The Roles of Mixing, Geothermal Heating, and Surface Buoyancy Forcing in Ocean Meridional Overturning Dynamics

by

Jeffery R. Scott

Sc.B., Electrical Engineering, Brown University (1985)
M.S., Civil and Environmental Engineering, Duke University (1995)

Submitted to the Department of Earth, Atmospheric, and Planetary Sciences in partial fulfillment of the requirements for the degree of

Doctor of Philosophy

at the

MASSACHUSETTS INSTITUTE OF TECHNOLOGY

September 2000

Signature of Author: _____
Department of Earth, Atmospheric, and Planetary Sciences
August 1, 2000

Certified by: _____
Jochem Marotzke
Professor of Physical Oceanography
Thesis Supervisor

Certified by: _____
Peter H. Stone
Professor of Meteorology
Thesis Supervisor

Accepted by: _____
Ronald G. Prinn
Chairman, Department of Earth, Atmospheric, and Planetary Sciences

The Roles of Mixing, Geothermal Heating, and Surface Buoyancy Forcing in Ocean Meridional Overturning Dynamics

by

Jeffery R. Scott

Submitted to the Department of Earth, Atmospheric, and Planetary Sciences
on September 1, 2000, in Partial Fulfillment of the Requirements for the Degree of
Doctor of Philosophy in Climate Physics and Chemistry

Abstract

The dynamics of the oceanic large-scale meridional overturning circulation are investigated through a series of numerical experiments using an idealized single-hemisphere general circulation model. In addition to the system's scaling behavior, the consequences of diapycnal mixing location, the impact of deep buoyancy fluxes, and the importance of the surface restoring timescale are considered.

As required by advective-diffusive balance, upwelling across isopycnals in low latitudes occurs where diapycnal mixing is specified. Downward mass transport into the abyss is relatively buoyant; the abyssal heat budget is such that this flow is subsequently cooled through deep convective mixing and re-warmed by diapycnal heat fluxes. Thus, mixing below the thermocline affects the abyssal stratification and upwelling profile, but does not contribute significantly to the zonally averaged circulation through the thermocline or the meridional oceanic heat transport. Boundary mixing is more efficient than interior mixing at driving the meridional overturning circulation; with interior mixing, the planetary vorticity constraint interferes with the communication of interior water mass properties and the eastern boundary. The results are consistent with thermodynamic considerations that suggest the strength of the overturning is a function of the vertical heat fluxes through the thermocline. Accordingly, diapycnal mixing must result in surface heat input to influence the portion of large-scale overturning that effects the meridional heat transport.

When a buoyancy flux (e.g., geothermal heating) is applied to the ocean floor, a perturbation deep meridional overturning cell on the order of several Sv is produced. The surface flow is also perturbed at high latitudes, allowing the additional heat to be released to the atmosphere. Rising motion is concentrated near the equator. The upward penetration of the deep cell is limited by the thermocline, analogous to the role of the stratosphere in limiting the upward penetration of convective plumes in the atmosphere. The magnitude of the advective response is inversely proportional to the deep stratification; with a weaker meridional overturning circulation and hence a less stratified abyss, the overturning maximum of the deep cell is increased. These results suggest that geothermal heat fluxes, typically ignored in general circulation models, might play a more significant role than thought in the determining the abyssal circulation.

For the lowest two decades of changes to diapycnal mixing diffusivity (κ), the system's response is largely "self-similar", but experiences a transition to a different regime at very high values of diffusivity. The maximum in overturning circulation obeys an approximate $^2/_3$ power scaling law over both regimes. In contrast, given changes in the imposed equator-to-

pole temperature difference ΔT, the behavior is not self-similar except in the meridional profile of surface heat exchange. Moreover, the power law scaling of overturning with ΔT is similar to that of κ, in contradiction with the $1/3$ law predicted by scaling arguments and the Marotzke (1997) theory. The ocean's dynamical behavior is also strongly influenced by the restoring timescale at which the surface temperature is restored; with weaker restoring, the deep sinking region of the ocean becomes more narrow in the zonal mean, and the maximum in meridional heat flux declines even though the maximum in overturning remains nearly constant. These results are interpreted by considering the fundamental thermodynamics of the system.

Thesis Supervisor: Jochem Marotzke
Title: Professor of Oceanography

Thesis Supervisor: Peter H. Stone
Title: Professor of Climate Dynamics

Acknowledgements

I would like to begin by thanking my co-advisors, Prof. Jochem Marotzke and Prof. Peter Stone. Both were very generous with their time and ideas. Jochem's enthusiasm for this work was infectious and helped me to persevere whenever the model's behavior was not readily understood. I consider myself quite fortunate to have been able to work so closely with Jochem over the last several years, and am thankful for the opportunity to work with him on several related projects. As the original questions posed in this thesis project dealt more extensively with coupled atmosphere-ocean dynamics; I am grateful to Peter for continued support during my tenure here, even when my focus shifted towards questions more firmly rooted in oceanography.

I am also indebted to my other two committee members, Prof. Kerry Emanuel and Prof. Carl Wunsch. Their expertise was also critical in the development of the ideas presented in this thesis. In particular, while my co-advisors provided guidance through the day-to-day analyses of model results, Kerry and Carl provided much of the vision on how this work is more broadly relevant to the fields of meteorology and oceanography, particularly in regard to thermodynamic considerations. Their continued emphasis on this theme led to a greater understanding of results and a more cohesive thesis. Alistair Adcroft also deserves mention, as he played an important role in the development of chapter 4.

I am grateful to Mary Elliff, Jane McNabb, Linda Meinke, and Joel Sloman for clerical, administrative, and computing assistance. All were willing to make an extra effort when asked. The graduate student 'process' can be frustrating at times, and their help was greatly appreciated.

I would also like to acknowledge the many students with whom I've had discussions over the years. In particular, the many discussions (and arguments) I've had with fellow classmates Brian Arbic and Constantine Giannitsis (among others) have enriched my scope of knowledge. Constantine also deserves mention for the many times he has helped me out when I have gotten stuck on long-forgotten mathematical subtleties.

And lastly, I would like to thank Janet, for her unwavering support through it all.

This work was supported jointly by the U.S. Department of Energy through the Climate Change Prediction Program and by the MIT Joint Program on Science and Policy of Global Change.

Table of Contents

Chapter 1 - Introduction ____ *9*

1.1 Motivation ____ **9**

1.2 Thermodynamic Considerations ____ **11**

1.3 Scaling Behavior ____ **13**

1.4 Thesis objectives and outline ____ **17**

Chapter 2 - Model Description ____ *19*

Chapter 3 - The Importance of Mixing Location ____ *23*

3.1 Introduction ____ **23**

3.2 Horizontal Location of Mixing ____ **24**

3.2.1 Boundary versus Uniform Mixing ____ 24

3.2.2 Low Latitude Mixing; Mid-Basin Mixing ____ 28

3.2.3 Highly Localized Mixing ____ 29

3.3 Depth-Dependent Mixing ____ **36**

3.3.1 Advective-Diffusive Balance and Stratification ____ 36

3.3.2. Mixing Below the Thermocline ____ 38

3.3.3. Abyssal Heat Balance ____ 41

3.4 Summary and Discussion ____ **46**

Chapter 4 - The Effect of Geothermal Heating ____ *51*

4.1 Introduction ____ **51**

4.2 Single Hemisphere Geothermal Heating ____ **54**

4.2.1 Preliminaries ____ 54

4.2.2 Initial Transient Response ____ 55

4.2.3 Perturbation Analysis ____ 57

4.2.4 Thermodynamic Interpretation of Response ____ 60

4.2.5 Dynamics of the Anomalous Meridional Overturning Circulation ____ 63

4.3 Alternate Forcing Scenarios ____ **66**

4.3.1 Alternate Background States ____ 66

4.3.2 Variations in Geothermal Heating Application ____ 68

4.4 Geothermal Heating In A Double Hemisphere Model ____ **71**

4.5 Summary and Discussion ____ **76**

Chapter 5 - Scaling Behavior of the MOC ____ *81*

5.1 Introduction ____ **81**

5.2 Scaling Behavior with κ ____ **84**

5.2.1 Overturning Streamfunction and Meridional Heat Transport ____ 84

5.2.2 Thermocline Depth ____ 90

5.3 Scaling Behavior with ΔT ____ **96**

5.3.1 Overturning Streamfunction and Meridional Heat Transport ____ 96

5.3.2 Thermocline Depth ____ 99

5.4 Effect of Surface Restoring Timescale ____ **103**

5.4.1 Varying τ ____ 103

5.4.1 Varying κ using a 30-day Restoring Timescale ____ 106

5.5 Summary and Discussion ____ **108**

Chapter 6 - Summary and Conclusions ____ *111*

6.1 Summary ____ **111**

6.2 Thermodynamic Conceptualization ____ **114**

6.3 Concluding Remarks ____ **119**

References ____ *121*

Chapter 1

Introduction

1.1 Motivation

Although the introduction of more powerful computers in recent years has allowed for more realistic simulations of our climate system, our understanding of these results has generally not kept pace with advances in computational resources. One difficulty in interpreting these results is our limited understanding of the fundamental dynamics of the large-scale ocean circulation. The ocean is an important component in the climate system, both in its capacity to store vast amounts of heat and as a dynamical agent of heat transport. The integration of oceanic observations with inverse models has led to improved estimates of global circulation patterns (e.g., Macdonald and Wunsch 1996), giving climate scientists a target when "tuning" the ocean component of their models. However, in addition to being able to simulate current climate, a goal of the climate modeling community is to understand climate change in both the past and future. Paleoclimate indicators can provide some hints as to the ocean circulation patterns of yesteryear, but in general lead to more questions than definitive answers. Oceanic circulation in future climates is even less certain. In order to facilitate our understanding of the ocean's role in climate, an improved understanding of the large-scale circulation is needed.

Most of the studies which have examined the climatic implications of the large-scale overturning circulation have focused on the stability of the so-called thermohaline circulation, hearkening back to Stommel's (1961) box model study on the roles of heat and freshwater surface forcing. The question of stability (and the related issue of predictability) is particularly relevant today given concerns that global warming might alter the fluxes of heat and freshwater at the ocean surface. Despite being pivotal to the issue of stability, the underlying

dynamics and thermodynamics of the meridional overturning circulation (MOC), even without the complication of competing temperature and salinity effects, have not been fully explored.

In part, our limited understanding of the MOC is due to uncertainty regarding the roles played by buoyancy-forcing, convection, and diapycnal mixing in the context of the fundamental thermodynamics. A related, yet equally fundamental problem, is to understand the process that determines the density structure of the ocean. Any prospect for a full analytical treatment is doubtful, inasmuch as rotational and frictional terms must also be included in any complete set of equations. Colin de Verdière's (1988) numerical modeling results were noteworthy in that his study was the first comprehensive attempt to diagnose and understand the simplified overturning circulation that arises without wind forcing. Marotzke (1997) added to our understanding by more carefully analyzing the different flow patterns and resultant density structures on the eastern and western boundaries. The east-west density differences, in turn, support a meridional overturning circulation through the build-up of vertical shear given thermal wind balance. Based on his numerical model's behavior, Marotzke also suggested an analytical treatment for the eastern and western boundary densities, in effect the first complete theory (the merits of this theory are discussed later in this chapter). Other experimental studies have also examined the buoyancy-forced problem (e.g., Rossby 1965; Rossby 1998), although the lack of rotation in some laboratory and numerical models is problematic, given that to leading order flows in the ocean are in geostrophic balance.

The objective of this thesis is to further our understanding of the large-scale ocean circulation by carefully examining the steady-state behavior of a single-hemisphere ocean model, given variations in buoyancy forcing and diapycnal mixing. As part of this study, we examine the impact of a buoyancy flux through the ocean floor, i.e., mimicking the effect of geothermal heating, a subject that has received only scant attention in the literature. Our configuration is very highly idealized, and like our predecessors, we omit the effects of wind forcing and salinity variations[1] (in this thesis we will treat temperature and density as conceptually similar). Nevertheless, we maintain that the single hemisphere ocean is an appropriate configuration to represent the fundamental dynamics of the MOC.

[1]Although our model includes salinity, it is restored to a surface salinity with the same profile as temperature. Thus, to a very good approximation salinity is a function of temperature only, and the two do not compete in determining the density. See chapter 2 for details.

1.2 Thermodynamic Considerations

In the absence of any ongoing sources of energy, frictional dissipation would ultimately spin down the ocean circulation to a motionless state. Possible external energy sources that could maintain a circulation include winds, tides, and geothermal heating [Weyl 1968; Faller 1968; Munk and Wunsch 1998 (hereafter MW)]. The direct effect of wind forcing has received considerable attention in the past few decades, both in theoretical and general circulation modeling studies, with fairly well established results. Wind stresses are thought to be responsible for the gyre structures observed in the oceans' surface currents. In addition, wind forcing generates overturning cells in the meridional plane, in effect providing a return pathway for upper level Ekman transport. Both of these structures contribute to the oceans' heat transport in the subtropics (Wang et al. 1995; Klinger and Marotzke 2000).

The oceanographic community's emphasis on the direct effect of wind forcing is in some ways puzzling, however, given that a MOC which transports heat meridionally is possible with or without direct wind input (n.b., Colin de Verdière 1988, Colin de Verdière 1989). Indirectly, wind forcing can lead to turbulent mixing through the breaking of wind-generated internal waves and through the interaction of wind-driven motions with topography (MW). Similarly, the interaction of tides with topography is also a likely contributor to turbulent mixing (MW; Polzin et al. 1997). Unfortunately, present-day limits of computational resources dictate that the external energy source for diapycnal mixing is couched in terms of the parameterization of eddy diffusivity.

It has been known for some time that the strength of the meridional overturning circulation in models depends strongly on this choice of the diapycnal (or vertical[2]) diffusivity (Bryan 1987; Colin de Verdière 1988; Zhang et al. 1999). However, given the different processes thought to play a role in the steady-state balance of the MOC, it is not directly apparent why this should be so. According to "Sandström's theorem" (Sandström 1908), the steady-state ocean circulation should be motionless except in a thin upper layer if surface heating occurs at higher geopotential than cooling. In other words, given heating in the tropics, the ocean should not be able to operate as a heat engine, extracting energy from the surface buoyancy forcing to maintain a vigorous MOC. However, Jeffreys (1925) argued that turbulent mixing could effectively lower the geopotential of heating, i.e., leading to horizontal temperature gradients at depth which could in turn lead to a strong circulation (see Colin de Verdière

[2]Given the aspect ratio of ocean models, diapycnal mixing is virtually equivalent to mixing along the vertical axis except in regions of sharply sloping isopycnals.

1993, MW, and Huang 1999 for a more thorough discussion of Sandström's theorem and the controversy surrounding its application to the ocean.). Inasmuch as diapycnal mixing is the immediate energy source for the large-scale overturning in this realization, we will avoid the use of the misleading descriptions "buoyancy driven" and/or "thermally driven" which are common in the literature.

The converse of Sandström's theorem suggests that deep heating from geothermal sources could also play a role in driving the MOC. It is an open question whether the geothermal buoyancy flux is able to directly drive a large-scale circulation (Faller 1968; Huang 1999). Given that geothermal heating is several orders of magnitude weaker than surface buoyancy forcing, geothermal heating has been heretofore ignored in ocean general circulation models (although Sandström's theorem would suggest that this scaling argument is specious). Geothermal energy might also contribute to turbulent mixing in the abyss.

In the absence of diapycnal mixing, a vigorous overturning circulation would fill the ocean depths with dense water. Thus, mixing is necessary to maintain a realistic vertical structure given upwelling of cold abyssal water, with the stratification determined by the ensuing vertical advective-diffusive balance. Munk (1966) examined this hypothesis in observed abyssal density profiles and tracer distributions. Neglecting the effects of horizontal advection, he concluded that the data are "not inconsistent" within a one-dimensional framework, with a uniform eddy diffusivity of u, although he also noted the likely importance of boundary mixing processes. The MW98 follow-up found a better fit with observations if the vertical diffusivity was allowed to vary with depth, and also more explicitly stated that the $O(10^{-4}\,m^2s^{-1})$ diffusivity was to be considered a spatially averaged value resulting from localized zones of enhanced mixing. In the real ocean, it is clear that ventilation of the thermocline through Ekman pumping also plays a role in setting the observed vertical structure (Luyten et al. 1983; Samelson and Vallis 1997; Samelson 1998).

In contrast to diapycnal diffusion, the overall effect of convective mixing of dense surface waters is to lower the center of mass of the system, hence lowering the overall potential energy. In other words, convection serves to remove heat that has been injected into subsurface waters through diapycnal mixing. Although convection is patently necessary in order to maintain high latitude deep-water formation (Zhang et al. 1992), model results suggest it is a sufficiently efficient process so as not to be rate limiting in determining the downward mass flux (Marotzke and Scott 1999). This latter study further notes that deep convective

mixing and downwelling are not necessarily co-located, which has important dynamical consequences (see also Rahmstorf 1995; Spall and Pickart 1999; Mauritzen and Häkkinen 1999).

A related issue is the "narrowness of sinking" of the large-scale circulation, as first discussed in Stommel (1962). Observations of abyssal water mass properties suggest that deep sinking occurs in select high-latitude regions of limited geographical extent. Stommel's pipe-model results suggested that narrow sinking was not a function of the imposed surface density gradient. Rossby (1965) concluded that the asymmetry was due to thermodynamics; more specifically, he stated that the process of convection[3] was much more efficient at heat transfer than diffusion. As a result, diffusion occurs over a larger area so that these fluxes are able to balance the heat lost through convection. Winton (1995) noted that narrow sinking resulted in a state of minimum overall potential energy, but once deep water properties were established, broad upwelling resulted in maximum downward heat penetration and therefore maximum available potential energy. Marotzke and Scott (1999) disputed Rossby's argument, providing an alternate explanation that invoked three-dimensional geostrophic dynamics (while suggesting that two-dimensional models were inappropriate to address this question in the context of oceanography).

1.3 Scaling Behavior

In view of the aforementioned difficulties in developing a theoretical model of the MOC, numerous studies have instead examined the scaling behavior. Commonly examined is the power law dependence of the overturning streamfunction maximum with vertical diffusivity. The sensitivity of other quantities such as thermocline depth and maximum meridional heat flux has also been computed.

A simple predictive scaling relationship for the overturning circulation was first presented by Bryan and Cox (1967) and is generally accepted as the de facto explanation of the scaling behavior (see also Welander 1971). The following balances are employed:

$$\text{vertical advective-diffusive balance: } W \sim \frac{\kappa}{D} \tag{1.1}$$

[3]These early works do not distinguish between the processes of convective mixing and net mass transport by downwelling, insofar as these processes are co-located in the two-dimensional framework (Marotzke and Scott 1999). Thus, it is not entirely clear if these early studies referred to the efficiency of the convective mixing process itself or to the efficiency of heat transport via a net vertical mass transport.

continuity: $$\frac{V}{L} \sim \frac{W}{D} \tag{1.2}$$

thermal wind balance: $$\frac{V}{D} \sim \frac{g\alpha}{f}\frac{\Delta T}{L} \tag{1.3}$$

where V and W are horizontal and vertical velocity scales, respectively, L and D are horizontal and vertical length scales, κ is a vertical (or diapycnal) diffusivity, and ΔT is the equator-to-pole temperature difference. By eliminating W from (1.1) and (1.2) and eliminating V using (1.3), the following scales for V and D are obtained:

$$V \sim \left(\frac{\kappa(g\alpha\Delta T)^2}{fL^2}\right)^{1/3}, \quad D \sim \left(\frac{\kappa f L^2}{g\alpha\Delta T}\right)^{1/3} \tag{1.4}$$

The meridional overturning Ψ can in turn be estimated as $\sim VDL$, suggesting a $\kappa^{2/3}$ dependence. Bryan (1987) was the first to test these ideas using numerical models, suggesting that both D and Ψ scale as $\kappa^{1/3}$. More recently, models with improved numerics (both vertical and isopycnal coordinate models) have shown that Ψ scales as $\kappa^{2/3}$ (Zhang et al. 1999; Park and Bryan 2000), in agreement with scaling law.

Despite this apparent success, on closer inspection it is less clear why a simple combination of (1.1)-(1.3) can predict the observed power law scaling. There are two problems with this approach. First, the thermal wind relation (1.3) predicts a zonal velocity scale as a function of the equator-to-pole temperature gradient. Since a scale relation for the *meridional* velocity is necessary to obtain a relation for Ψ, it has implicitly been assumed that the north-south density gradient is directly proportional to the east-west gradient. Recent results show that this may not be a problem after all; Marotzke's (1997) analytical theory suggested that this proportionality was indeed the case, which was confirmed numerically by Park and Bryan (2000). The second problem is more subtle, and has apparently thus far escaped scrutiny. In (1.1), the depth scale D is an advective-diffusive scale height, as scaled from the thermodynamic equation. In (1.3), however, the depth scale is a distance over which a horizontal velocity is established through thermal wind shear, as scaled from the momentum equation. (This depth is the zero-crossing depth in the zonal mean, a.k.a. the depth of the "level of no

motion[4]"or baroclinic node; in this thesis we will henceforth use the terminology "zero-crossing depth" to refer specifically to the depth of vanishing horizontal velocity in the zonal mean). It is not clear *a priori* that these two quantities are proportional to each other, much less even related. Compounding the confusion is the difficulty in measuring a depth scale; studies have typically estimated a scale height as the e-folding depth of the top-to-bottom density difference (e.g., Bryan 1987) or calculated a temperature-weighted average height (e.g., Park and Bryan 2000), neither of which directly measures the advective-diffusive scale height or the zero-crossing depth.

The dependence of this depth scale on external parameters is yet another problem with the scaling argument. As noted in Park and Bryan (2000), a scaling argument implicitly assumes a "self-similarity" of solutions. In other words, given a change in external parameters, a contour plot of any internal quantity should show only a multiplicative change, not a change in the shape of the contours. The scaling argument presumes that northward shear in the thermocline accounts for the upper limb of the MOC; the northward flow is then balanced by southward flow in the abyss. Hence, a change in the depth over which the northward shear occurs also implies a change in the pattern of overturning streamfunction, as no self-similar solution is possible as long as the depth of the ocean is fixed. Park and Bryan dismiss this concern by arguing that as long as the depth scale is small compared to the depth of the ocean, a weakly stratified abyss prevents the overturning circulation from "feeling" the presence of the ocean bottom [as first noted in Bryan and Cox (1967)]. Thus, they conclude that a self-similar scaling is possible, at least over a limited parameter range of κ.

Early analytical attempts at developing a "thermocline theory" (i.e., solving the equations employed in the scaling argument—the geostrophic/hydrostatic momentum equations, continuity, and the advective-diffusive density equation) resulted in a class of "similarity solutions" (Robinson and Stommel 1959; Stommel and Webster 1962; Robinson and Welander 1963). In order to solve the full set of partial differential equations, these solutions were assumed to be separable in the vertical. Thus, the structure of the thermocline was assumed to be of the same analytical form, albeit with a different stretching factor, everywhere in the horizontal. More recent efforts have suggested that the similarity structure is more appropriate as an advective-diffusive internal boundary layer which forms below the wind-driven ventilated thermocline structure (Young and Ierley 1986; Salmon 1990; Samelson and Vallis

[4]This is somewhat of a misnomer, as it is only the zonally averaged horizontal velocity that vanishes; the vertical velocity is at its maximum value at this depth, and it is not required that horizontal velocity vanishes at any specific longitude.

1997; Vallis 2000). Even if one is willing to accept the similarity assumption used in these solutions, the mathematical complexity of these solutions effectively limits the vertical structure to a narrow class of solutions, limiting their utility. Moreover, these solutions offer limited physical insight into the problem (see Pedlosky 1996, pp. 171-176 for additional historical perspective on the so-called thermocline problem).

In light of the difficulties with both the scaling argument and the similarity theory, the Marotzke (1997) theory represents a breakthrough in our understanding of the MOC. The fundamental assumptions of this theory are as follows. In the tropics and along the western boundary, temperature is assumed to decay exponentially from a prescribed profile of sea surface temperature. The scale height is determined as part of the solution. Implicit in this assumption is that the primary vertical balance is advective-diffusive, assuming a constant vertical velocity. Along the eastern boundary, surface downwelling produces a deep mixed layer (the depth being a function of latitude), with exponential decay below. The system of equations is closed by assuming that isopycnals are flat along the eastern boundary, so that the depth of the unstratified mixed layer matches the depth of that isopycnal at the equator. (Isopycnals are also assumed to be flat along the equator, given that to leading order no zonal pressure gradient can be maintained in the absence of wind forcing.) All of these assumptions seem plausible given the observed model behavior.

Thus, by assigning density profiles on the eastern and western boundaries, the Marotzke theory incorporates the physical behavior of the system. The scaling argument and the similarity solutions, on the other hand, do not "know" about the behavior on the eastern boundary. Another strength of the theory is that the advective-diffusive scale height is distinguished from the zero-crossing depth. Therein also lies a major weakness of the theory, however: An ad hoc assumption for the zero-crossing depth is employed, although reasonable agreement between the theoretical and model results is achieved. It is interesting to note that Marotzke's analytical results show the same power law dependences on κ and ΔT as the scaling argument; in this regard, the Marotzke theory would seem to suggest that the aforementioned problems with the scaling argument are of little consequence in predicting the behavior of the MOC.

1.4 Thesis objectives and outline

Our approach here will be to examine the behavior of a buoyancy-driven sector model of the MOC in a series of numerical experiments. Through these experiments we will address the following questions:

- What is the role of mixing processes (i.e., diapycnal mixing and convection) in the dynamics of the large-scale circulation? Is the location of mixing important?

- How does the MOC depend on the buoyancy gradient at the surface? How do bottom boundary fluxes of buoyancy affect the MOC?

- Is it possible to define a thermocline depth in an ocean without direct wind forcing, and if so, how does it vary with diapycnal mixing and buoyancy forcing?

- Can the MOC's scaling behavior be considered self-similar?

- Does the application of thermodynamic principals help explain the MOC dynamics?

The goal is to build on the qualitative discussion and theory put forth in Marotzke (1997), thus providing a more fundamental understanding of the MOC.

In chapter 2, we describe the numerical model in more detail. As mentioned, our configuration is highly idealized in order to facilitate our understanding of the dynamics. As compared with previously published work, our model is noteworthy in two important ways. First, our numerics are state-of-the-art, with the main improvement being the use of an isopycnal mixing scheme (Gent and McWilliams 1990). This scheme eliminates spurious horizontal mixing across isopycnals that is otherwise present in coarsely resolved (i.e., non-eddy resolving) models. Second, our "control" configuration specifies mixing only at the boundaries, with zero interior mixing, as first implemented in Marotzke (1997). Not only is this scheme likely to be closer in spirit to the inhomogeneous mixing in the real ocean (MW; Polzin et al. 1997), but it simplifies the dynamical interpretation of results.

In chapter 3, we present a systematic and comprehensive exploration of spatially varying diapycnal mixing. We juxtapose various extreme scenarios, in that mixing is concentrated entirely at low or high latitudes; at the western boundary, the eastern boundary, or the inte-

rior; in or below the thermocline. To our knowledge, the MOC's sensitivity to mixing in so clearly identifiable regimes of the ocean has never been investigated. Moreover, we offer new interpretations of the deep-ocean heat budget and of how planetary vorticity conservation helps us to understand the MOC.

The effect of geothermal heating is examined in chapter 4. To the best of our knowledge, geothermal heating at the ocean bottom has been omitted from all previously published ocean general circulation model results [the only exception being our companion study using a global ocean model, Adcroft et al. (2000)]. We begin with a perturbation analysis of the flow and temperature structure that results from a uniform heat flux of 50 mW m^{-2} through the ocean floor. Because our model is coarsely resolved, we cannot resolve dynamically active convective plumes; hence, our focus is on understanding the impact of non-local geothermal heating in the context of the background large-scale circulation. The sensitivity of these results to different model forcings is then examined, including several experiments in a double-hemisphere ocean basin.

Chapter 5 examines the dynamical behavior of the MOC given variations in κ and ΔT, with careful attention given to thermodynamic considerations. Although the scaling with κ has been examined at length, we extend the range of parameter space. Moreover, we examine the scaling of the thermocline depth more rigorously than in previous studies. Unlike the scaling behavior with κ, the scaling of the MOC with ΔT has been subject to only cursory examination. In the process of these scaling analyses, we are naturally led back to Stommel's (1962) question about the narrowness of sinking and how the MOC structure depends on surface boundary conditions.

In Chapter 6, we begin by summarizing our major findings. Building on these results, we synthesize a speculative thermodynamic model of the MOC. Lastly, we suggest some direction for future research efforts.

Chapter 2

Model Description

We employ the vertical coordinate, primitive equation model MOM2 (beta version 2.0), as described in Pacanowski (1996). Default parameters are listed in Table 1, with any deviations noted in the text. The ocean configuration and forcing are identical to that in M97: the domain is a 60° wide single hemisphere sector, ranging from the equator to 64°, with a constant depth of 4500 meters; surface temperature and salinity are forced using an identical, zonally uniform profile, given as follows:

$$(T,S) = \frac{(T_\Delta, S_\Delta)}{2}\left(1+\frac{\cos \pi y}{L_y}\right)+(T_o,S_o) \tag{2.1}$$

with $(T_\Delta, S_\Delta) = (13.5°\text{C}, 0.75)$, so that the peak-to-peak amplitudes are 27°C and 1.5, respectively, and $(T_o, S_o) = (0°\text{C}, 34.0)$ (salinity is dimensionless in the practical salinity scale). Given these identical forcing profiles, the model can be thought of as being forced by buoyancy[5]. As such, in this thesis we do not distinguish between temperature and density in the language of our discussion. Unless specified otherwise, the surface layer is relaxed to (2.1) using a 30-day relaxation time constant in the experiments presented in chapters 3 and 4. In chapter 5, we examine the effect of changing this time constant, although our main scaling analyses are based on runs that employ a 3-day restoring timescale. For simplicity, no wind stress is imposed, nor does the model include the effects of sea ice. Horizontal resolution is 1.875° zonally by 2° meridionally, using 30 vertical levels ranging from 50 meters at the surface to 250 meters at the lowest level.

[5]Higher-order effects from the non-linear equation of state are included in the model but are not thought to be important in the results presented here.

TABLE 1. Summary of numerical parameters.

Parameter	Value
Basin width, length	60°, 64°
Basin depth	4500 m
Horizontal, vertical viscosity	3.3×10^{4} m^{2}s^{-1}, 10^{-2} m^{2}s^{-1}
Horizontal, isopycnal diffusivity	0 m^{2}s^{-1}, 10^{3} m^{2}s^{-1}
Diapycnal[6] boundary, interior diffusivity (κ)	10×10^{-4} m^{2}s^{-1}, 0 m^{2}s^{-1}
Isopycnal diffusion thickness	10^{3} m^{2}s^{-1}
Longitude, latitude grid spacing	1.875°, 2°
Number of levels	30
Temperature, salinity restoring timescale	30 days (unless noted)
Time step, momentum	30 minutes
Time step, tracers	12 hours

As in M97, diapycnal mixing is imposed in the columns adjacent to the north, south, east, and west sidewalls, and is set to zero elsewhere; this is thought to mimic the effect of enhanced mixing due to a sloping lateral boundary. Diapycnal mixing at the equator is a surrogate for the global integral of mixing throughout the rest of the world's oceans. Although there is evidence of enhanced mixing at the equator (Gregg 1987; Peters et al. 1988) and the dynamics are unique due to the vanishing of the Coriolis parameter (Gill 1982), our choice of the equator for our southern wall is for practical reasons, as cross-equatorial flow involves complicated dynamics (Marotzke and Klinger 1999) that are beyond the scope of our investigation. To insure that equatorial dynamics were not important in our findings, we spun-up a run with the southern boundary mixing moved one grid cell northward (i.e., removed from the equator), with only minor differences resulting.

[6]We employed the MOM 2 full tensor option, which operates as follows. Diapycnal mixing is implemented through vertical diffusion, which is a reasonable approximation given that the slope of isopycnals is quite flat over much of the ocean. In addition, the horizontal diffusive flux terms $\kappa\,\partial_x(T,S)$ and $\kappa\,\partial_y(T,S)$ are included so that diapycnal mixing is represented even in the case of sharply sloping or vertical isopycnals (the effect of these horizontal fluxes is neglibible for weakly sloping isopycnals, given our large diffusivity for along-isopycnal mixing).

For computation efficiency, some of the experiments were run at half resolution, i.e., 3.75° x 4°, 16 vertical levels. In these runs, the diapycnal mixing coefficient along the boundaries was decreased 50% for comparative purposes with the standard runs, and the horizontal viscosity was changed to resolve the Munk boundary layer at the new zonal grid spacing. The weak deep mixing run and control run as presented in section 4 were run using 90 evenly spaced vertical levels; this was done to minimize any adverse numerical effects and to allow for a smoother representation of stratification. In several direct comparisons (not shown), model results did not differ significantly between similarly configured runs at different vertical and/or horizontal resolution.

All model runs were integrated to equilibrium, as defined by a basin-averaged surface heat flux of 5×10^{-3} W m^{-2} or less, where practical, and/or when overturning is discernibly within 0.1 Sv of its final value. The spin-up procedure is as follows. The control run was integrated to equilibrium at coarse resolution from an isothermal, motionless ocean, interpolated to standard resolution and allowed to re-equilibrate. All other experiments were started from the control run (at either the standard or coarse resolution) or from the equilibrated state of another experiment.

In order to minimize numerical "wiggles" resulting from zero diapycnal mixing in the ocean interior, we employed MOM's flux corrected transport advection scheme, a non-linear compromise between upstream and central differences (Gerdes et al. 1991). In effect, this scheme minimizes numerical noise through the introduction of some diapycnal mixing. We maintain this scheme's supplementary mixing is inconsequential here, based on trial experiments using MOM's other advection schemes and from the results of runs with very weak boundary mixing. The reader is referred to M97 for a discussion of other numerical issues involved with the boundary mixing implementation

Before proceeding, some additional comments are in order regarding the boundary layers that occur in the model solution. Reasonable treatment of western boundary currents is possible, albeit using an unrealistic viscosity coefficient due to our coarse grid spacing. As noted in Huck et al. (1999), however, the parameterization of the lateral boundary conditions can influence the large-scale circulation. Here, two notable features of our solution—narrow upwelling along the eastern and western boundary and deep downwelling in the northeast corner—are enhanced by (or perhaps even caused by) by our use of no-slip side boundaries with

Laplacian momentum dissipation[7]. Huck et al. showed that the model solution differs when a linear frictional closure scheme for tangential velocity is introduced into the vorticity equation, such as proposed in Winton (1993). It is not clear which boundary parameterization is superior for the purpose of modeling the real ocean, given a lack of observational evidence and our limited understanding of eddy dissipation processes (see Huck et al. for a more complete discussion). An additional complication is that our coarse grid does not permit resolution of these narrow boundary layers; presumably, the internal radius of deformation is the relevant scaling. Despite this seeming miasma of issues related to boundary layer implementation, we believe the qualitative behavior observed in our experiments is robust, reflecting the fundamental thermodynamics of the large-scale circulation rather than local dynamical features specific to the model implementation. The effect of other model deficiencies, particularly the absence of wind stresses and topography, is addressed in later chapters.

[7]The so-called "Veronis effect" (Veronis, 1975) whereby a Cartesian implementation of diffusion is thought to effect spurious horizontal mixing in the western boundary, producing upwelling, does not occur here given our use of MOM's the isopycnal mixing scheme. Huck et al. (1999) argue that the lateral boundary parameterization induces upwelling which in turn causes the Veronis effect, rather than vice-versa.

Chapter 3

The Importance of Mixing Location

3.1 Introduction

Since the advent of ocean general circulation models (Bryan and Cox 1967; Bryan 1969), the standard parameterization for unresolved diapycnal stirring has been through vertical diffusion of heat and salt, typically using a spatially uniform diffusivity coefficient. Recent improvements in modeling techniques allow for a more realistic representation of isopycnal and diapycnal mixing processes (Redi 1982; Gent and McWilliams 1990), although values for the diffusivities must still be chosen [or calculated as ad hoc mixing parameters, e.g., as some function of the buoyancy frequency, as in Cummins et al. 1990, or as some function of the Richardson number, as in the Pacanowski and Philander (1981) scheme]. Energy necessary for diapycnal mixing is thought to come from winds and tides (Munk and Wunsch 1998, hereafter MW98) and perhaps geothermal sources (Huang 1999). It is by no means established that this necessary energy is spatially dispersed; rather, the very nature of the sources, and the importance of bottom topography in extracting this energy (MW98; Polzin et al. 1997), suggests that a large portion of this mixing may be localized. Indeed, microstructure and tracer release measurements of turbulent mixing (Polzin et al. 1997; Ledwell et al. 1993; Ledwell et al. 1999) found strong mixing, with diffusivities on the order of 10^{-4} m^2s^{-1}, above rough bottom topography, but found an order of magnitude less above smooth abyssal plains and in the thermocline.

Our focus here is to examine the dynamical implications of spatially varying diapycnal mixing, both in the horizontal and vertical. The overriding goal is to better understand the dynamics of both the rising and sinking branches of the MOC, in particular clarifying the roles of diapycnal mixing and deep convective mixing. Owing to its direct impact on climate, the

meridional heat flux is one important attribute of the MOC. Also typically diagnosed is the maximum in the meridional overturning streamfunction, as a proxy for tracer transport; this property of the MOC can be important, for example, in the carbon cycle and distribution of biological nutrients. Additionally, the MOC plays an important role in governing deepwater properties. We will address the role of diapycnal mixing in determining each of these aspects of the large-scale circulation.

To date, there have been only a few model studies that specifically examine the dynamical consequences of mixing location. Samelson (1998) applied localized mixing on the eastern boundary to an idealized wind- and buoyancy-forced single hemisphere, planetary geostrophic model. Using an idealized single-hemisphere ocean general circulation model, Cummins et al. (1990; hereafter CHG) parameterized vertical diffusivity as a function of N^{-1}, effectively increasing mixing at depth, particularly below the thermocline. Cummins (1991; hereafter C91) examined the results of several additional runs with specified increased mixing below the thermocline. Using a similar model without wind-forcing, Marotzke (1997; hereafter M97) imposed mixing only along the boundaries and applied the results as a foundation for a self-contained theory predicting the strength of the MOC. Marotzke and Klinger (2000) investigated the effects of equatorially asymmetric vertical mixing.

Our configuration is very highly idealized, but we maintain that the single hemisphere ocean is an appropriate configuration to represent the fundamental dynamics of the MOC.

This chapter is organized as follows. The ramifications of highly localized mixing (i.e., ranging from boundary mixing to mixing at a single column) are examined in section 3.2. In section 3.3 we present experiments with depth-dependent diapycnal mixing, leading to some original notions about the deep ocean heat balance and the structure of the overturning cell. We conclude with a summary in section 3.4. The material in this chapter closely follows that presented in Scott and Marotzke (2000).

3.2 Horizontal Location of Mixing

3.2.1 Boundary versus Uniform Mixing

In the model runs of M97, boundary flows set up an east-west temperature gradient which, through thermal wind balance, supports a vigorous MOC. We have repeated M97's bound-

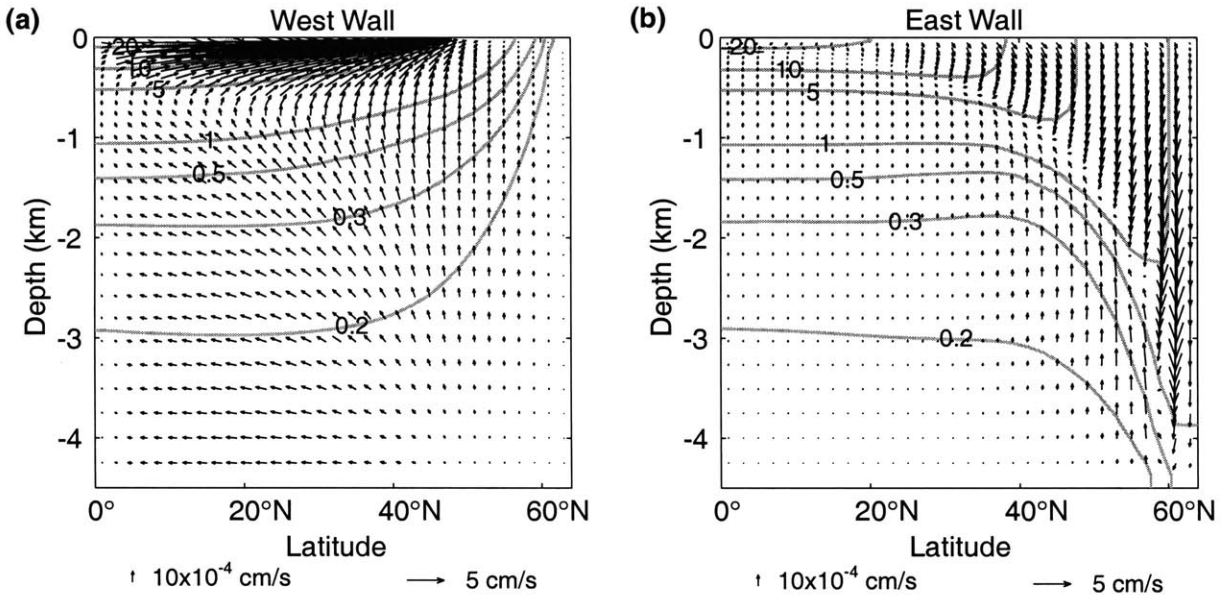

FIGURE 3.1: Boundary mixing run, $\kappa = 10 \times 10^{-4}\ \mathrm{m^2 s^{-1}}$. (a) Temperature (contour levels as indicated) and flow along the western wall; (b) temperature and flow along the eastern wall. Vertical and horizontal velocity scales are shown for reference.

ary mixing control run here; minor differences are due to our use of improved resolution and the isopycnal mixing scheme. As in M97, upwelling occurs all along the west wall (Fig. 3.1a), advecting dense deep waters into the thermocline. On the east wall (Fig. 3.1b), however, the vertical flow pattern is more complicated. Upwelling occurs at depth, but surface flow downwells to increasing depths at high latitudes. Since the downwelling surface water is relatively warm, the eastern wall is less dense than the western wall, providing the necessary shear for zonally integrated southward flow at depth and northward flow in the upper ocean.

The meridional mass transport stream function for the control run is shown in Fig. 3.2a. Over 5 Sv (Sv = $10^6\ \mathrm{m^2 s^{-1}}$), or almost half of the net mass transport, upwells adjacent to the equator, where diapycnal mixing is concentrated. To examine the effect of the boundary mixing parameterization, we equilibrated a run with uniform diapycnal mixing diffusivity of $1.15 \times 10^{-4}\ \mathrm{m^2 s^{-1}}$, i.e., that which produces an area-weighted diffusivity equivalent to that of the control run. Detailed analyses of a similarly configured uniform mixing run, albeit with cruder numerics, are presented in Colin de Verdière (1988). Superficially, the MOC of the uniform-mixing run (Fig. 3.2b) shows little difference from the boundary mixing run. The maximum of the overturning stream function is 1.7 Sv less in the uniform case, reducing the ocean's northward peak heat transport from .55 to .47 PW (PW = 10^{15} watts). With mixing

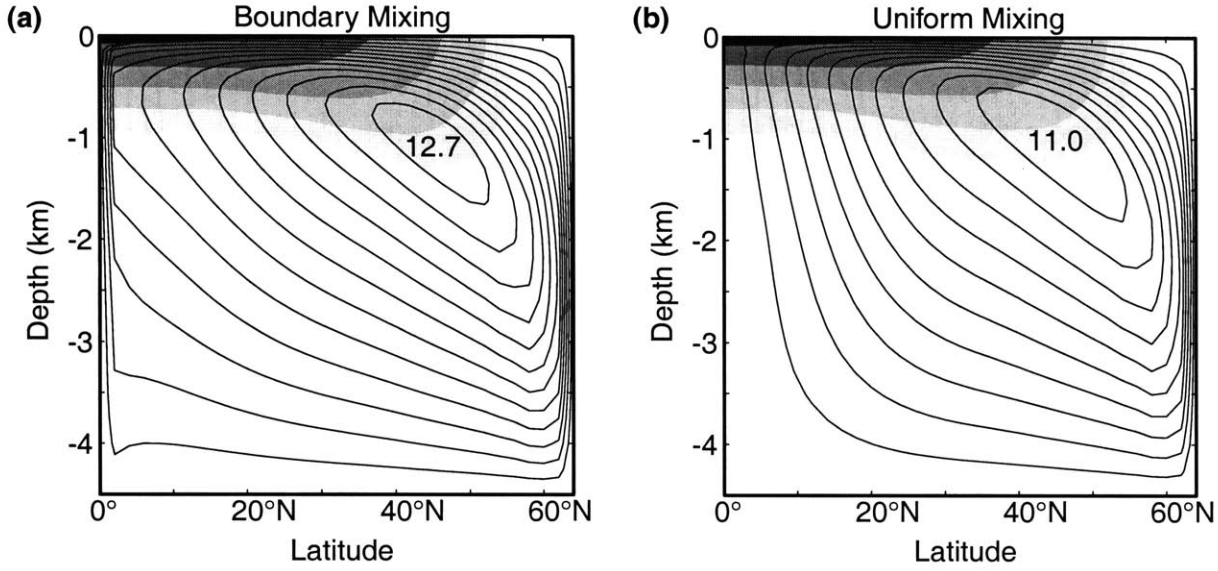

FIGURE 3.2: Meridional overturning streamfunction (contours) and zonally averaged temperature (shading) for (a) boundary mixing run, $\kappa = 10 \times 10^{-4}$ m^{2}s^{-1} and (b) uniform mixing run, $\kappa = 1.15 \times 10^{-4}$ m^{2}s^{-1}. In this and all subsequent plots of overturning streamfunction and zonally averaged temperature, overturning contours interval is 1 Sv; isotherms (shaded) are at 0.05, 0.1, 0.2, 0.4, and $0.8 \times \Delta T$ ($\Delta T = 27$°C); flow is oriented clockwise around overturning maximum.

spread out more evenly over the low latitudes, a much smaller proportion of the upward mass transport flows adjacent to the southern boundary. As would be suggested by our discussion in the previous section, strong vertical flows are present along the east and west boundaries, even in the uniform mixing case. Some of this flow recirculates zonally, eschewing any contribution to the MOC (see Bryan, 1987, for a diagnosis of the meridionally averaged circulation and its scaling behavior with vertical diffusivity), while some of western upwelling moves northward along isopycnals. As such, it is not immediately clear what component of these boundary flows is diapycnal.

To determine which boundary flows are directly induced by diapycnal mixing, presumably through advective-diffusive balance, and which are a largely a consequence of the boundary layer parameterization, we ran an experiment where we expanded the region of diapycnal mixing to two boundary grid columns around the model sidewalls. For consistency, we decreased the magnitude of κ by 50%. We also resolved the Munk boundary layer across two zonal grid points. As with the uniform mixing run, imposing mixing away from the boundaries results in a decreased maximum in the overturning streamfunction (not shown), although the reduction here is only 0.3 Sv. Near the equator, both meridional grid columns with mixing show strong upwelling, as shown in Fig. 3.3a, while interior flows are very weak in the

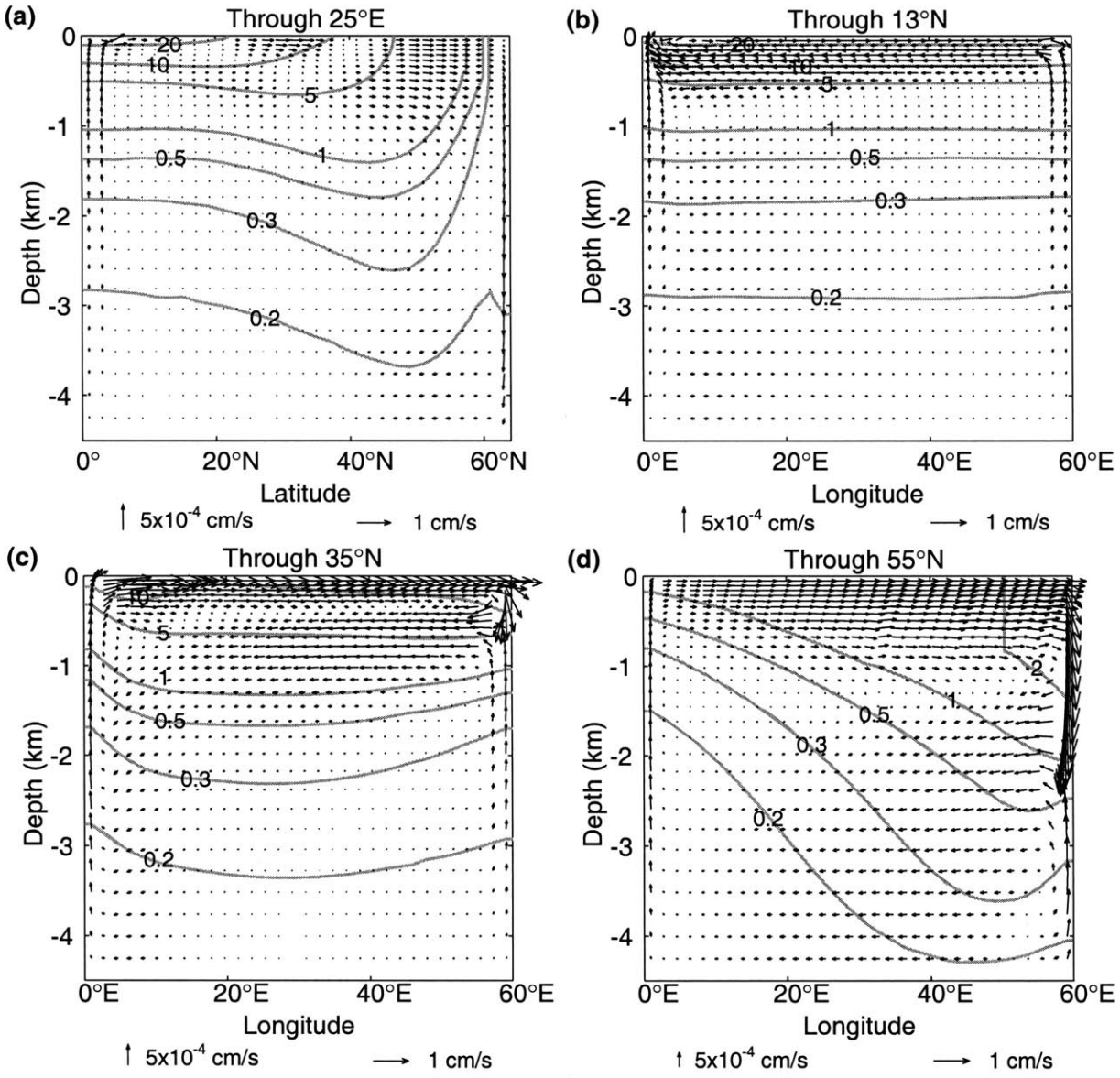

FIGURE 3.3: Two-column boundary mixing run, $\kappa = 5 \times 10^{-4}$ m^{2}s^{-1}. (a) Temperature and flow along the meridional plane through 25°E; (b) temperature and flow along the zonal plane through 13°N; (c) temperature and flow along the zonal plane through 35°N; (d) temperature and flow along the zonal plane through 55°N.

meridional-vertical plane. In low latitudes, there are two columns of strong upwelling at both the eastern and western boundaries (Fig. 3.3b). This result is consistent with Colin de Verdière (1988), who diagnosed that the primary balance in low latitudes was between diffusive heating and cold upwelling. Similarly, Samelson (1998) observed strong upwelling in low latitudes along the eastern boundary, where his mixing was concentrated. Although some upwelling is evident in two columns at the boundaries at mid-latitudes (Fig. 3.3c), the magnitude is much larger in the columns directly adjacent to the boundary. At high latitudes,

nearly all upwelling in the west occurs adjacent to the boundary, as shown in Fig. 3.3d; in the east, some upwelling is apparent in both columns, although there is a large disparity in the velocities, as in the mid-latitude section. These results suggest that the mixing at low latitudes, in effect, drives local upwelling through vertical advective-diffusive balance. At middle and high latitudes, where stratification is generally weak, a large percentage of the vertical flow at the east-west boundaries is the result of mass convergence and subsequently a component of the vertical flow is oriented along isopycnals.

3.2.2 Low Latitude Mixing; Mid-Basin Mixing

Motivated by these results, we wish to examine whether mid- and high-latitude mixing plays any significant role in the dynamics of the MOC. Fig. 3.4a shows the meridional overturning streamfunction given boundary mixing from the equator to 36°N, with no diapycnal mixing to the north. As compared with the control run (Fig. 3.2a), the center of the overturning cell is several hundred meters higher in the water column, but there are no apparent differences in the zonally averaged temperature profile and the difference in overturning maximum is only 0.3 Sv. In addition, there are only slight differences in the east and west wall boundary layer flows in mid- and high-latitudes (not shown).

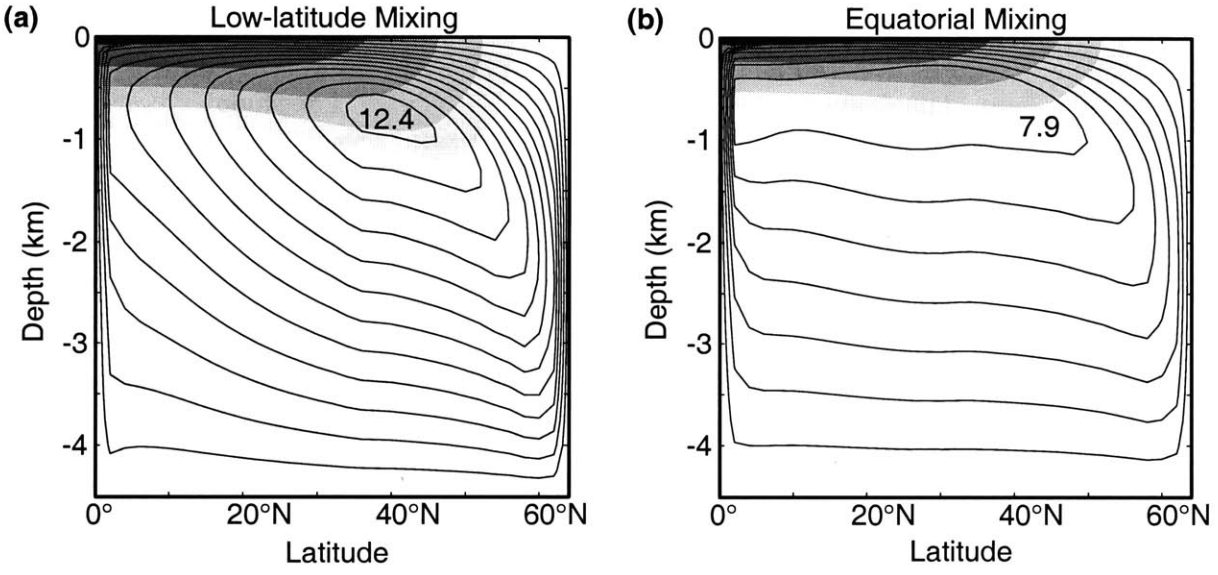

FIGURE 3.4: Meridional overturning streamfunction (contours) and zonally averaged temperature (shading) for (a) low-latitude boundary mixing run, $\kappa = 10 \times 10^{-4}$ m^{2}s^{-1} between 0-36° latitude, otherwise diffusivity is set to zero; and (b) equatorial mixing run, $\kappa = 10 \times 10^{-4}$ m^{2}s^{-1} between 0-2° latitude, otherwise diffusivity is set to zero.

If we further concentrate all mixing at the equator (Fig. 3.4b), the maximum in overturning drops by 38% to 7.9 Sv, as we have reduced the area of mixing from the previous low-latitude mixing experiment by 50%. Thus, the sub-tropical mixing on the east and west walls does contribute in driving the MOC. This result is consistent with significant upwelling into the thermocline along these latitudes, as suggested by the overturning pattern in runs with sub-tropical mixing, viz. Figs. 3.2a and 3.4a.

As mentioned in the introduction, the results from recent microstructure measurements suggest elevated mixing in the water column above the mid-Atlantic ridge. To this end, we ran a variation on our control run where we moved the mixing on the eastern and western boundaries to two adjacent meridional strips down the middle of the ocean, preserving the area-averaged diffusivity. This experiment produced a similar pattern of overturning as the control run (not shown). However, consistent with other runs that imposed interior mixing, the overturning cell was slightly weaker, comparable in magnitude with the uniform mixing experiment.

3.2.3 Highly Localized Mixing

The results of the previous sub-section suggest that the MOC cell depends critically on the meridional distribution of diapycnal mixing, with the zonal distribution being less crucial. In this sub-section we take these experiments to their logical extreme, localizing mixing to a single grid column, which also facilitates a more detailed examination of the dynamical significance of interior versus boundary mixing.

The diapycnal diffusivity in the "mixing column" was chosen so that the area-weighted diffusivity in latitudes 0°-36°N matched that of the control run. However, to control numerical difficulties we also added a background diffusivity of 0.1×10^{-4} m^2s^{-1}, the value typically assumed for the "pelagic diffusivity" (MW98). In a run with uniform diffusivity set at this background value, the overturning streamfunction maximum is 2.3 Sv, considerably weaker than that observed in this set of experiments. We equilibrated runs with the mixing column at three zonal locations—the western boundary, at mid-basin, and at the eastern boundary—and at latitudes ranging from 2°N to 50°N.

Fig. 3.5 shows the maximum in overturning streamfunction for the three series as a function of the mixing column latitude. As the mixing location moves further north, the MOC de-

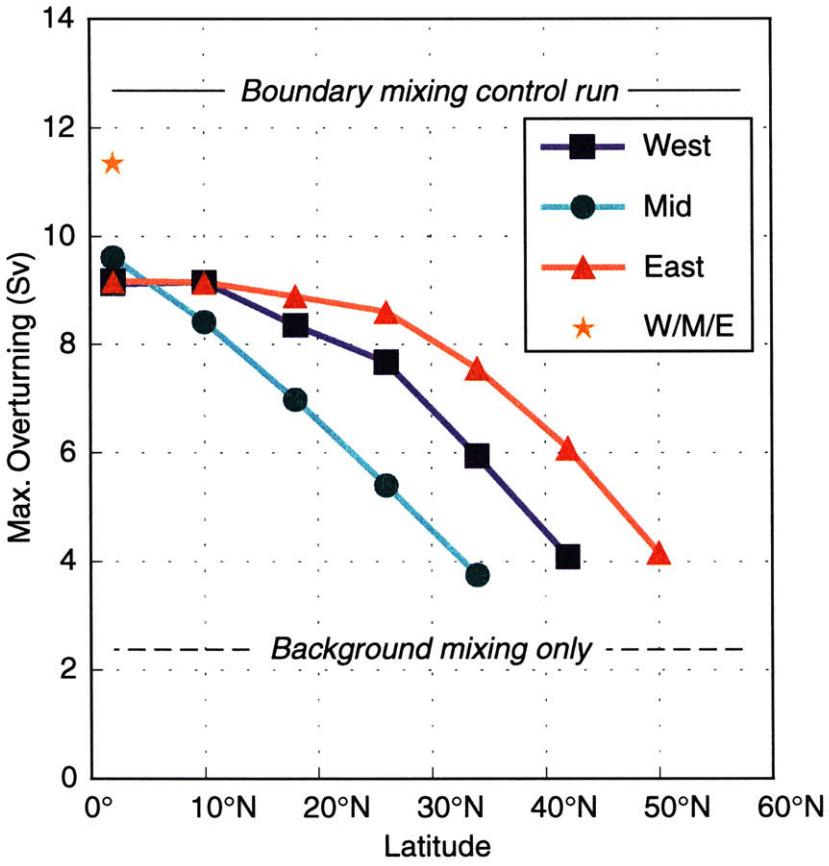

FIGURE 3.5: Maximum in overturning streamfunction for highly localized mixing experiments. The abscissa reflects the meridional location of the mixing column with $\kappa = 160 \times 10^{-4}$ $m^2 s^{-1}$, otherwise the diffusivity is set to a background value of $\kappa = 0.1 \times 10^{-4}$ $m^2 s^{-1}$ (these runs were done using 3.75°x4° resolution). The three series show results for different zonal locations of the mixing column, i.e., adjacent to the western wall, at mid-basin, and adjacent to the eastern wall. The '★' indicates the result when mixing is equally divided into three equatorial columns at these zonal locations.

creases in intensity, most noticeably when the mixing is located in the interior. Conversely, the circulation remains strongest when the mixing is located on the eastern boundary.

Consistent with the previous results, nearly all the MOC's upwelling occurs where mixing is located. In Figs. 3.6 and 3.7b the temperature and flow for the surface and bottom layers, respectively, are shown for a mixing column that is located at 18°N along the western boundary. In this configuration, the deep western boundary current is effectively short-circuited by the upwelling at the mixing column. An examination of the surface temperature immediately suggests why all of the highly localized mixing experiments plotted in Fig. 3.5 produce weaker overturning than the control mixing run: where upwelling occurs, the surface is quite cold, approximately 10°C colder than neighboring grid points, so the diffusion of heat into the thermocline is far less efficient than in the less localized mixing runs. In the

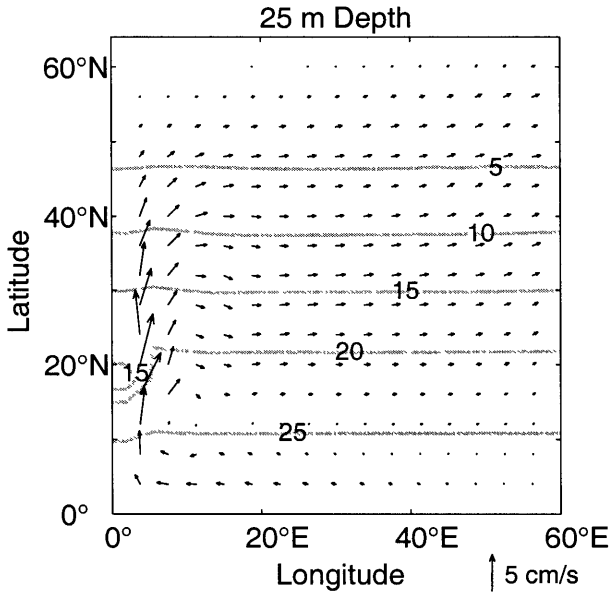

FIGURE 3.6: Plan view of the uppermost model level (25 m depth) circulation and temperature (contours), with the mixing column located along the western boundary at 18°N. Velocity scale is shown for reference.

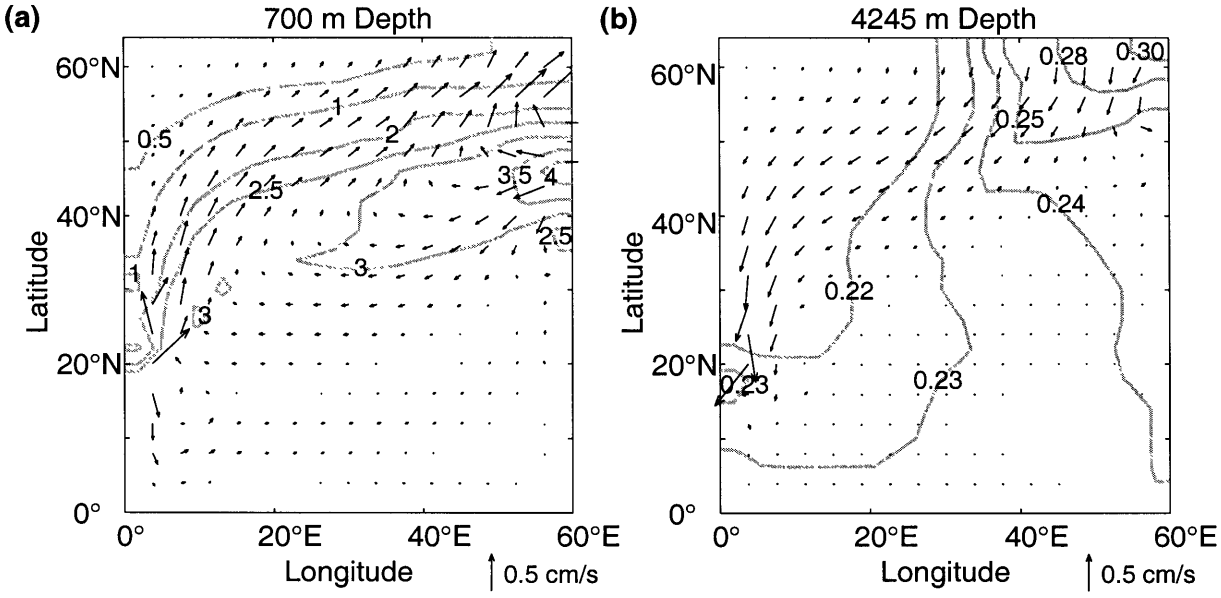

FIGURE 3.7: Plan view of the circulation and temperature (contours) with the mixing column located along the western boundary at 18°N. (a) thermocline level (700 m depth); (b) lowest model level (4245 m depth).

mid-basin, equatorial mixing run the surface anomaly in temperature is about 1°C less than when the mixing is at the equatorial western or eastern boundary, consistent with its slightly stronger overturning circulation. We ran two additional experiments to further test whether a direct link exists between overturning strength and the realized surface temperature at the

mixing location(s). First, we divided the mixing evenly between three equatorial columns located at the west, east, and mid-basin. As indicated by the '★' on Fig. 3.5, the overturning circulation was 2 Sv stronger, consistent with the steady-state temperature at these three points being much closer to the restoring profile than in the single column mixing runs. Second, we changed the surface restoring time constant from 30 days to 2 days. With the mixing column located in the southwest corner, the circulation increased to match that of the control run (but since the mixing column experiments employ weak background mixing, we caution that the nearly exact agreement is not quite as "clean" as this result might suggest).

As the mixing column moves north, the surface restoring temperature decreases, providing a simple explanation for the noted decrease in overturning strength. The streamfunction maximum in the eastern and western localized mixing runs falls off more slowly than temperature, consistent with analytical and model scaling results that suggest a power law dependence of less than one (Welander 1971; Huang 1999). Yet, this decrease in temperature does not provide a complete explanation of the results shown in Fig. 3.5, as the overturning actually decreases *more rapidly* than temperature for the mid-basin runs. There is also a disparity between the eastern and western series that increases as a function of latitude, suggesting that important dynamical differences in the large-scale overturning occur as a function of the zonal location of mixing.

From simple thermal wind considerations one might expect diffusive warming on the eastern boundary to support a strong MOC, whereas it is not clear how warming on the western boundary can support even a weak MOC. In reality, the dynamics are more complicated than suggested by this argument. Assuming that low-latitude diffusive heating leads to warming of waters in the thermocline, irrespective of whether mixing occurs on the east or west (the assumption that advective-diffusive balance sets the low-latitude stratification will be addressed in the next section), a meridional temperature gradient exists at high-latitudes in concert with strong zonal flow and subsequent downwelling on the eastern boundary. This downwelling is the main mechanism that warms the eastern boundary, thus helping to provide the shear necessary for the MOC. Note that the high-latitude flow and temperature structure is similar in the thermocline whether mixing is on the west (Fig. 3.7a), east (Fig. 3.8a), or mid-basin (Fig. 3.9a).

Instead, it is at lower latitudes where the distinction between the eastern and western localized mixing runs is more apparent. Notice, first, that the MOC is confined to the north of the mixing latitude. When mixing occurs on the eastern wall, the deep western boundary current

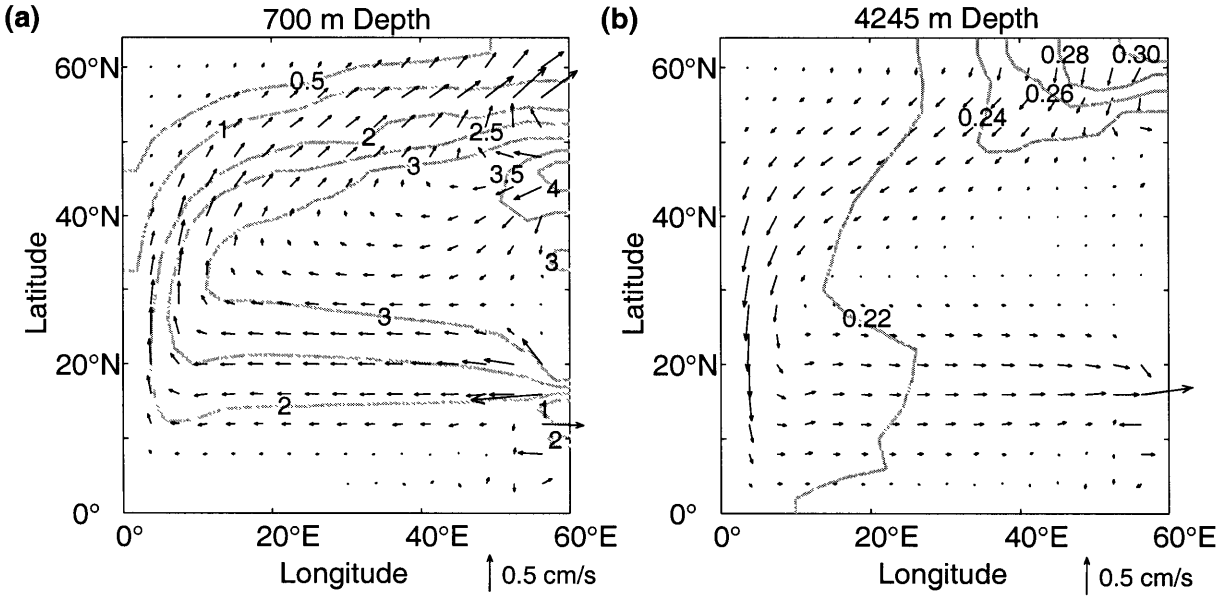

FIGURE 3.8: Plan view of the circulation and temperature (contours) with the mixing column located along the eastern boundary at 18°N. (a) thermocline level (700 m depth); (b) lowest model level (4245 m depth).

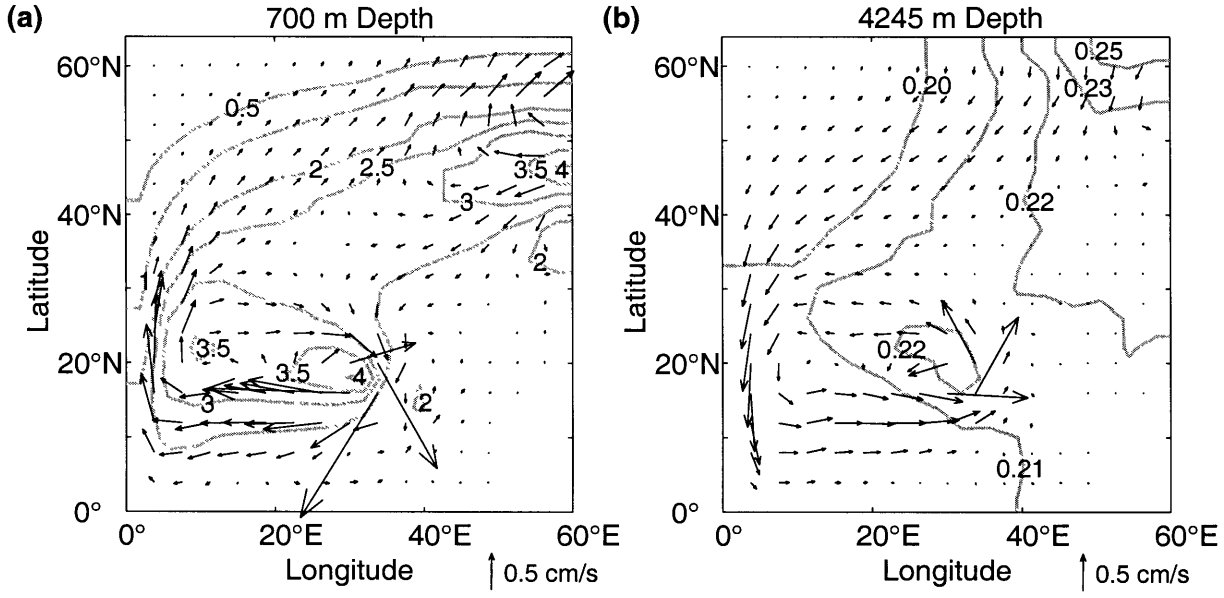

FIGURE 3.9: Plan view of the circulation and temperature (contours) with the mixing column located at mid-basin (32°E) and 18°N. (a) thermocline level (700 m depth); (b) lowest model level (4245 m depth).

turns and flows eastward across the basin (Fig. 3.8b) at the latitude of the mixing column. The low-level convergence into the eastern boundary causes upwelling from the abyss and divergence in the thermocline, producing opposite (westward) flow across the basin (Fig. 3.8a). In order to support this flow geostrophically, it must be colder in the tropics, as

this depth is above the level of no motion. It must remain warm northward of the mixing latitude, or else geostrophic eastward flow would occur; note the large tongue of water greater than 3°C.

In contrast, when mixing occurs only at the western boundary, significant zonal flow does not occur at low latitudes (Fig. 3.7a[8]). At this depth the temperature in the tropics is a full degree higher than with localized eastern mixing, yielding the result that the tropical thermocline is actually deeper in the run with smaller overturning. This may seem surprising, as it has long been assumed that the meridional overturning scales as the thermocline depth (Welander 1971), but the caveat here is that the overturning does not extend to these tropical latitudes.

Building on these differences, we now address why the aforementioned disparity in the eastern and western mixing series increases with mixing latitude. As the mixing column moves northward and f increases, geostrophic effects become more pronounced. With mixing on the western boundary, it becomes increasingly difficult for geostrophic currents to advect the diffusive warming over to the eastern boundary at mid-latitudes. Conversely, as mixing on the eastern boundary moves northward it approaches the site of warm water injection, forming a cohesive warm anomaly which supports the dominant circulation—an anticyclonic gyre above a deep cyclonic gyre—even as the mixing column moves quite far to the north.

From analytical considerations one might expect the dynamical behavior exhibited by the interior localized mixing runs to be different yet again from the boundary mixing runs. Assuming a geostrophic ocean interior, the planetary geostrophic vorticity equation

$$\beta v = f \frac{\partial w}{\partial z} \tag{3.1}$$

implies that any deep convergence (producing upwelling and hence vortex stretching) must be balanced by northward meridional flow into a latitude of higher planetary vorticity. Similarly, any lateral divergence in the thermocline must be balanced by southward flow. As the results in this section suggest, both the strength of local diapycnal upwelling and the me-

[8]A careful observer will notice the wave-like pattern in Fig. 7a along the western boundary to the north of the mixing latitude. To a lesser extent, the same behavior is present to the south of the mixing latitude when the mixing is located on the east (as shown in Fig. 8a). Since this behavior does not affect the conclusions presented here, we did not investigate further whether we were in fact observing stationary Rossby waves or spurious "wiggles" related to contrast between the intense local and weak background diffusivities.

ridional profile of upwelling are a function of diapycnal mixing. As the latter implies something about meridional velocity, a map of mixing seemingly provides quantities on both sides of (3.1); consequently, the meridional velocity which satisfies the vorticity constraint will in general not match the velocity suggested by the upwelling requirements (see Spall 2000 for an analytical treatment of the geostrophic circulation induced by imposed interior vertical flow). For example, uniform upwelling produces a horizontal recirculation that is equal in magnitude to the upwelling mass flux, as noted in Stommel and Arons (1960). It is a simple exercise to show that upwelling must decrease with latitude as β, i.e., as $\cos(\theta)$, in order to eliminate this recirculation. At the boundaries, however, frictional effects become dominant in the vorticity budget, whether the lateral boundary parameterization is no-slip or free-slip (Spall 2000). Hence, upwelling can occur when flow impinges on boundaries without concomitant meridional velocity or horizontal recirculation of flow.

When mixing is highly localized in the ocean interior, the magnitude of $\partial w/\partial z$ is quite large, producing a strong recirculation in both the abyss and in the thermocline, as shown in Figs. 3.9b and 3.9a, respectively (see Pedlosky 1996, pp. 405-409, for an analytical treatment of a localized abyssal sink). Note that at both depths, the recirculation is associated with a warm anomaly extending westward from the mixing column. In the thermocline, vortex compression produces a recirculation of opposite sense as the flow at depth, consistent with anomalous warmth above the level of no motion. In order to support the upper level recirculation geostrophically, some of the diffusive heat flux is "trapped" between the mixing column and the western wall. The westward propagation of the anomaly is due to the β-effect, the dynamics of which are described in Stommel (1982) for a geothermally driven warm anomaly. Notice that the anomaly is not advected to the east wall, where it could instead support the MOC. The magnitude of the warm anomaly is to some degree controlled by the upwelling strength; weak upwelling allows for a more intense warm anomaly, which in turn is able to satisfy the geostrophic vorticity constraint. As the mixing column moves further north, f/β increases monotonically, thus requiring a larger recirculation which is in turn balanced through an increase in the magnitude of the warm anomaly (via weaker upwelling). As such, the mid-basin mixing series plotted in Fig. 3.5 decreases rather sharply with mixing latitude.

The maximum in meridional heat flux also decreases sharply as the mixing column moves northward (not shown), as might be expected given the decrease in overturning strength. However, there is less disparity in the three series as compared to that shown in Fig. 3.5. Although the overturning is weaker with mid-basin mixing, a small "eddy" contribution to

the meridional heat flux (i.e., due to deviations from the zonal mean) is positive at the latitude of maximum flux, whereas the contribution is negative for both other series, particularly with mixing located on the eastern boundary. We also note that the latitude of maximum meridional heat flux, approximately 20°N for our standard boundary mixing run, moves to the north if the mixing column is moved northward of this location. Hence, the shape of the zonally averaged profile of surface heat exchange is altered when mixing is located only in mid- or high latitudes [this contrasts with the results presented in chapter 5, where the magnitudes of (boundary) diapycnal mixing and the imposed equator-to-pole temperature are varied, resulting in little change in the profile shape].

To close this section, we return to our comparison of the boundary mixing control run with the uniform mixing run. As with localized interior mixing, uniform mixing leads to horizontal recirculation (as evidenced by stronger western boundary currents) supported by a warm anomaly (or, equivalently, less anomalous cooling) on the western side of the basin interior, consistent with the reduction in overturning maximum.

3.3 Depth-Dependent Mixing

3.3.1 Advective-Diffusive Balance and Stratification

It has long been assumed that advective-diffusive balance plays an important role in setting the stratification of the ocean. Although wind also plays a role in determining the density structure in the thermocline (Luyten et al. 1983), its effects are not included in model runs here, so we may assume that advective-diffusive balance applies equally well in the thermocline as at depth in our model results. Through application of the spatially averaged advective-diffusive equation,

$$w\frac{d\rho}{dz} = \frac{d}{dz}\left(\kappa\frac{d\rho}{dz}\right) \tag{3.2}$$

MW98 found that a reasonable fit with the observed abyssal density structure could be obtained by assuming constant w while allowing κ to vary with depth. They further argue that horizontal advection acts as an agent of lateral homogenization, in effect spreading the resultant stratification at locally intense mixing sites into more weakly mixed areas (see also Samelson 1998).

Our question is as follows: Can this procedure be used to explain the stratification observed in the model results? For our purposes, the results are the same whether we apply (3.2) pointwise or as a spatial average, since in our control run κ is either zero (producing no upwelling) or the prescribed boundary value. Since here κ is not a function of depth, (3.2) can be readily solved to yield:

$$\rho'(z) = \rho'(0)e^{\alpha z} \tag{3.3}$$

$$\rho(z) = \rho(0) + \frac{\rho'(0)}{\alpha}\left(e^{\alpha z} - 1\right) \tag{3.4}$$

where $\alpha = w/\kappa$. Plugging the density at the bottom boundary into (3.4) yields:

$$\rho(-H) = \rho(0) + \frac{\rho'(0)}{\alpha}\left(e^{-\alpha H} - 1\right) \tag{3.5}$$

If we assume several e-folding depths from the ocean surface to depth so as to neglect the exponential term in (3.5), (3.4) can be re-written as:

$$\rho(z) - \rho(-H) \approx \frac{\rho'(0)}{\alpha} e^{\alpha z} \tag{3.6}$$

Fig. 3.10a shows a comparison of $T(z) - T(-H)$ with $\partial T/\partial z$ as measured at the western equatorial boundary (the behavior is qualitatively similar throughout the tropics). According to (3.3) and (3.6), both curves should be linear, with similar slope, when plotted on a logarithmic scale. Only in the upper 1500 meters does this appear to be true.

The lack of agreement between the model's observed and expected temperature structure from (3.3) at depth is explained by examining $w(z)$ at the equator, as plotted in Fig. 3.10b. Upwelling increases quasi-linearly from the abyss into the thermocline before abruptly falling off in the top few hundred meters. The aforementioned agreement in the thermocline is attributed to the fact that over much of the thermocline, the variation of w is small, roughly between $3 - 3.5 \times 10^{-6}\,\mathrm{ms}^{-1}$. Returning to the question of how well (2) explains the model's observed stratification, we plug the model's $w(z)$ into a numerical one-dimensional advective-diffusive equation solver, using the surface and bottom temperatures as boundary conditions. The resulting solution is nearly an exact match with the model's temperature profile. In other words, horizontal advection (i.e., due to sloping isopycnals) does not play any sig-

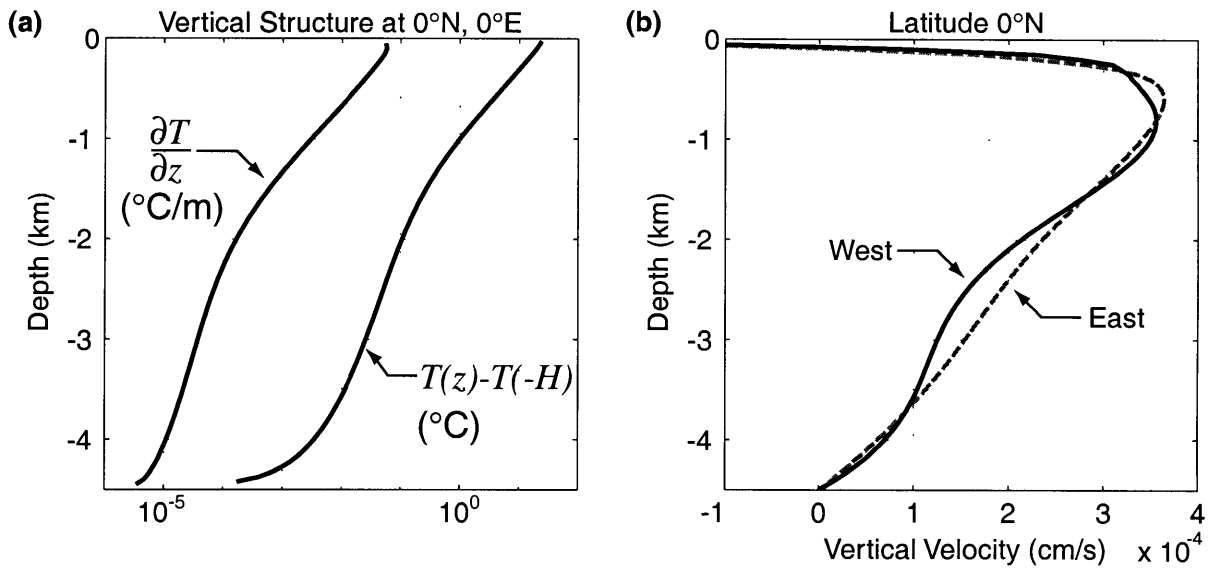

FIGURE 3.10: (a) Vertical potential temperature structure in low-latitudes along the boundary, as exemplified by this plot of $T(z)-T(-H)$ and $\partial T/\partial z$ at 0°E, 0°N. (b) Vertical velocity adjacent to the equatorial boundary, as shown for the westmost and eastmost gridpoints.

nificant role in setting stratification, except at the bottom boundary where $w(z)$ vanishes (MW98 note that their analysis should in theory be carried out in isopycnal coordinates; however, given that our model is essentially forced by density, and there is no effect from isopycnal advection of density, one would expect exact agreement between the model and the one-dimensional result in this coordinate system).

3.3.2. Mixing Below the Thermocline

The results of this simple analysis lend credence to studies that assume exponential decay of density in the thermocline (e.g. M97), but at the same time beg the question of what controls the vertical profile of upwelling at depth. To address this, and the broader question of the effect of deep mixing on the MOC, we performed three additional runs: a weak thermocline mixing case, with our standard boundary mixing below 1000 meters and exponentially decaying boundary diffusivity toward the surface; a weak deep mixing case, retaining the standard boundary mixing in the top 1000 meters but exponentially decreasing the boundary diffusivity below; and a strong deep mixing case where the boundary mixing is exponentially increased below 1000 meters. These vertical profiles are illustrated in Fig. 3.11. Note that our choice of 1000 meters for the thermocline depth was determined a posteriori, based on results from the control experiment.

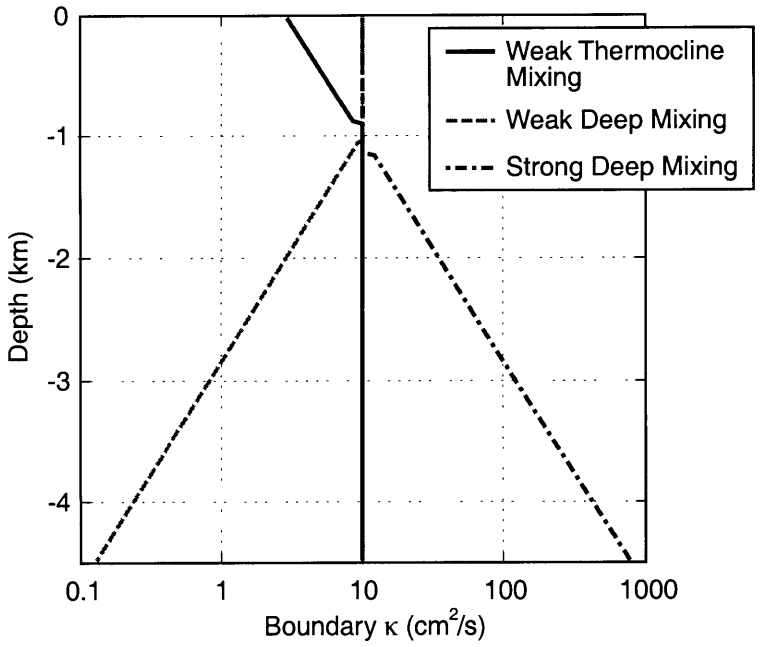

FIGURE 3.11: Vertical profile of boundary diapycnal diffusivity for weak thermocline mixing, weak deep mixing, and strong deep mixing experiments.

When mixing is decreased in the thermocline, the thermocline depth decreases and the maximum in overturning strength is reduced to 7.0 Sv. The model's meridional heat flux is also considerably weaker. This result is consistent with thermodynamic considerations and is not discussed further.

The overturning streamfunction for the weak deep mixing case is shown in Fig. 3.12a. The maximum in overturning strength decreases by only 0.2 Sv as compared with the control run (Fig. 2a), and there is no apparent change in the zonally averaged thermocline. However, upwelling at depth along the equator is much weaker, so that upwelling through the abyss is more evenly distributed meridionally rather than concentrated where mixing (albeit weak) is parameterized.

In contrast, the strong deep mixing run (Fig. 3.12b) gives rise to vigorous upwelling at the equator, producing a deep secondary maximum in overturning. Approximately 3 Sv upwells near the equator at depth but subsequently downwells in the sub-tropics. In as much as the equatorial upwelling through the thermocline here is similar to that in the control and weak deep mixing runs, the overturning maximum is increased by less than 1 Sv. The maximum meridional heat transport in the three runs varies by less than 0.01 PW, again suggesting that

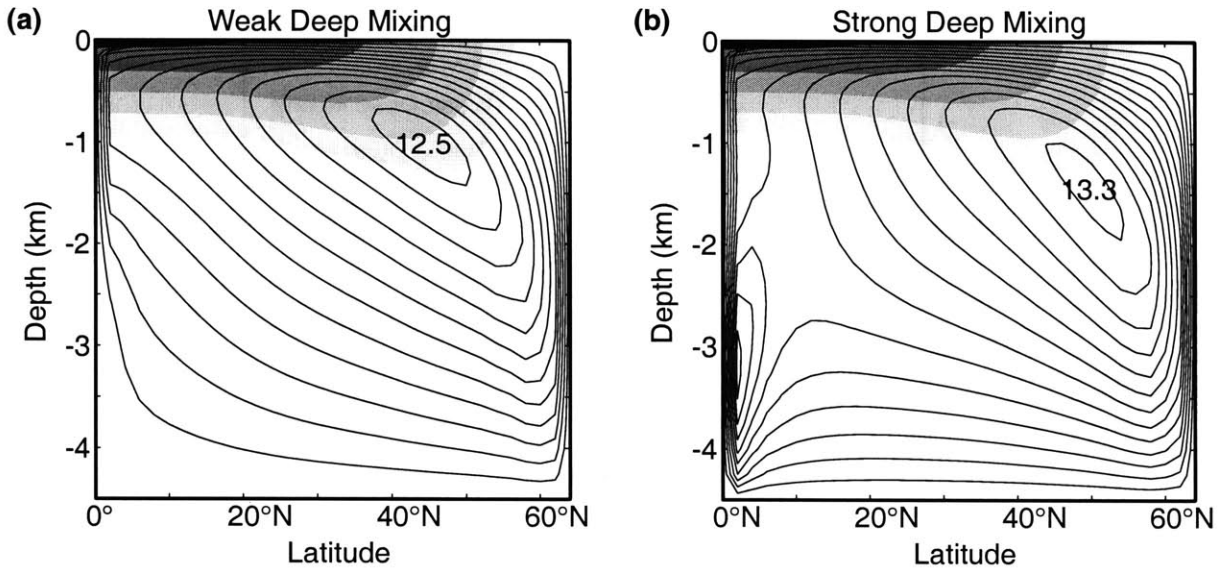

FIGURE. 3.12: Meridional overturning streamfunction (contours) and zonally averaged temperature (shading) for (a) weak deep mixing and (b) strong deep mixing runs.

any changes in the deep circulation do not affect the flow through the surface layer or thermocline.

Our strong deep mixing run is similar to those discussed in CHG, although their parameterization of vertical diffusivity as a function of N^{-1} implies increased mixing with depth within the thermocline. C91 performed several experiments with varied mixing at depth, although his profile of vertical diffusivity exhibited a rather sharp increase at the base of the thermocline, in contrast to our slow exponential increase. In both these studies, the increase in deep abyssal mixing was an order of magnitude less than that here. Despite these differences in the implementation of deep mixing, all studies concur that the meridional heat flux is not sensitive to deep mixing. In contrast with our results, however, the CHG and C91 results suggest that the maximum in overturning streamfunction can in fact be quite sensitive to deep mixing. Anticipating that this inconsistency is due to our vertical profile of $\kappa(z)$, we ran our model with sharply increased diffusivity near the base of the thermocline [i.e., similar to C91's profile, although our increase was somewhat less steep than that indicated by his Fig. 1]. In this run we found that the strength of the MOC did increase more significantly, as compared to our other runs, again with only minor change in the meridional heat flux. Nevertheless, our maximum in overturning was somewhat less sensitive to deep mixing than in CHG and C91, although we are hesitant to draw immediate conclusions from this observation and instead offer that the sensitivity is a strong function of the shape of $\kappa(z)$ and the thermo-

cline depth. Further, we note that our secondary meridional cell is much stronger than that shown in CHG's Fig. 4a, which we attribute to our boundary mixing implementation. With strong equatorial mixing the secondary cell is quite distant from the high-latitude maximum in overturning, allowing for less superposition of the deep circulation and the large-scale buoyancy-driven overturning[9].

3.3.3. Abyssal Heat Balance

In order to understand how the steady-state dynamics are affected by deep mixing, it is useful to first examine the abyssal heat budget, as illustrated in Fig. 3.13. Downwelling water in the northeast corner is relatively buoyant (Marotzke and Scott 1999), producing a warm anomaly with associated cyclonic flow in the deep ocean. Some of the flow immediately turns and upwells along the eastern boundary; as illustrated in Fig. 3.1b, the strongest upwelling occurs adjacent to downwelling, tending to cool the eastern boundary higher in the water column (note the cold anomaly between 30-40°N on the eastern boundary in Figs. 3.7a, 3.8a, and 3.9a). Most of the flow however continues westward across the basin, passing near deep convection. In these model runs deep convective mixing reaches the bottom in the north-western corner, which is relatively stagnant (and therefore cold) because the upper western boundary current separates from the "coast" between 40°N and 50°N. As discussed in Marotzke and Scott (1999), convective mixing acts as a heat sink, cooling the deep flow, and is not a source for mass flux. As the flow proceeds along the western boundary, along the equator, and at the eastern boundary, it is warmed somewhat by diffusion.

To reconcile the abyssal heat budget, first consider the signs of the relevant flux terms. In steady state, convective mixing causes a heat loss, and diffusion produces a heat gain. That leaves us with the vertical advective heat gain, which is proportional to the following expression:

$$\int wT\,dA = \int_{downwelling} w_D T_D + \int_{upwelling} w_U T_U \qquad (3.7)$$

where the U and D subscripts refer to upwelling and downwelling, respectively. This term seemingly could be positive or negative, but we suggest it must yield a heat gain (i.e.,

[9]It is also possible that their use of a Cartesian mixing scheme contributes to their sensitivity. For example, the maximum of the MOC is deeper in M97's Cartesian boundary mixing run than in our isopycnal mixing run. With a deeper maximum, more superposition with this secondary deep circulation is possible.

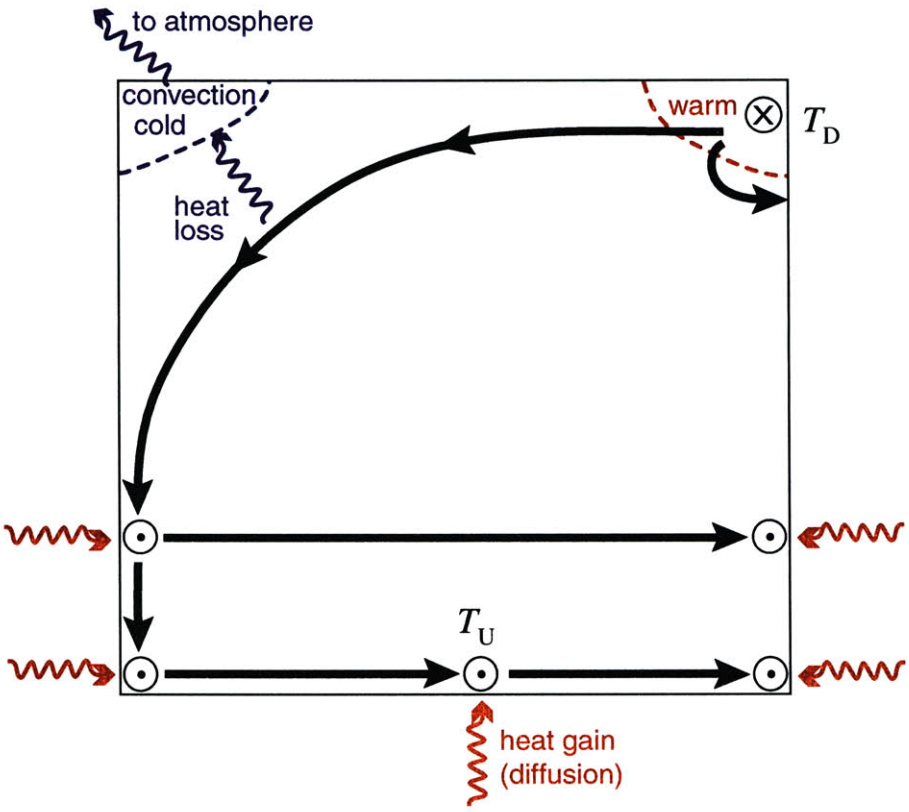

FIGURE 3.13: Illustration (plan view) of abyssal flow and heat budget. Flow downwells (as indicated by the circled '×') in the northeast corner at temperature T_D and subsequently loses heat as it flows adjacent to deep convection in the northwest. Flow then proceeds along the western boundary; some flow upwells (as indicated by the circled '•') in the western boundary, some flow reaches the equator and upwells, and some flow moves acoss the basin before upwelling in the east. Downward diffusion of heat along the boundaries is not quite balanced by upwelling so that the flow is warmed in low-latitudes, upwelling at average temperature T_U.

$T_D > T_U$, and by continuity $w_D = w_U$), unless there are other deep diabatic sources/sinks such as geothermal heating (see chapter 4). Diffusive heating occurs at low latitudes, at the tail end of the abyssal flow pathway, and therefore the system cannot effectively balance diffusive gains by convective losses. In other words, the dynamically significant balance is between the convective loss and the advective heat gain. With greater diffusive heat input, the difference $T_D - T_U$ is decreased, in order that the increased diffusive flux offsets the decreased advective flux. In short, it is this three-way balance that allows for our observed MOC insensitivity in maximum overturning.

Figs. 3.14a and Fig. 3.15a show the temperature and stratification ($\partial T/\partial z$) at the west and east sides of the equator, respectively, for the depth-dependent mixing runs. With strong

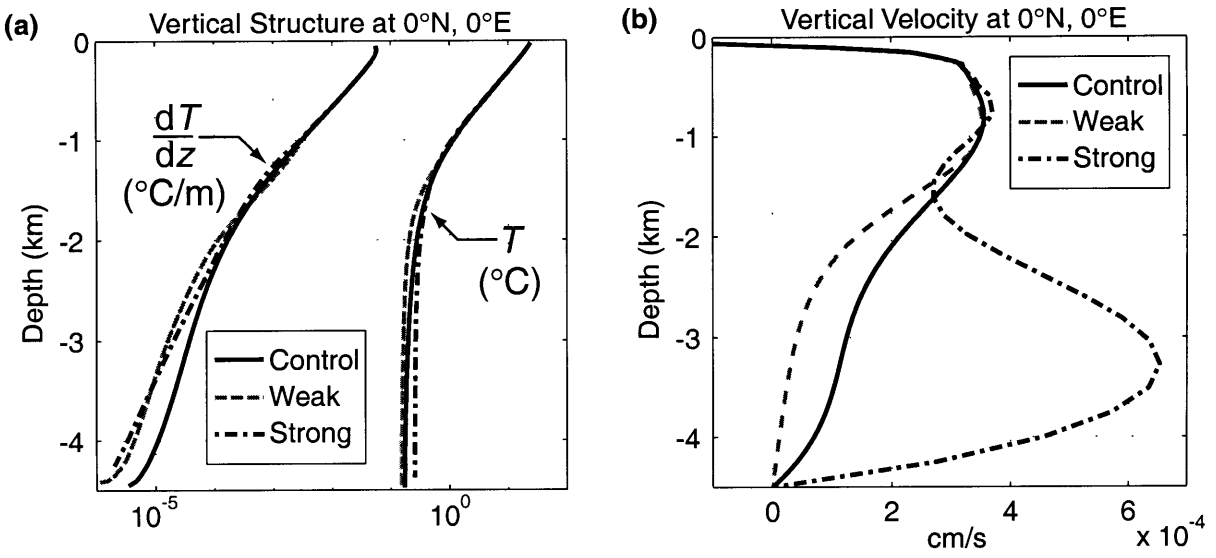

FIGURE 3.14: (a) Vertical potential temperature structure and (b) vertical velocity at the western extreme of the equator for the control boundary mixing, weak deep mixing, and strong deep mixing runs.

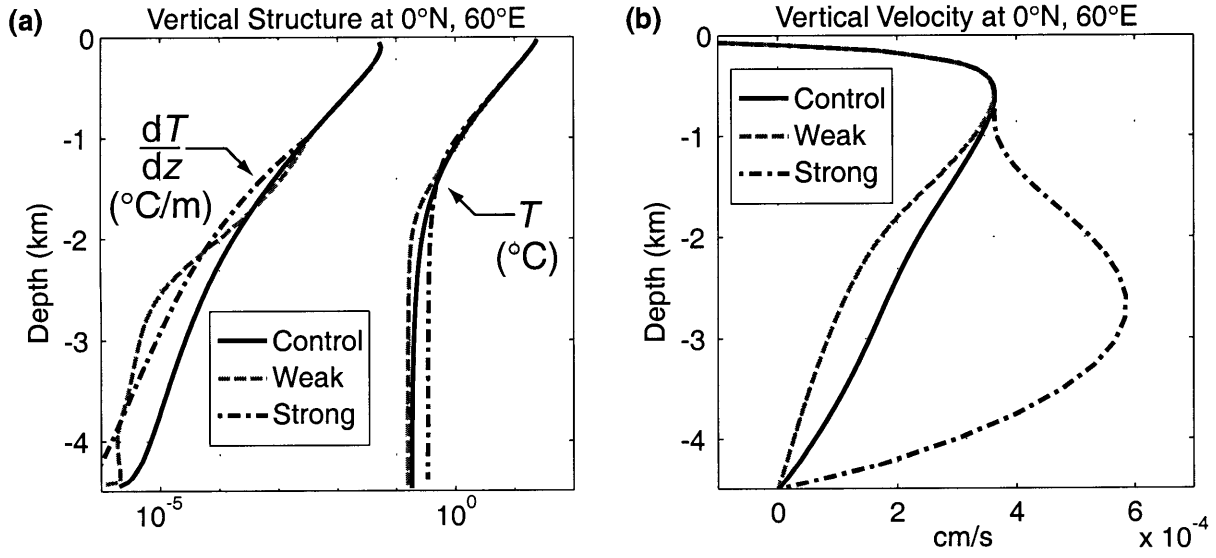

FIGURE 3.15: (a) Vertical potential temperature structure and (b) vertical velocity at the eastern extreme of the equator for the control boundary mixing, weak deep mixing, and strong deep mixing runs.

deep mixing, the bottom water is warmer, consistent with the larger diffusive heat flux to the bottom, but the downwelling water is likewise warmer (not shown). Surprisingly, the abyss is less stratified in both the weak and strong mixing cases. With weak deep mixing, less heat is diffused downward, whereas in the strong mixing case diffusion is so efficient at mixing heat that the temperature gradient is degraded. This latter result is in contrast with CHG and

C91, where stronger stratification with increased deep mixing was observed. Our aforementioned run with sharply increased diffusivity near the base of the thermocline was also more weakly stratified. However, when we scaled back the increase in deep mixing by an order of magnitude [i.e., so that area-weighted diffusivity was more similar to that in C91, increasingly six-fold beneath the thermocline], we too observed increased stratification at depth. More specifically, the deep ocean stratification doubled, although stratification in the 1000 meters below the thermocline was weaker. We speculate that some "optimum" profile of $\kappa(z)$ could lead to a maximum stratification at depth, although further research along these lines is beyond the scope of this paper.

As suggested by the plots of meridional overturning streamfunction, upwelling at the equator varies considerably between deep mixing runs (Figs. 3.14b and 3.15b). A weaker diffusive flux requires less upwelling for steady-state balance, and therefore it is no longer necessary for such a large percentage of abyssal upwelling to occur at the equator. Conversely, in the strong deep mixing case the large equatorial diffusive heat flux must be balanced by strong upwelling. Without sufficient mixing in the thermocline, however, this upwelling essentially "detrains" from the larger cell, flowing horizontally and downward away from the equator. We conclude that deep mixing affects the deep stratification and upwelling pattern, but since the water that downwells into the abyss is buoyant, as warm as the water at the base of the thermocline (see Fig. 3.1b), it does not play a role in determining the strength of the MOC.

Finally, our analysis of the abyssal heat budget suggests an explanation for some subtle differences in the behavior on the east and west for the three mixing scenarios. First, we note that the stratification in the west is less affected by the magnitude of deep mixing. Because the abyssal flow reaches the western boundary directly after convective heat loss, diffusion has had less opportunity to modify stratification. Moreover, the temperature in the northwestern corner, which is linked to the coldest surface temperature, is virtually unchanged between runs. In the east, the effect of deep mixing is much more pronounced. The ocean is virtually unstratified in the bottom 2000 meters in the weak mixing run, and stratification also falls off more sharply (as compared to the control run) in the strong mixing case. Second, any differences in the upwelling profile are consistent with thermal wind balance of the zonally averaged deep overturning circulation. More specifically, note that the western boundary upwelling in the weak deep mixing run is sharply reduced. As a result, some heat penetrates downward on the west (mixing may be weak, but is still non-zero), so the nearly unstratified eastern boundary is colder than the west throughout much of the abyss (Fig 3.16a). The resulting east-west temperature difference is such that zonally averaged

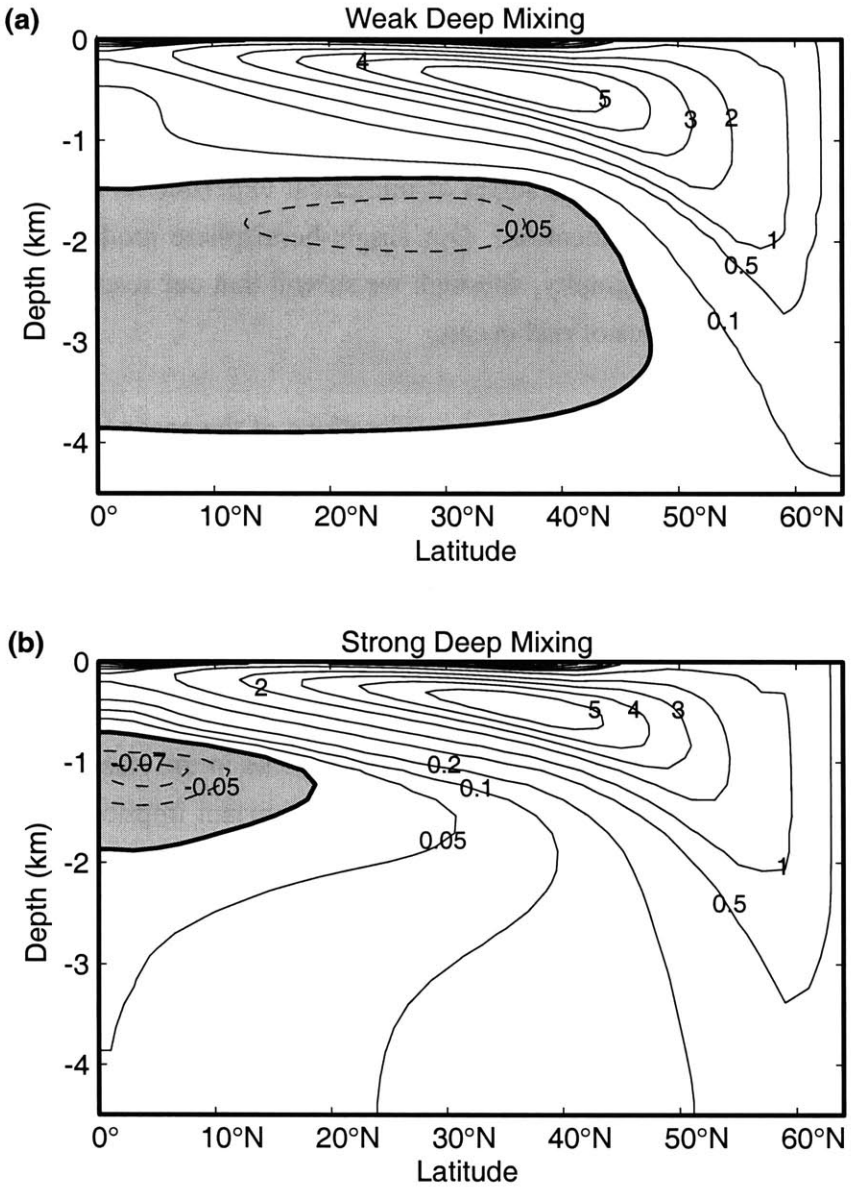

FIGURE 3.16: Potential temperature difference between the eastern and western boundary for (a) weak deep mixing and (b) strong deep mixing runs. The difference is negative in shaded areas.

southward flow increases from the bottom upward, consistent with the overturning pattern observed in Fig. 3.12a. In the strong deep mixing run, upwelling on the eastern boundary peaks higher in the water column as compared to the west, which in turn produces a dipole pattern east-west temperature difference at depth (Fig. 3.16b). The warmer eastern boundary near the bottom is necessary to support the shear required for the deep equatorial overturning cell, but the east must also be colder near the base of the thermocline in order to attenuate the northward flow associated with the top of this cell.

3.4 Summary and Discussion

In this chapter we have presented a series of numerical experiments that explore the large-scale consequences of mixing location. Our single-hemisphere model is highly idealized, lacking wind forcing and topography, although we submit that our results provide context for speculation about the dynamics of real ocean.

Our findings suggest that thermodynamic considerations of the ocean circulation, as first discussed in Sandström (1908) and Jeffreys (1925), are indeed fundamental: The strength of the MOC is a direct function of the amount of heat which diffuses into the thermocline. Greater heat penetration leads to temperature gradients at increased depth, producing zonal flows which downwell at the model's eastern boundary, which in turn effects a negative density difference between the eastern and western boundaries. Through thermal wind balance, the boundary density difference can support a vigorous MOC (Marotzke 1997). This elucidation provides justification for the advective-diffusive depth scale in the classical Welander (1971) scaling of the meridional overturning strength. One important implication is that mixing at low-latitudes, where the surface temperature is high, is more efficient at diffusing heat into the interior and hence more effective at driving the MOC.

Comparison of boundary mixing with interior mixing indicates that planetary geostrophic vorticity balance in the interior, the cornerstone of the Stommel and Arons (1960) theory for the abyssal component of the large-scale overturning circulation, actually hinders the process leading to east-west density differences which can support the MOC through thermal wind shear. Horizontal convergence at depth and divergence in the thermocline requires horizontal recirculations for vorticity balance; in order to support these recirculations geostrophically, the diffusive heat flux is to some extent trapped between the upwelling and the western boundary. With boundary mixing, where frictional effects enter the vorticity balance, heat penetration into the thermocline leads to stronger zonal flows which downwell to greater depth at the eastern boundary.

Our model results suggest that deep downwelling waters are relatively buoyant, and the base of the thermocline is established by the water mass properties of this downwelling flow. The magnitude of deep mixing does affect the bottom water temperature, which is in general some average of the water mass properties tied to deep convective mixing and the properties of the deep mass injection (Marotzke and Scott 1999; Huck et al. 1999). However, given that

the water mass properties of the deep downwelling flow match those much higher in the water column, it is not necessary to "pull" the circulation through the abyss via diffusion, and hence only thermocline mixing is necessary to generate a surface-forced large-scale overturning cell. Rather, the parameterization of mixing at depth plays a role in setting stratification and determining location and strength of diapycnal upwelling in the abyss. Mixing at depth may play a more significant role in the real ocean which is not addressed here, namely its capacity to homogenize water masses of different origin (e.g., North Atlantic Deep Water and Antarctic Bottom Water). Our results show that the deep circulation pattern induced by deep mixing (or lack thereof) is confined below the thermocline and does not transport any significant amount of heat, and therefore does not play a significant role in determining the oceanic meridional heat transport. The fact that the bottom water temperature is affected by the deep mixing has only minor impact on the meridional heat flux, in contrast with the argument put forth in Cummins et al. (1991) to explain this insensitivity. The maximum in the overturning streamfunction may be affected by deep mixing through superposition of the deep circulation with the surface-forced overturning, depending on the vertical profile of mixing in the abyss.

Our description of the abyssal heat budget, when taken with the aforementioned distinction between boundary and interior mixing, suggests that the Stommel-Arons model is at best incomplete in capturing the large-scale abyssal dynamics. Not only does the Stommel-Arons solution implicitly assume that downwelling and deep convection are co-located, its inviscid formulation can not account for upwelling through mass convergence at the boundaries. Observation evidence in favor of the Stommel-Arons model has thus far proven to be elusive (Wunsch, 1996, pp. 65-72). We suggest that for future progress in understanding the large-scale circulation and its role in the climate system, a new paradigm for the abyssal circulation is needed.

Mechanical energy is necessary to drive mixing, most likely through the actions of winds and tides (Munk and Wunsch 1998), although we have generally ignored this consideration here in the spirit of our highly idealized experiments. Dissipation of tides is thought to produce elevated mixing at depth near rough bottom topography, as implied by microstructure observations at the mid-Atlantic ridge (Polzin et al. 1997). Although this latter study also found evidence for elevated mixing in the water column above rough bottom topography, presumably through upward internal wave propagation, the measurements suggest that the mixing in the water column at thermocline depths is only slightly above background "pelagic" values. Recent microstructure measurements off Cape Hatteras indicate strong mixing at thermocline

depths (of order $10^{-2} - 10^{-4}$ m^2s^{-1}) above rough bottom topography, although of very limited spatial extent (Toole and Polzin 1999). Similar measurements in the Gulf Stream, above gently sloping terrain, suggest only slightly elevated levels of mixing. To date, significant areas of elevated mixing in the thermocline have not been located (see Gregg 1987 for a review of thermocline mixing). If found, these sites could contribute to the $O(10^{-4}$ $m^2s^{-1})$ spatially averaged diffusivity typically employed in ocean general circulation models to obtain realistic North Atlantic deep-water production.

Other limitations of our idealized configuration that merit further study include effects from more realistic boundaries. Our boundary mixing is parameterized in vertical columns many kilometers wide, which provides an equal area of mixing at all depths. In the real ocean, the boundaries are more horizontal than vertical, and mixing likely occurs over a significantly reduced length scale normal to the boundary. Moreover, the effect of diapycnal mixing on sloping boundary has been shown to have dynamical consequences (Garrett 1991; Thompson and Johnson 1996), which may influence the large-scale circulation. The presence of sloping boundaries at high latitudes affects the volume of deep mass transport by requiring deep convection to occur in the open ocean (Spall and Pickart 2000), which may alter our depiction of the abyssal heat balance.

In part due to the lack of observed thermocline mixing, other ideas regarding the importance of the Southern Hemisphere in driving North Atlantic Deep Water production have recently been gaining favor. One possibility is that the winds over the Antarctic Circumpolar Channel (ACC) lead to enhanced mixing there, as discussed in Wunsch (1998). Using a general circulation model of an idealized ocean basin, Marotzke and Klinger (2000) found increased cross-equatorial transport with enhanced mixing in the Southern Hemisphere, consistent with our results that show upwelling occurs where mixing is located. However, if mixing is concentrated in the latitude band of the ACC, our model results suggest that this would not be effective in driving a strong MOC, as the cool surface temperatures would lead to weak diffusive heat flux penetrating into the thermocline.

A second variation on the role of the Southern Ocean is that the wind stress over the ACC produces a "Drake Passage effect" whereby these winds induce northward Ekman transport which can only return southward geostrophically below the sill of the Drake Passage, hence requiring its transformation into North Atlantic Deep Water (Toggweiler and Samuels 1993). The flow is subsequently returned to the surface though Ekman suction in the Drake Passage. In coarse resolution general circulation models, a nearly linearly relation between northern

deep-water production and Southern Hemisphere winds has been observed (McDermott 1996), perhaps obviating the need for any significant sources of mixing in order to produce a vigorous overturning circulation (Toggweiler and Samuels 1998). Again, we caution the direct applicability of our idealized model to the real ocean, in as much as we do not have any wind-induced upwelling, nor does our model do justice when it comes to representing the complexity of the oceans' water mass properties. Although model results show that the presence of the channel can lead to increased thermocline depth (e.g., Gill and Bryan, 1971), the thermodynamic considerations we have examined suggest that it must be investigated *how* this mechanism leads to the east-west temperature differences necessary to support a pole-to-pole overturning cell in thermal wind balance.

Chapter 4

The Effect of Geothermal Heating

4.1 Introduction

As the interior of our planet slowly cools over geologic time, heat is lost through the lithosphere. Approximately 70% of this heat flux is absorbed into the abyssal oceans and marginal basins (Sclater et al. 1980). Prior work has argued that both local hotspots (forming rising plumes) along the mid-ocean ridge axes (e.g. Stommel 1982) and the more pervasive diffusive heating away from the ridge systems (e.g. Thompson and Johnson 1996) play important roles in the abyssal circulation. Nonetheless, to the best of our knowledge geothermal heating at the ocean bottom has been omitted from all previously published ocean general circulation model results [the only exception is our own companion study using a global ocean model, Adcroft et al. (2000)]. In this chapter, we rectify this situation by examining the impact of geothermal heating in the context of an idealized ocean's large-scale overturning circulation.

To begin, let us compare the estimated 32 TW (1 TW = 10^{12} watts) of geothermal heating through the ocean floor (Stein et al. 1995) with other important energy fluxes in the climate system. The meridional oceanic heat flux is approximately 2000 TW (Macdonald and Wunsch 1996) and the solar flux of energy at the ocean surface is greater still by an order of magnitude. Presumably, the contrast between these numbers underpins modelers' justification for the omission of the geothermal flux. However, as first noted by Sandström (1908), the net heating of the oceans occurs in the tropics, at higher geopotential, and is therefore unable to directly drive a strong large-scale overturning circulation. More recently, Huang (1999) used a simple tube model of the ocean circulation to suggest that surface heating can produce a weak circulation that is rate-limited by diffusive mixing, as first suggested by Jef-

freys (1925), whereas deep heating can produce a very strong circulation, rate-limited by friction. Thus, it is not clear *a priori* that even a weak geothermal energy flux is necessarily negligible. By area-integrating the geothermal buoyancy flux times the depth of the ocean floor, one can estimate the generation of potential energy by geothermal heating (Huang 1999). This calculation suggests that only a small fraction of the heating, about 0.05 TW, results in potential energy generation. However, the energy available for mixing in the open ocean is also quite small; wind and tidal dissipation both contribute about 1 TW (Munk and Wunsch 1999; Wunsch 1998), although it is less certain to what extent these mechanical sources are converted to potential energy. Given our limited understanding of the energetics of the large-scale circulation, it is unclear whether the increase in potential energy due to geothermal heating is significant and/or should lead to a measurable increase in the kinetic energy.

Until recently, nearly all attention has focused on the dynamics of plumes at mid-ocean ridges. Hydrothermal venting at high temperatures (roughly 350 °C) can produce steady-state plumes or transient thermals, also known as "megaplumes" or event plumes. A typical black smoker can release 60 megawatts, whereas event plumes are thought to produce a heat flux several orders of magnitude greater (Lupton 1995). These local sources entrain surrounding waters as they rise to a level of neutral buoyancy, or spreading level. The amount of entrained water is not negligible, owing to the disparity between the ambient and venting water temperatures; Kadko (1995) estimated that the total vertical transport may be as large as 12 Sv, i.e., the same order of magnitude as the meridional overturning circulation. The influence of rotation causes entraining fluid to circulate cyclonically, whereas the flow is anti-cyclonic in the spreading phase [see Helfrich and Speer (1995) for a review of hydrothermal convective plume growth]. In the absence of background flow, the β-effect would propagate tracers and temperature perturbations westward (Stommel 1982). Evidence of this westward propagation has been observed at depth (Lupton and Craig 1981). Joyce and Speer (1987) showed that if a background Stommel and Arons (1960) abyssal flow is included (directed north and eastward), characteristics originating from a plume may tend westward or eastward, depending on the ratio of the background flow velocity to the long baroclinic Rossby wave phase speed [see also Speer (1989)].

Although less remarkable for their local dynamical effect, low temperature venting occurs at both mid-ocean ridge axes and along ridge flanks. Ocean crust that is older than about 50-70 million years does not produce significant hydrothermal circulations (Stein et al. 1995), yet continued cooling and radiogenic decay maintain a background heat flux of 38 to 46 mW m^{-2}

(Sclater et al. 1980). What is perhaps most notable from a thermodynamic perspective is the division of heat flux into the ocean. Stein et al. (1995) estimated 34 ± 12% is released through hydrothermal heat flux, and of this only 29% occurs directly along the ridge axes. Murton et al. (1999) suggested that the heat flux through high temperature venting might be as low as 1% of the total flux. Joyce et al. (1986) employed a scaling argument to show that the weak background heat flux has a negligible effect on the local potential vorticity balance. However, in this chapter we will consider the non-local effect of the background heating through the ocean floor, which we will show has a measurable effect on the abyssal circulation.

In keeping with the exploratory nature of this thesis, geothermal heating is represented by a uniform heat flux of 50 mW m^{-2} through the ocean floor (unless otherwise specified). We did not parameterize any hydrothermally generated salinity flux through the bottom boundary. All experiments with geothermal heating were spun up from a similarly configured steady-state run without applied geothermal heating. For computational purposes the model is coarsely resolved and thus can not resolve dynamically active convective plumes. In our model runs we will assume that diapycnal mixing rates are determined through a prescribed diffusivity, investigating the role of deep heating rather than the likelihood that geothermal heating leads to measurable deep mixing (the latter being a more difficult problem, in our opinion).

We begin this chapter with a perturbation analysis of the flow and temperature structure that results from geothermal heating. A dynamical interpretation of these results is provided. The sensitivity of these results to different model forcings is then examined, including several experiments in a double-hemisphere ocean basin (in this configuration, the northern and southern basins are identical; also, we no longer prescribe diapycnal mixing all along the equator, just along the four sidewalls). We conclude with some thoughts on how these results might apply to both a more realistic ocean model and the real ocean. The material in this chapter closely follows that presented in Scott et al. (2000).

4.2 Single Hemisphere Geothermal Heating

4.2.1 Preliminaries

Before proceeding to the model results, consider the ramifications of a simple uniform diffusive response to the geothermal heating. In steady-state balance, the extra heat input through the bottom boundary must eventually be released to the atmosphere through the surface boundary condition. Given our surface restoring timescale of 30 days[10] and a mixed layer depth of 50 meters, a sea surface temperature increase of only 0.006 °C is required to "radiate" away an additional 50 mW m^{-2}. The vertical temperature structure in this diffusive model can be deduced by balancing the additional deep heat input with the diffusion of an anomalous temperature gradient

$$\rho_o c_p \kappa \partial_z T' \quad \sim \quad \rho_o c_p \kappa \Delta T'/H \quad = \quad 50 \text{ mW m}^{-2} \tag{4.1}$$

We find that for an ocean depth H of 4500 meters, the top to bottom anomalous temperature difference is 0.5 °C (assuming $\kappa = 1.15 \times 10^{-4}$ $m^2 s^{-1}$, our area-averaged vertical diffusivity). Our calculation of T' at the surface implies that virtually all of this temperature difference occurs in the abyss. In other words, the presence of geothermal heating leads to a lowest order change in the oceans' deep water properties! In light of this simple calculation, it is somewhat surprising that the effect of geothermal heating has not received more attention. An important caveat, however, is that this analysis presumes that a purely diffusive response is dynamically possible; on a rapidly rotating planet, even small changes in the temperature structure produce an advective response through geostrophic balance.

In the other extreme, the additional geothermal heat flux could be lost through a purely advective response, i.e., through an increase in anomalous vertical velocity (w') in the model's surface layer. To get an order of magnitude estimate of this advective response, we will assume a prescribed sea surface temperature. In the zonal mean, the equation for anomalous heat loss at the surface is as follows:

[10]Our "standard" surface restoring timescale of 30 days effectively removes heat from the ocean much more rapidly than would be achieved through radiative processes (Marotzke and Pierce, 1997). To examine the sensitivity of the geothermal response to the surface boundary condition, in section 4.3 we compare the results from our standard model to a model run which employs a 450-day timescale. Our scaling result is insensitive to this timescale.

$$\frac{\rho_o c_p \Delta z}{L_y} \int_0^{L_y} \nabla \cdot (\mathbf{u}' T) dy \quad = \quad 50 \text{ mW m}^{-2} \tag{4.2}$$

where L_y is the meridional extent of the model and Δz is the depth of the surface layer. The left hand side of (4.2) can be simplified and scaled as follows:

$$\equiv \frac{\rho_o c_p \Delta z}{L_y} \int_0^{L_y} \frac{\partial (w'T)}{\partial z} dy \quad \sim \quad \frac{\rho_o c_p \Delta z}{L_y} \frac{w' \Delta T}{\Delta z} L_y \tag{4.3}$$

where ΔT is the imposed equator-to-pole temperature difference. Using continuity to scale $w' \sim v' \Delta z / L_y$ gives:

$$\sim \quad \frac{\rho_o c_p \Delta z}{L_y} v' \Delta T \tag{4.4}$$

(4.2)-(4.4) suggests that $v' \sim 0.01 \text{ cm s}^{-1}$. Like the hypothesized diffusive response, this represents a small change from the background state. Even if the anomalous meridional velocity were concentrated in the western boundary current, v' is still much smaller than the local background flow. A more significant advective response would be possible only if localized in longitude and latitude, e.g., in a single grid cell, in which case anomalous flow as large as 10 cm s^{-1} could exist in an area of weak temperature gradient.

4.2.2 Initial Transient Response

In response to uniform geothermal heating of 50 mW m^{-2}, convective mixing in the lowest model layers is triggered in the tropics, except near the deep western boundary current (Fig. 4.1). Convection occurs here because the flow is sluggish and near the terminus of the abyssal flow pathway, and has therefore been exposed to warming from the bottom boundary longer than more newly injected deep water. Since the abyssal waters are very weakly stratified, even weak heating from below is sufficient to initiate convective adjustment. Continued geothermal heating leads to increased convective penetration, effectively distributing the boundary heat flux over an expanding column of water. Analogous to a convective plume in the tropical atmosphere, however, penetration is ultimately limited by an area of sharply increased stratification. In the atmosphere, this increase in stratification is delineated by the

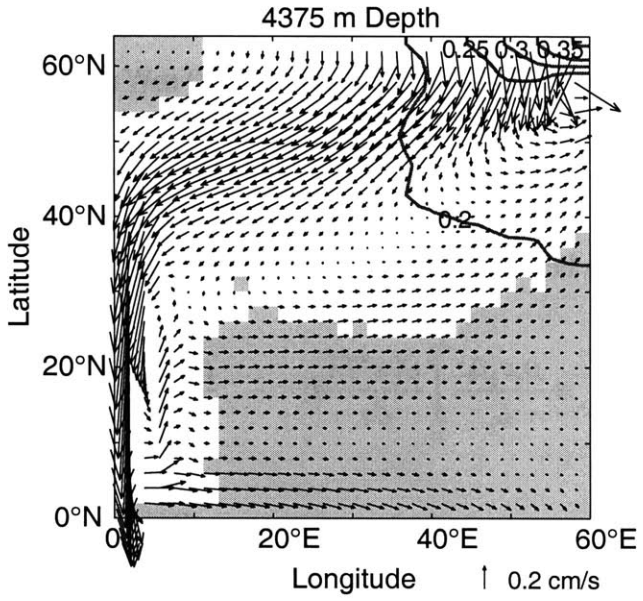

FIGURE 4.1: Plan view of bottom model layer, 50 years after uniform geothermal heating is first applied. Flow is indicated by vectors and is representative of the background state flow, as the model's advective response requires on the order of centuries to develop. Shading indicates grid cells undergoing convective mixing (i.e., cooling these locations). As compared to the background state prior to geothermal heating, the deep convective region in the northwest is increased in area, and all convective mixing in the tropics is new.

tropopause, whereas the analog in the ocean is the base of the thermocline. Present-day geothermal heat fluxes are too small to allow for any significant penetration of convective mixing into an existing thermocline.

On the timescale of a few hundred years, a perturbation circulation develops in response to changes in the deep temperature structure. At steady state, flow through the abyss is increased, and tropical deep convective mixing is no longer triggered from below. We will not attempt to further diagnose the spin-up of this circulation, but will instead focus on the steady-state response.

This transient behavior provides a qualitative link between the local hydrothermal plume models and our steady-state geothermal response, as the lack of maintained convection from below in the latter might otherwise obscure this connection. This link serves as partial justification of modelers' routine dismissal of geothermal fluxes, as any geothermal response can have very little *direct* impact on the circulation through the thermocline, and therefore cannot affect the oceanic heat transport to any measurable degree. Accordingly, the real oceans' large-scale response to geothermal heating is highly constrained by the large fluxes of heat at

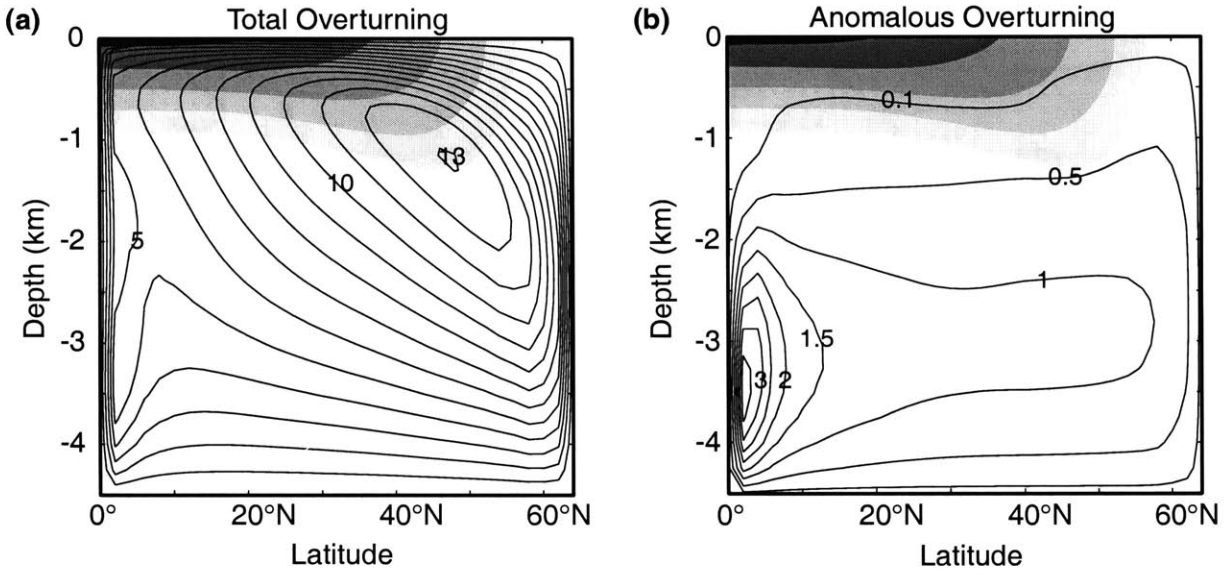

FIGURE 4.2: Meridional overturning streamfunction (contours) and zonally averaged temperature (shading). (a) Steady-state run with uniform geothermal heating; (b) same as (a), except showing anomalous overturning as compared to a similarly configured run without geothermal heating. Contours are labeled in Sv, with solid contours indicating clockwise flow; isotherms (shaded) are at 0.05, 0.1, 0.2, 0.4, and 0.8 of $\Delta T = 27\,^{\circ}\mathrm{C}$.

the surface and the downward penetration of these fluxes through the action of diapycnal mixing and/or wind stress.

4.2.3 Perturbation Analysis

In Fig. 4.2a, we show the steady-state meridional overturning circulation and zonally averaged thermal structure of our standard run. Compared to an identically configured run without geothermal heating (Fig. 3.2a), the main meridional overturning circulation is similar, and its maximum in overturning near 50°N at 1 km depth is increased by only 0.4 Sv. However, the perturbation response obtained by subtracting the steady-state circulation without geothermal heating shows a much stronger response centered at low latitudes (Fig. 4.2b). A deep meridional overturning cell is produced, with an overturning maximum of 3.8 Sv. All rising motion in the zonal mean occurs alongside the equator; net sinking occurs at all other latitudes, but is concentrated primarily in the tropics and at high latitudes. Also note that the cell is essentially confined to the coldest ocean waters, as in the zonal integral only 0.1 Sv flows through the thermocline.

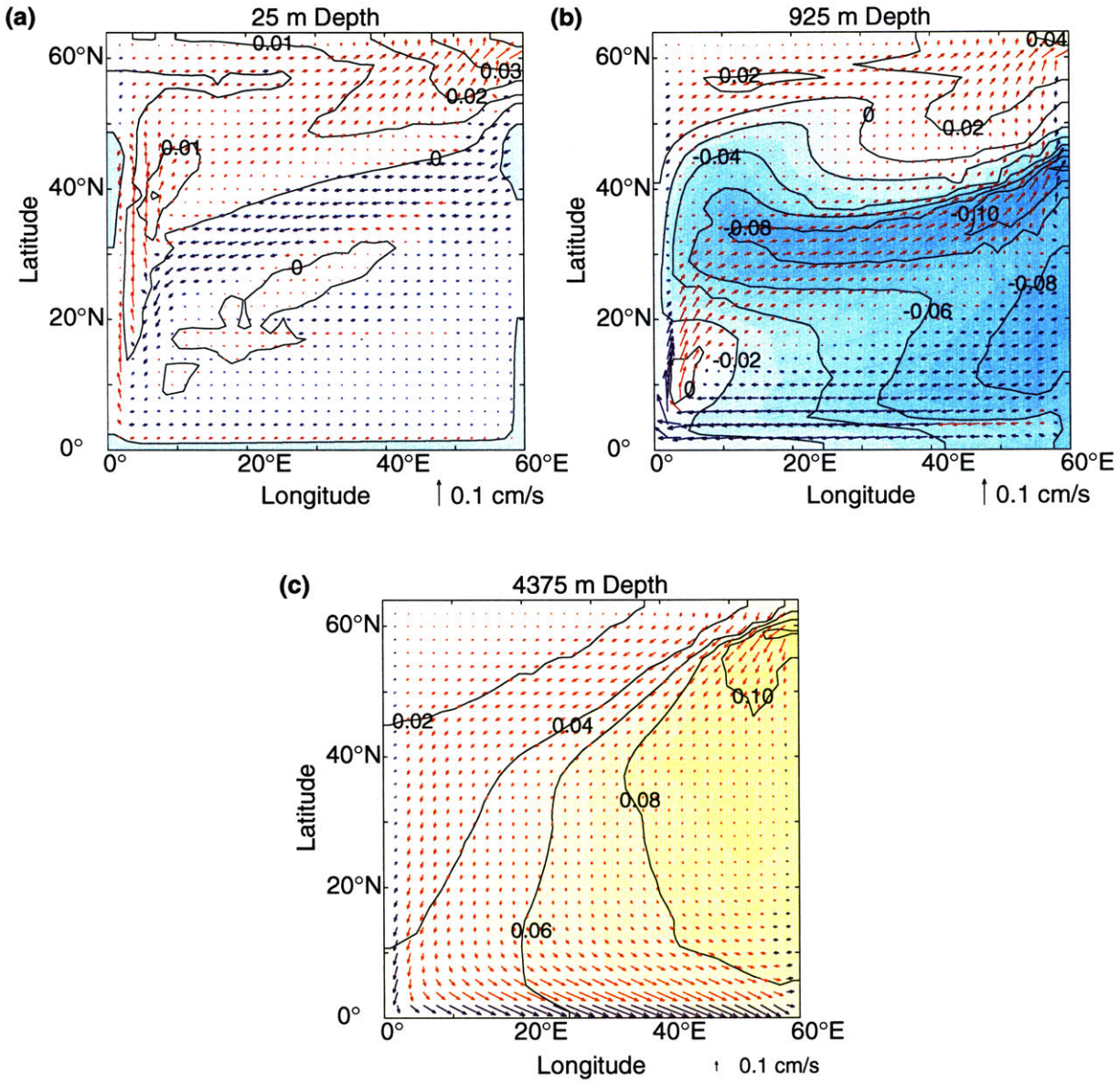

FIGURE 4.3: Plan view of the anomalous circulation and anomalous temperature (contours and color shading) obtained by subtracting the geothermal run results from the background state. Blue vectors indicate anomalous upwelling and red arrows indicate anomalous downwelling. (a) Surface model layer (contour interval 0.01 °C); (b) layer near the base of the thermocline, 950 m depth (contour interval 0.02°C); (c) lowest model layer (contour interval 0.02°C).

The surface perturbation in temperature and flow is shown in Fig. 4.3a. Anomalous warming occurs primarily in the northeast corner, where in the background state surface waters downwell to the lowest layers of the abyss. The maximum temperature anomaly is 0.04 °C, which is still small in comparison to the approximate 27 °C difference between the equator and pole, but is nearly an order of magnitude larger than the uniform diffusive response. Except

for an area near the western boundary current, much of the ocean surface is actually slightly *colder* (anomalous temperature of less than 0.01°C) in the geothermal simulation.

This perturbation temperature structure at the surface is accompanied by slight changes in surface flow patterns. Given a background state of nearly zonal flow into the eastern boundary (in the absence of applied wind forcing), the flow vectors indicate less downwelling at the eastern boundary between 40-50°N, with increased downwelling further north. Closing this loop requires anomalous meridional flow, advecting warmer waters northward which in turn produces the patch of anomalous warming. This alteration in eastern boundary flow leads to a mid-latitude cold tongue near the base of the thermocline, as observed in Figure 4.3b (we will postpone a discussion of why the tropics are colder in this figure until later in this section). The perturbation flow in the thermocline is over an order of magnitude smaller than the background flow, so the impact of geothermal heating on the upper ocean circulation is indeed quite small.

In contrast, the magnitude of the perturbation flow in the abyss is significant in the context of the relatively sluggish background flow. A comparison of the perturbation flow pattern in Fig. 4.3c and background flow vectors (see Fig. 4.1, which shows the deep flow prior to any significant advective response) suggests that geothermal heating serves to augment the existing deep flow, except perhaps in the tropics where the background flow is more zonal. In the background state, flow is injected into the northeast as the warmest water in the abyssal layer, but is then cooled by deep convective mixing in the northwest, and re-heated by diffusive heating from above along the boundaries in the tropics (see chapter 3 for a comprehensive discussion of the abyssal heat balance). Geothermal heating along this flow pathway produces anomalous warming throughout the bottom layer. Fig. 4.3c indicates an increase in the volume of downwelling water into the northeast, where a maximum temperature anomaly of 0.12 °C occurs. In the northwest corner, however, the anomalous warming is much weaker. Here, the convective connection to the surface effectively transports any anomalous heat out of the abyss, creating an anomalous zonal temperature gradient at high latitudes. In the tropics, water is warmed as it flows eastward, completing the abyssal pathway of the large-scale overturning circulation; this heating helps to maintain an anomalous zonal temperature gradient, albeit weaker than at higher latitudes. We will subsequently show that this zonal gradient is not localized in the bottom layer, and that the vertical structure of the east-west temperature difference is an essential feature of the dynamical response. The vigorous anomalous flow into the equator is consistent with the upwelling noted in our description of the overturning cell.

The steady-state dynamical response invites several questions. Why is the anomalous upwelling narrow and the downwelling broadly distributed? Why does geothermal heating produce an anomalous meridional circulation at all? In the remainder of this section, we will show that the anomalous deep circulation is ultimately governed by the requirement that the geothermal heat flux is exported out of the abyss to the surface, where it can be "radiated away" to the atmosphere through our restoring boundary condition.

4.2.4 Thermodynamic Interpretation of Response

Consider the possible means by which the bottom layer can achieve a steady-state balance given geothermal heat input. The most direct route of heat loss is through convective exchange to the surface. The fact that the deep convective "pipeline" expands from one grid cell in the northeast corner to several, in the geothermal run, does suggest that some additional heat is lost through convective mixing. However, this mechanism is quite ineffective at removing heat input not local to the site of deep convection. Because deep convective mixing occurs at high latitudes, it is near the beginning of the abyssal flow pathway, hence only brief exposure to geothermal heating has occurred. Moreover, given that the coldest water in the bottom layer occurs at the deep convection site (Marotzke and Scott 1999), geostrophic dynamics diverts flow around this area of convective mixing, not through it. Ultimately, anomalous convective heat loss is quite limited, even if it were possible to re-route the abyssal flow pathway back to high latitudes after extended exposure to geothermal heating. Penetrative convective mixing from below, as observed in the tropics during the transient response, can effectively distribute the geothermal heat across the abyss, but cannot penetrate the thermocline. Hence, any convective heat exchange to the surface is prohibited at low latitudes.

Weaker diffusive heat flow into the bottom layer constitutes a second conceivable means by which heat balance can be achieved. The decrease in stratification on the eastern boundary (Fig. 4.4; there is little change in the western boundary stratification due to the rapid flow) indeed leads to smaller diffusive heat flux in the steady-state geothermal run. However, a rough estimate of the heat flux from the term $\rho_o c_p \kappa \partial_z T$ suggests that even in the non-geothermal run, the area-averaged deep diffusive flux is $5\,\mathrm{mW\,m^{-2}}$, about an order of magnitude smaller than the geothermal flux. Hence, any decrease in downward diffusive fluxes through weakened stratification is relatively modest.

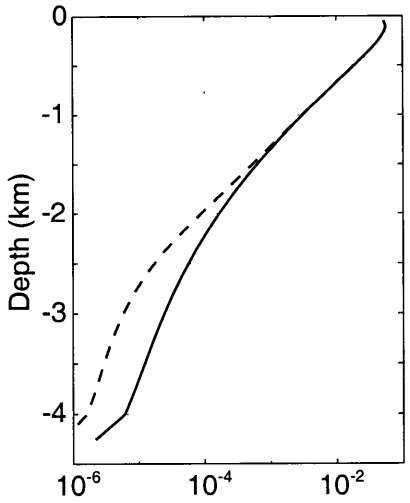

FIGURE 4.4: Plot of vertical potential temperature structure $\partial T/\partial z$ (in °C m^{-1}) versus depth along the equator at 60°E. The geothermal run results are represented by the dotted curve, and the solid curve shows the background state.

We are left with the conclusion that geothermal heating must invoke a response in vertical velocity, at least in the deep ocean, to remove the excess heat input. The vertical advective heat gain is proportional to the following expression (as described in chapter 3):

$$\int wT\,dA = \int_{downwelling} w_D T_D + \int_{upwelling} w_U T_U \tag{4.5}$$

where the U and D subscripts refer to upwelling and downwelling, respectively. On one hand, a vertical response is intuitive—more inflow into the abyss minimizes the temperature gain at the bottom, simply by reducing transit time. Prior to geothermal heating, (4.5) is negative (i.e., downward) because relatively warm water is injected into the bottom layer but upwelling occurs at colder temperatures. With geothermal heating, the advective response in the upper ocean leads to even warmer downwelling waters, so the overall result is to convey more anomalously warm water into the abyss (i.e., the $\overline{w}_D T'_D$ and $w'_D \overline{T}_D$ terms in the heat budget are both negative quantities). This observation is seemingly at odds with the steady-state requirement that the magnitude of the advective heat gain decreases with geothermal heating. Therefore, a more significant increase in the magnitude of the upwelling term must occur. As mentioned, anomalous upwelling occurs along the equator, where waters are being warmed through geothermal heat fluxes. In the geothermal run, a much larger percentage of the upwelling occurs along the western boundary, where temperatures are relatively cold. Thus, the increase in T_U outweighs the first term in (4.5).

Having established that geothermal heating must generate anomalous vertical motion in the bottom layer, consider the vertical extent of this flow. Fig. 4.2b shows that much of the perturbation cell in the tropics is confined to the lowest 2000 meters. A significant percentage of the flow here simply recirculates at low-latitudes, and is thus ineffective at transporting heat out of the lower abyss. The two arguments presented heretofore that necessitate the vertical response in the bottom layer—namely that water flows around the location of deep convective mixing and that background diapycnal heat fluxes are weak—also apply to the lower abyss, implying that an advective response across mid-depth must occur.

Above mid-depth, the component of the anomalous circulation through the high-latitudes is critical in communicating the geothermal heating to the surface. Anomalous northward flow into the northeast is not limited to the surface layer, but occurs throughout the top 2500 meters. Because deep mixed boundary layers occur along the back wall and eastern walls, as shown in Figs. 4.5a and 4.5b, respectively, heat fluxes into these convecting columns can be quickly communicated to the surface. Without the efficient convective mixing process, a more significant advective surface perturbation would be required, as estimated in the beginning of this section.

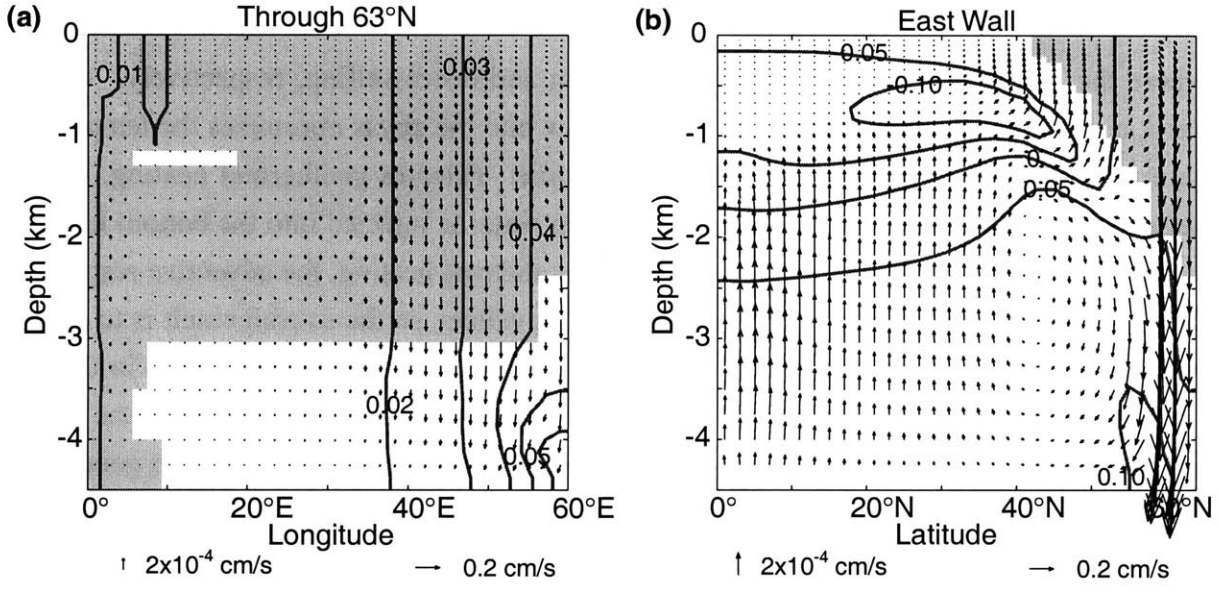

FIGURE 4.5: Plot of anomalous circulation and anomalous temperature (contours) in (a) the zonal plane against the model's back wall; (b) the meridional plane adjacent to the eastern boundary. Shading represents grid cells with active convective mixing.

4.2.5 Dynamics of the Anomalous Meridional Overturning Circulation

In thermal wind balance, the strength of the meridional overturning circulation is a function of the density difference between the eastern and western walls (Marotzke 1997). We will use this balance to obtain an order of magnitude estimate of the perturbation deep cell, based on the increase in temperature as a function of the zonal transit time across the tropics, which is in turn a function of the background large-scale circulation. From the non-geothermal run we can estimate the depth of the abyss and obtain an average zonal velocity. Given an approximate deep zonal velocity of 0.1 cm s^{-1}, it takes water roughly 200 years to cross the basin. Our applied geothermal heat flux can heat a 3000 meter column of water by 0.03 °C in this "transit time" (Joyce et al. 1986). This value roughly agrees with the model's anomalous temperature difference between the east and west walls in the tropical abyss, as shown in Fig. 4.6. (It is more difficult to predict the boundary density difference at high latitudes *a priori*, as we have argued the warming is a function of the increase in downwelling along the boundary). To convert this boundary density difference into an overturning rate, we compute the shear in meridional velocity through the abyss from the thermal wind relation:

$$\frac{\Delta v'}{\Delta z/2} = \frac{g}{f\rho_o}\frac{\Delta \rho'}{\Delta x} \tag{4.6}$$

where $\Delta\rho'$ is the anomalous east-west density difference and Δz is the depth of the abyss (i.e., so that $\Delta z/2$ is approximately the depth of the southward branch of the anomalous cell). If we assume that the meridional velocity increases linearly from maximum southward flow at the ocean bottom and vanishes at the center of the anomalous cell (i.e., so that the average southward velocity is $\Delta v'/2$), the estimate of overturning strength is:

$$\Psi' \approx \frac{\Delta v'}{2}\Delta x\frac{\Delta z}{2} = \frac{\alpha g}{8f}\Delta T'\Delta z^2 \tag{4.7}$$

where $\alpha = 1.8\times10^{-4}$ K^{-1}, the thermal expansion coefficient. Near the equator, use of (4.7) is problematic, as the geostrophic relation breaks down and the f^{-1} dependence implies an infinite response. If we take $f \sim 10^{-5}$ s^{-1}, the value of the Coriolis parameter at 4°N, our estimate for the anomalous overturning is 6 Sv. This estimate is somewhat too large, but is the correct order of magnitude. The estimate is more accurate at higher latitudes. For example, at 45°N $\Delta T' \sim 0.07$ °C and $f \sim 10^{-4}$ s^{-1}, hence the estimated overturning strength is slightly over 1 Sv, in general agreement with Fig. 4.2b.

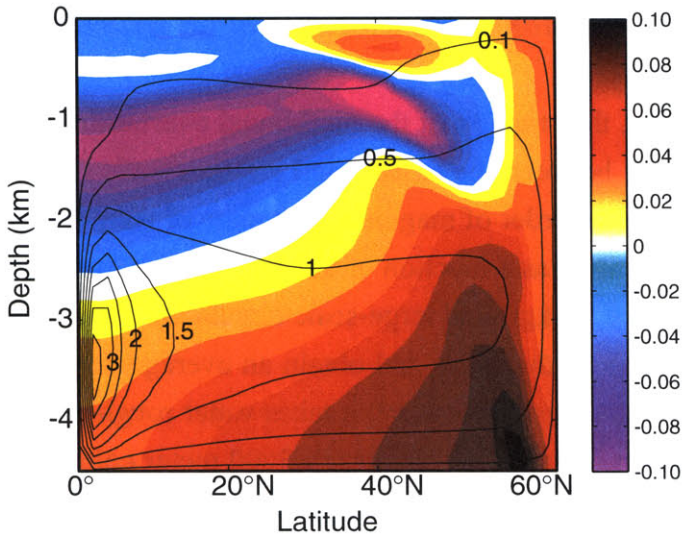

FIGURE 4.6: Contour plot of $\Delta T'$, the anomalous temperature difference between the eastern and western boundaries, overlaid by the anomalous meridional overturning circulation.

We have been careful to obtain our *a priori* estimate of anomalous overturning maximum based on the southward branch of the deep cell. As seen in Fig. 4.6, $\Delta T'$ varies considerably in the northward branch of the cell, i.e. between 1500 and 3000 meters depth. In fact, $\Delta T'$ changes sign near the top of the anomalous cell, providing southward shear. This reversal is necessary or else the anomalous northward velocities would continue through the thermocline. As shown in Fig. 4.7, this reversal is accomplished by cooling at the top of the anomalous cell where upwelling occurs, primarily the eastern side of the basin. This is perhaps somewhat surprising—why should an extra heat flux through the bottom boundary lead to nearly 0.1 °C cooling in the thermocline? Given that the tropics are sharply stratified, any weak upwelling that continues above the top of the anomalous cell leads to anomalous cooling. Hence, anomalous cooling throughout the tropical thermocline is observed (see also Fig. 3b).

Let us now return to our initial goal, that of explaining the anomalous cell's narrow upwelling. In geophysical fluid systems, both stratification and rotation can influence the dynamical behavior by restricting vertical motions (e.g., Cushman-Roisin 1994). First, consider the importance of rotation. Given our estimate for the background deep zonal flow, the Rossby number U/fL is O(10^{-5}). This number remains quite small even within a few degrees of the equator, suggesting that rotational terms dominate the momentum equation throughout the basin. Second, we estimate the internal Froude number U/NH as O(10^{-3}) using a representative model value of N (2×10^{-3} s^{-1}). Hence, although the stratification is weak in the

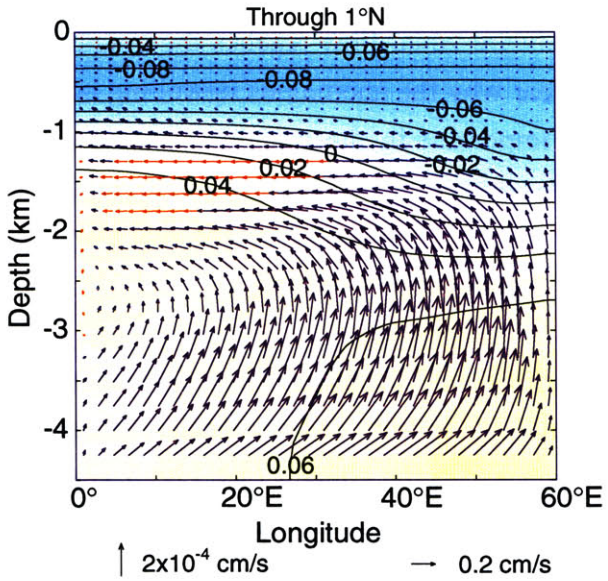

FIGURE 4.7: Plot of anomalous circulation and anomalous temperature in the zonal plane adjacent to the equatorial boundary.

abyss, it is also sufficient to restrict vertical motion. Although both processes are clearly important, the ratio of the Rossby number to Froude number suggests that flow is mostly influenced by rotation. This analysis is consistent with the observed geothermal response, in that limited vertical motion does occur, but all upwelling occurs adjacent to the equator, where f is as small as permitted by our crude resolution.

Away from the equator, weak downwelling occurs in the ocean interior, as observed in meridional cross sections (not shown). The vorticity equation $\beta v = f\partial_z w$ implies meridional flow if vertical convergence is non-zero. In the southward branch of the anomalous cell $\partial_z w < 0$ whereas $\partial_z w > 0$ in the northward branch. The vorticity equation could also permit a reversed anomalous circulation, i.e., with narrow sinking at the equator and weak upwelling in the interior. However, this circulation would flow counter to the background overturning, and therefore would be ineffective at removing the surplus heating. We ran an additional experiment (not shown) with an inverted equator-pole temperature gradient, which produced a background state with deep sinking at the equator. Given this surface forcing, we obtained an anomalous geothermal response of narrow sinking at the equator and broad upwelling in the ocean interior, consistent with this argument.

In contrast with the interior flow, anomalous upwelling occurs at the tropical eastern and western boundaries (as shown for the eastern boundary in Fig. 4.5a). On the east, upwelling

occurs when anomalous eastward zonal flow reaches the boundary. At the western boundary, it is not immediately clear why the anomalous upwelling occurs. As discussed in Spall (2000), viscous terms are important in the potential vorticity budget at the boundaries. Anomalous eastern and western boundary upwelling occurs regardless of whether diapycnal mixing is concentrated at the boundaries, as the geothermal response was qualitatively similar in a model with uniform diffusivity (not shown).

It is edifying to note similarities between the geothermal heating response and the effect of enhanced deep diapycnal mixing. In both cases, a deep anomalous overturning cell is produced with rising motion adjacent to the equator (see Fig. 3.12b for the overturning streamfunction with enhanced deep mixing, using an otherwise similarly configured model). Dynamically, both geothermal heating and increased deep diffusion lead to greater heat fluxes into the model's bottom layer. There is a fundamental difference in the nature of the response, however. With enhanced deep mixing, the rising motion of the deep cell occurs where forced by mixing (i.e., adjacent to the equator, where mixing is concentrated in these runs) as required by advective-diffusive balance. In contrast, the geothermal heating response can be interpreted as a free response constrained by rotational dynamics.

From a modeling perspective, it is somewhat problematic that anomalous upwelling is concentrated in the grid cells adjacent to the equatorial boundary, suggesting an unresolved equatorial boundary layer. Equatorial dynamics could seemingly be very important in determining the magnitude of the geothermal response. Since the anomalous overturning maximum might conceivably be dependent upon the equatorial grid spacing, we re-ran the geothermal heating simulation with resolution decreased by 50% (to increase resolution further was beyond our computational resources), but found only a slight decrease in the magnitude of the anomalous overturning cell (not shown).

4.3 Alternate Forcing Scenarios

4.3.1 Alternate Background States

Our analyses in the previous section suggest that the magnitude of the geothermal response is a function of the background state flow and density structure. To test this hypothesis, we reran our geothermal simulation with both stronger and weaker background meridional overturning circulations.

A stronger background overturning can be achieved through increased diapycnal mixing (Bryan 1987; Marotzke 1997). Here, we increased the boundary mixing strength four-fold, which produced a maximum overturning of 31 Sv at steady-state (as compared to 12.7 Sv for the standard run). The anomalous geothermal response in overturning is shown in Fig. 4.8a. There are several reasons why this response is considerably weaker than our standard geothermal response. First, increased mixing thickens the thermocline, thus decreasing the depth of the abyss while increasing its stratification. Consequently, the build-up of meridional shear resulting from east-west boundary temperature differences occurs across a reduced depth, producing a weaker overturning cell. Second, the background flow's transit time through the abyss (primarily a function of overturning strength) is decreased, resulting in weaker anomalous zonal temperature gradients, again reducing the build-up of meridional shear. And finally, the increased effectiveness of diffusive processes implies that a weakening in stratification can lead to a more significant reduction in deep diffusive heat fluxes. In other words, the system is better able to offset the geothermal heating through a diffusive response, making the advective response less critical as a means to re-establish a steady-state heat balance.

The anomalous geothermal response with boundary diapycnal mixing strength reduced by 80% is nearly double that of the standard experiment (Fig. 4.8b). Here, the background state

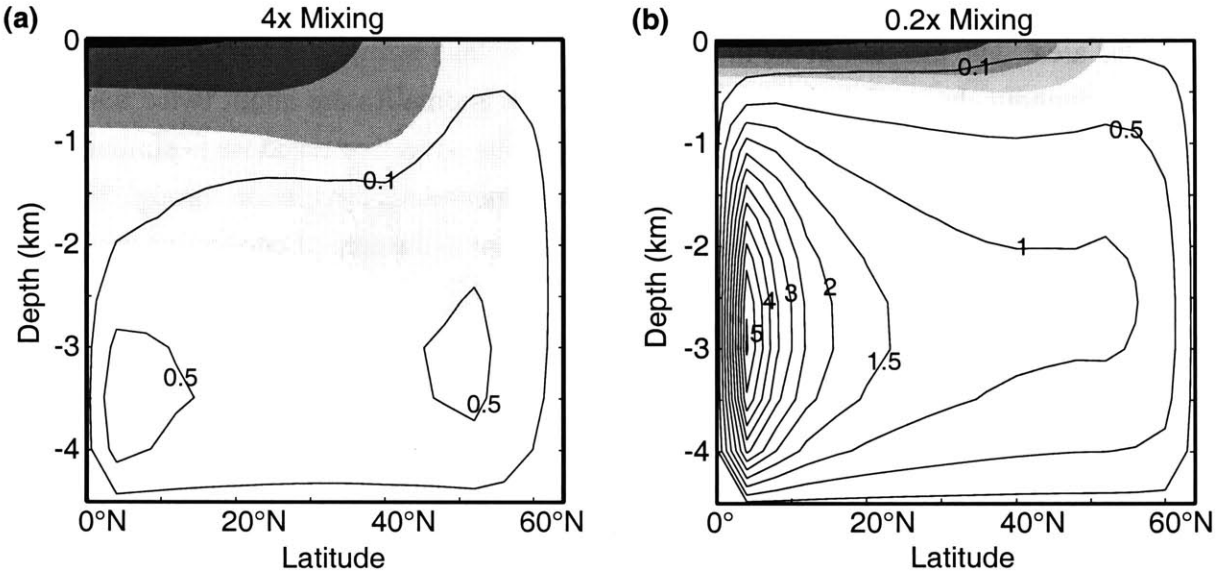

FIGURE 4.8: Anomalous meridional overturning circulation due to geothermal heating, given (a) a four-fold increase in boundary mixing strength; (b) an 80% decrease in boundary mixing strength.

overturning maximum is 4.6 Sv, the same order of magnitude as the geothermal response, indicating that non-linear interactions are likely to be significant. The opposite of the arguments employed in the stronger mixing case apply; namely, the abyss is deeper and less stratified, the transit time through the abyss is longer, and diffusive fluxes are extremely weak (although we suggest the latter is of little consequence given that these fluxes are already quite small in the standard run). Note that the increased response occurs primarily at low latitudes, as compared to Fig. 4.2b. The anomalous circulation through high latitudes—whereby heat is effectively communicated to the atmosphere through advection into deep mixed layers—is little changed, as the applied geothermal heating is unchanged from our standard run. Given the sluggish deep circulation, here convective mixing along the bottom boundary is maintained even as the system has reached a steady-state response to geothermal heating. Accordingly, the warmest waters in the bottom layer are now found in the tropical eastern boundary rather than the northeastern corner (not shown). Anomalous cooling in the thermocline peaks at 0.3°C, double that of the control experiment.

To examine the sensitivity of our results to the surface restoring boundary condition, we also equilibrated a geothermal heating run using a 450-day restoring timescale (not shown). The background state for this run is described more fully in chapter 5, but the salient features include a decrease in the depth and area of high-latitude mixed boundary layers and a narrower deep sinking region that is adjacent to the model's northern boundary at mid-basin. As might be expected given the decreased efficiency of the surface boundary condition in removing heat anomalies, the positive temperature anomaly at the surface is increased in both magnitude and area. The increase in the magnitude of anomalous warming is not limited to the surface; throughout the model, the positive temperature anomalies are about twice that of the standard geothermal run. Qualitatively, the anomalous advective response is similar to our standard run, with a slight increase (~0.5 Sv) in the anomalous circulation through high latitudes, which we attribute to the aforementioned decrease in the area of convective mixing.

4.3.2 Variations in Geothermal Heating Application

As discussed in the introduction, the flux of geothermal heat is enhanced in the vicinity of the mid-ocean ridges. To examine how localization affects the anomalous response, we ran two variations of our geothermal heating experiment. In the first, we specified stair-step fluxes of 100-200-100 mW m^2 across a 12° longitude span through the center of the ocean basin, maintaining the background 50 mW m^2 at other locales. This new forcing represented a 30% increase in total geothermal heating. Note that this is only a partial representation of the pos-

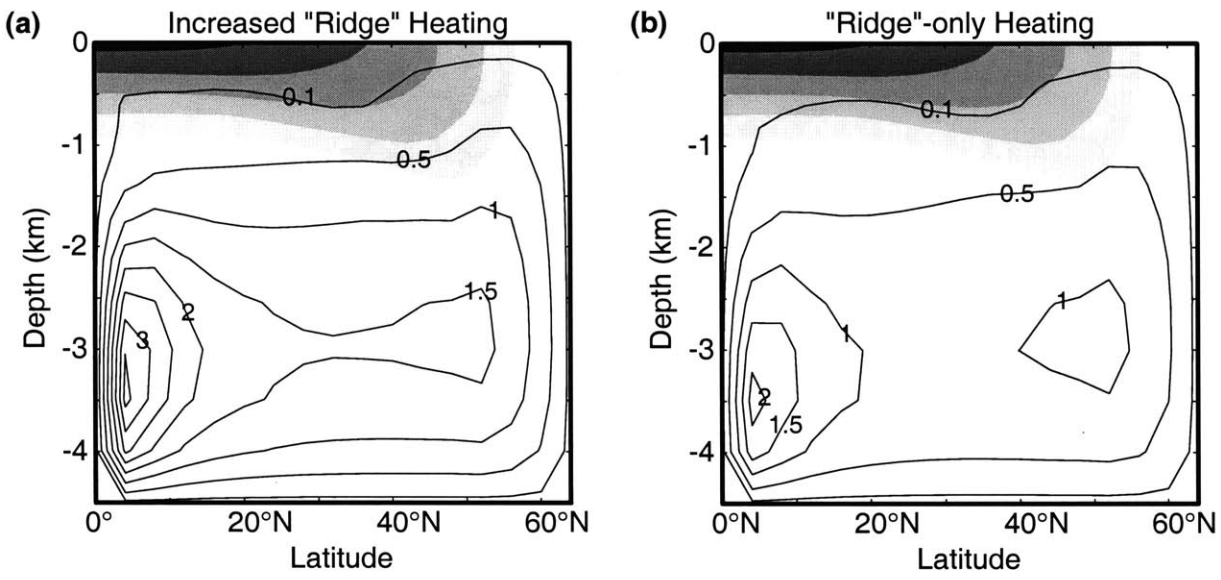

FIGURE 4.9: Anomalous meridional overturning circulation given (a) an increase in geothermal heating along a 12° meridional strip through the middle of the basin, maintaining heating elsewhere; (b) a more significant increase in heating along this mid-ocean "ridge" with zero geothermal heat input elsewhere, so as to maintain the total heat input of the uniform geothermal heating run.

sible effects from ridge heating, as we maintain a flat bottom in all runs. The low-latitude response (Fig. 4.9a) shows only a modest increase in maximum overturning as compared to the uniform heating run at this resolution. More significant is the degree to which the anomalous overturning extends to higher latitudes. In the second variation we located all anomalous heating along a 200-400-200 stair-step, which maintained the total heat flux of the uniform forcing run. In this run the maximum overturning at low-latitudes is reduced considerably (Fig. 4.9b), but the anomalous downwelling through high latitudes is similar to the uniform heating run.

These two additional runs, taken together, uphold the arguments presented heretofore. When the total geothermal heating is increased, the anomalous high-latitude circulation must increase, as this component represents the only means by which excess heat is transported out of the abyss. The strength of the anomalous low-latitude circulation is largely a function of the east-west density difference. Increased heating along the "ridge" produces a local maximum in temperature (as shown in Fig. 4.10), which leads to anomalous cyclonic circulation. However, the fact that a local maximum exists makes it clear that the ridge heating is only partially communicated to the eastern boundary. This behavior is analogous to that of localized interior mixing, which is also less effective at driving a meridional overturning circulation (see chapter 3 for a discussion). On the western side of the "ridge" there is a fairly sharp

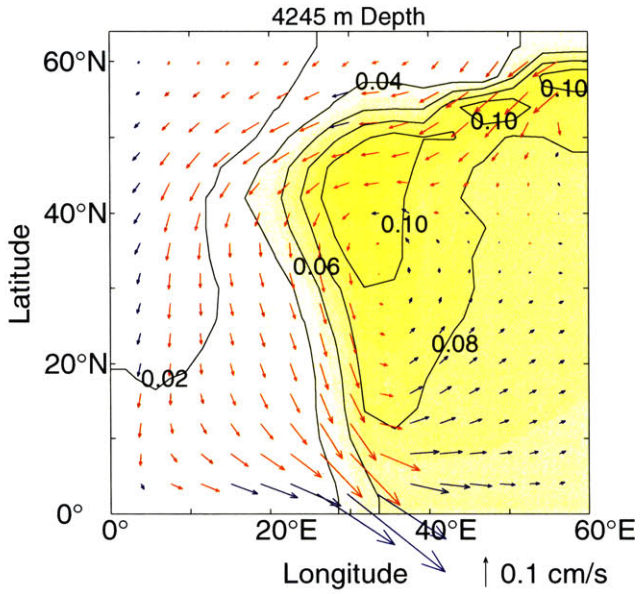

FIGURE 4.10: Plan view of the anomalous circulation and anomalous temperature of the bottom model layer in the "ridge"-only geothermal heating run.

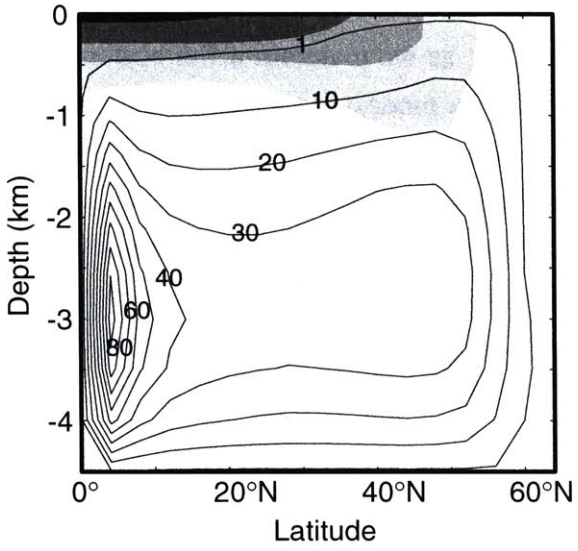

FIGURE 4.11: Anomalous meridional overturning circulation produced by a uniform geothermal heating of 5 W m^{-2}.

anomalous temperature gradient. As required by geostrophic balance, a significant portion of the anomalous circulation flows along this gradient, with less flow through the deep western boundary current as observed in the uniform heating run.

To test the sensitivity of the response to the magnitude of geothermal heating, in as much as the heating rate has not been constant through geologic time [see Kadko et al. (1995) for a review], we ran an experiment with an arbitrarily chosen uniform 5 W m^{-2} geothermal heating, a two order increase from our control run. The choice was not meant to be realistic, but simply to represent an extreme case whereby geothermal fluxes are closer in magnitude to surface heat fluxes. As shown in Fig. 4.11, the resulting anomalous circulation is quite remarkable. The response is essentially an exaggerated version of our results given a weaker background circulation. Here, the anomalous response constitutes the dominant flow except in upper thermocline waters. The bottom portion of the thermocline has been eroded in the tropics, and the anomalous overturning maximum is 94 Sv. There is also a secondary maximum in the anomalous streamfunction at high latitudes. Like our control geothermal heating simulation, the portion downwelling at high latitudes is about one-third of the overall maximum. Even in this extreme, with the predominant ocean circulation now primarily driven by geothermal heating rather than diapycnal mixing, the resulting maximum meridional heat transport is only 0.1 PW greater than the non-geothermal run. This result suggests that more realistic changes in geothermal heating rates are not likely to affect climate directly through the oceans' heat transport.

4.4 Geothermal Heating In A Double Hemisphere Model

In this section we extend our results by adding a second hemisphere to our ocean basin, setting up an asymmetric background flow pattern through a 1°C pole-to-pole difference in surface restoring temperature profiles (the northern hemisphere is more dense, and hence northern-originated water fills much of the abyss). The dynamics of the two-hemisphere flow is discussed in detail in Marotzke and Klinger (2000). We wish to test whether the equatorial upwelling observed in the single hemisphere runs is a robust feature or due to the limited geographical extent of the model. In addition, introducing a second hemisphere adds two notable complexities to the system: a second competing source for deepwater, and the possibility of cross-hemisphere flow. We will examine how these affect the dynamics of the anomalous response to geothermal heating.

In Fig. 4.12, the anomalous meridional overturning in the double hemisphere system is shown. Anomalous upwelling occurs all along the equator, although there is no longer any 'boundary' mixing here, as was parameterized in the single hemisphere model. Total equatorial upwelling is about the same as in the single hemisphere run, although some of the tropi-

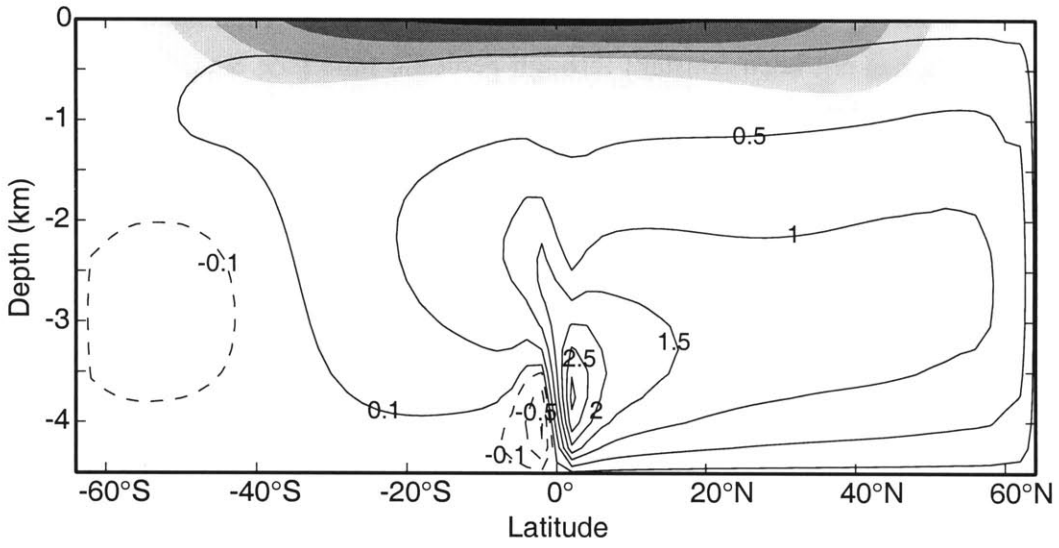

FIGURE 4.12: Anomalous meridional overturning circulation in a double hemisphere basin given uniform geothermal heating of 50 mW m^{-2}.

cal downwelling occurs in the southern hemisphere, as evidenced by the counter-clockwise cell abutting the equator to the south. As before, the geothermal heat flux is lost to the atmosphere locally in the northeast corner (Fig. 4.13a; the structure in the northwest is due to a slight change in the pattern of high-latitude convective mixing). Since the area-integrated geothermal heat flux is now twice as large, this anomalous surface warming is greater in magnitude and covers a larger area than in the single hemisphere run. The anomalous overturning through the northern hemisphere high latitudes is only slightly enhanced from the single hemisphere results (viz. Fig. 4.2b vs. Fig. 4.12). As we have argued that this component of the circulation is critical in communicating the geothermal heat fluxes to the surface, the lack of a bigger response is surprising (i.e., given that the anomalous circulation must now transport twice as much heat from depth to mixed layer), and suggests that the anomalous circulation is a more efficient heat conveyor in the double hemisphere system. To address why this is so, it is necessary to focus on the more subtle differences brought about by the addition of the second hemisphere.

Fig. 4.13a shows that the enhanced downwelling in the northeast is to large extent supported by anomalous upwelling at 40-50°S (as implied by the 0.1 Sv contour in Fig. 4.12), which then flows westward and joins the western boundary current. The anomalous upwelling at these latitudes opposes the background flow which downwells and produces southern ocean intermediate water (Klinger and Marotzke, 1999). Unlike the process of deep mass injection in the northern hemisphere, sinking waters in the southern hemisphere are insufficiently

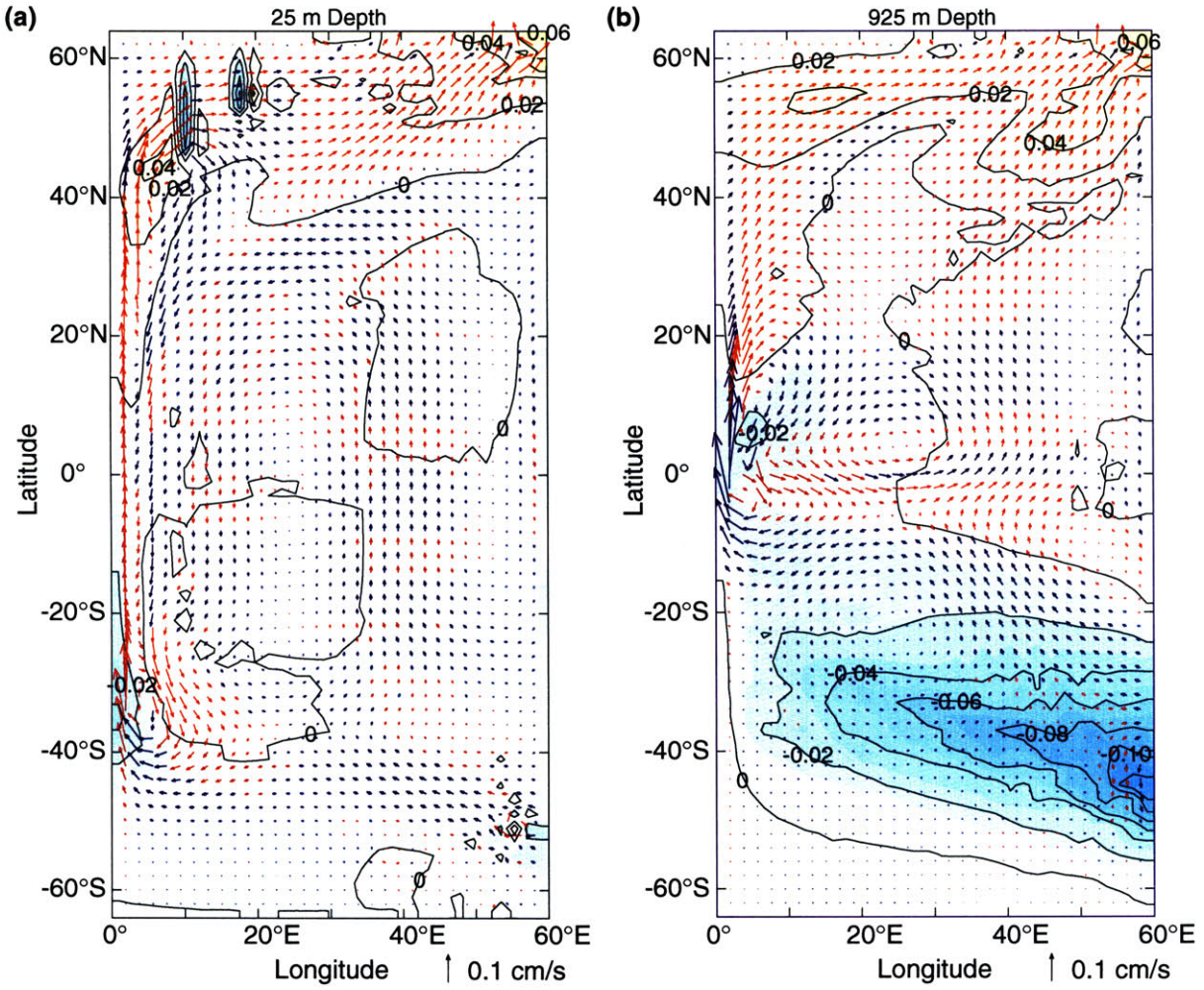

FIGURE 4.13: Plan view of the anomalous circulation and anomalous temperature for the double hemisphere, uniform geothermal heating simulation. (a) Surface model layer; (b) layer near the base of the thermocline, 935 m depth; (c) Lowest model layer (next page). Contour interval on all plots is 0.02°C.

dense to penetrate into the abyss. Recall that in the single hemisphere run, the anomalous surface circulation is fed by anomalous upwelling at 40-50°N (Fig. 4.3a), giving rise to a cold tongue at the base of the thermocline. In the double hemisphere basin, a more pronounced cold tongue extends from the eastern boundary in the southern hemisphere than in the northern hemisphere (Fig. 4.13b). The northern hemisphere cold tongue in the double hemisphere run is also much less pronounced than in the single hemisphere run (viz. Fig. 4.13b vs. Fig. 4.3b).

Our explanation as to why the anomalous high latitude circulation into the northern deep mixed layers is seemingly more efficient is as follows. The northern hemisphere thermocline is less anomalously cold in the double hemisphere run, so advection into the northern hemi-

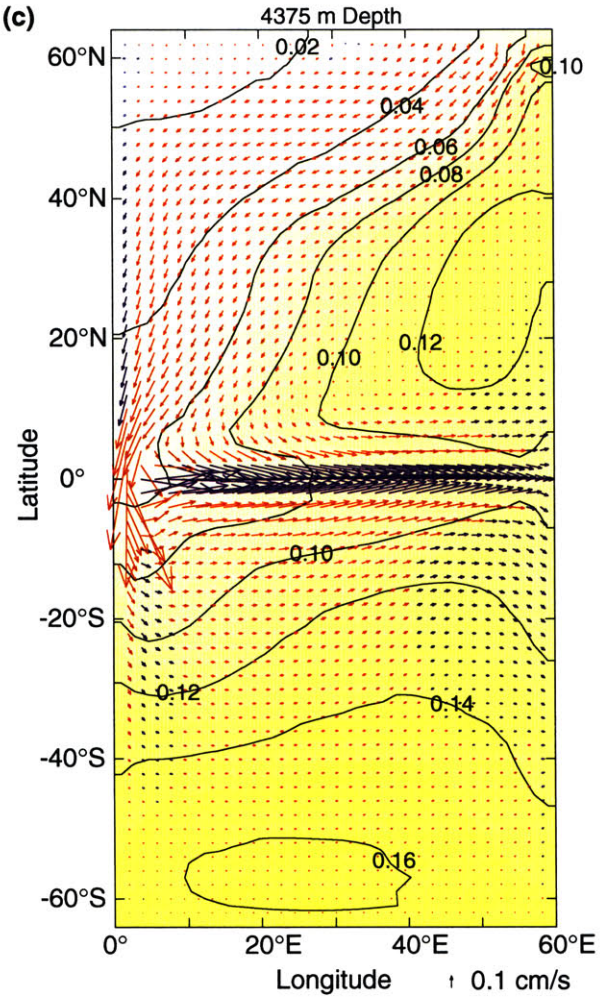

sphere's deep mixed boundary layers conveys a greater heat content. Thus, by diverting anomalous flow through the southern hemisphere, the double hemisphere system is able to effectively transport geothermal heat fluxes to the surface through a weaker advective response.

Anomalous intrahemisphere flow in the abyss is weak, as shown in Fig. 4.13c. As compared to the single hemisphere run, the flow pattern in the northern hemisphere is little changed except for slightly stronger zonal flow along the equator. In the southern hemisphere, the warming is nearly uniform zonally, with the largest anomalous temperatures at high latitudes. Here, the weak background abyssal flow crosses the equator in the western boundary prior to flowing southeast [Marotzke and Klinger's (2000) Fig. 5b]. In thermal wind balance, the zonal uniformity of the temperature response can not support a strong anomalous meridional overturning south of the equator. However, some of the anomalous flow in the southern hemisphere circulates zonally, rising in the eastern boundary and sinking in the western

boundary, and therefore is not observed in the zonal integral. Along both boundaries, anomalous flow augments the background flow [sinking along the western boundary is necessary for thermal wind balance of the cross-hemisphere meridional overturning circulation (Marotzke and Klinger 2000)].

As confirmation of the arguments presented in this section, we ran two additional double hemisphere geothermal heating runs. In the first, we applied the geothermal heating only in

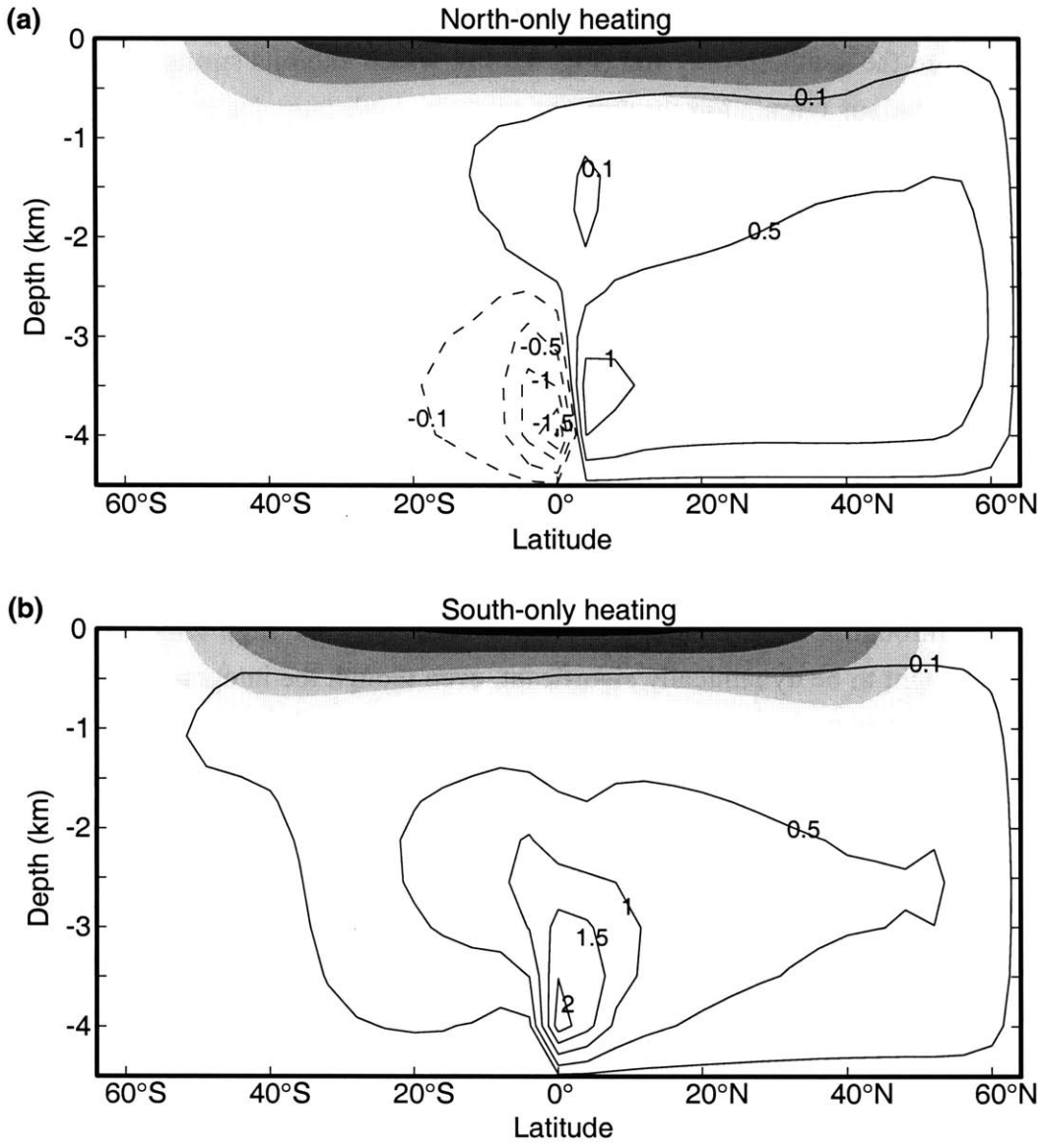

FIGURE 4.14: Anomalous meridional overturning circulation in a double hemisphere basin given (a) geothermal heating of 50 mW m^{-2} in the northern hemisphere, with no geothermal heat input in the southern hemisphere; (b) geothermal heating of 50 mW m^{-2} in the southern hemisphere, with no geothermal heat input in the northern hemisphere.

the northern hemisphere, and in the second we applied the flux only in the southern hemisphere. To lowest order, the response to heating across the full basin can be viewed as the superposition of these separate runs. In the northern-only run (Fig. 4.14a), the counterclockwise cell in the southern hemisphere is more pronounced; here, the deep heating leads to anomalous weak warming in the southern hemisphere abyss, albeit with more zonal structure than when heated directly. The anomalous warming pattern in the northern hemisphere abyss is little changed (not shown). Also note that the extension of the anomalous overturning into the southern hemisphere high latitudes is less pronounced than in Fig. 4.12. Therefore, it is not surprising that stronger anomalous flow into northern high latitudes is observed as compared to the southern-only run (Fig. 4.14b), which exhibits stronger intrahemispheric flow (the anomalous circulation through the northern high latitudes is weaker than the full-basin heating run in both cases, as the area-integrated heat flux is decreased by half). The southern-only run is also notable in that all anomalous downwelling occurs in the northern hemisphere, producing a single overturning cell.

4.5 Summary and Discussion

Our experiments illustrate the effect of geothermal heating on the large-scale circulation in an idealized ocean basin. Prior work has focused on the dynamical response to high temperature venting, which can penetrate to greater heights than either low-temperature venting or warming through a weak conductive flux. Hence, only the high temperature forcing is generally thought to be dynamically significant, even though the integrated heat flux through the low temperature sources is much greater than that of local hotspots (Murton et al. 1999). Both effects are ignored in ocean general circulation models. However, our results suggest that the omission of the low temperature fluxes may be problematic: We find that the integrated effect of uniform weak heating through the ocean bottom produces a significant change in the model's deep circulation, on the order of several Sv. Although the meridional heat transport of the anomalous circulation is insignificant as compared to that of the background surface-forced circulation, the deep circulation may have an important indirect effect on climate through the transport of carbon and other nutrients, which have their concentration maxima at depth.

We find that the model's response to geothermal heating is largely advective, as suggested by the change in the meridional overturning circulation. A simple diffusive response is not realized, which would require a significant perturbation in deep-water properties. In the pres-

ence of a background flow field, heating of the abyss does not occur uniformly; in a rotating system, these anomalous temperature gradients are then balanced geostrophically through anomalous flow. The change in deep circulation is governed by the requirement that the flow communicate the geothermal heating to the surface in order that steady state is achieved. Convecting boundary layers that are coincident with deep mass transport can effectively pipe anomalous heat to the surface, precluding the need for strong anomalous flow at the surface. To lowest order, the geothermal response serves to augment the pre-existing background circulation. A more stratified abyss and/or a stronger background overturning reduce the magnitude of the geothermal response. When geothermal heating is applied to a double hemisphere ocean model, our findings are largely consistent with those in a single hemisphere.

In low latitudes, a maximum in the model's anomalous overturning circulation results from a zonal temperature gradient that is established as deep eastward flow is warmed. All anomalous upwelling (in the zonal mean) occurs adjacent to the equator, although some of this anomalous flow simply recirculates in the tropics. The thermal wind relation can be used to estimate the magnitude of this local maximum, presuming that the background flow and stratification are known. The thermal wind relation also can be used to relate the anomalous overturning strength to zonal temperature gradients at mid- and high latitudes.

Weak geothermal heating at depth is able to drive an anomalous overturning circulation because the heating occurs at low geopotential, thus increasing potential energy. Although geothermal fluxes are much smaller in magnitude than surface heat fluxes, the latter occur at high geopotential and thus require diapycnal mixing in order to drive a meridional overturning circulation.

Without the context of a background circulation, however, uniform geothermal heating is unable to generate a coherent large-scale response. Consider the model's response to geothermal heating in a temperature-only "box" ocean governed by uniform surface forcing. Without an imposed meridional temperature gradient or applied wind stress, the resulting ocean is isothermal and no background circulation is established. If we apply geothermal heating uniformly along the ocean floor, we generate unstable columns of water everywhere. Convective adjustment redistributes this heat throughout the full depth of the water columns, so that at the surface the additional heat is released to the atmosphere. With steady heating from below and restoring at the surface (cooling), every water column is in a constant state of convective adjustment. This configuration closely resembles the classical Rayleigh-Bénard convection problem with rotation (n.b., Emanuel 1994, chapter 3); presumably, with a suffi-

ciently high-resolution model, the steady-state solution would consist of an array of Rayleigh-Bénard convective overturning cells (the wavenumber of these cells would likely be on the order of the ocean depth[11]). Given our limited resolution, however, the convective adjustment parameterization is the only active process in the model, conveying the deep heating directly to the surface. At no time would any large-scale motion occur. From an energetic standpoint, even though geothermal heating embodies the necessary characteristic of heating at low geopotential, in the absence of a forced circulation or maintained stratification it is insufficient to produce a large-scale circulation.

The connection between diffusive heating and geothermal heating as "driving" mechanisms can be extended further. Both produce heating at depth, which can be conveyed back to the surface through convective mixing. The efficiency of convection versus diffusion as mixing processes forms the basis of Rossby's (1965) argument as to why oceans' high latitude sinking is narrow. While we disagree with this conclusion [see also Marotzke and Scott (1999) and chapters 5 and 6], our results corroborate the abstraction of convection as a means by which the ocean can remove heating necessary to sustain motion, whether the heating is diffusive or geothermal.

Our model is highly idealized and is therefore at best only a crude representation of the real ocean, but it is tempting nonetheless to speculate that geothermal heating might similarly affect our oceans' circulation. Although we have not made a direct comparison between our single hemisphere model and the North Atlantic, it is implicit that our model represents a simplified depiction of North Atlantic Deep Water circulation. However, we would be remiss in not pointing out several limitations that obscure how these results might apply to the real ocean. First, our model has no topography; as such, all geothermal heating occurs at a single depth, in contrast with the real ocean where the heating is effectively spread across a wide range of depths. Second, our model has a single source of deep water (even in our double hemisphere configuration), whereas the real ocean is characterized by deep water formation in both the Northern Hemisphere and Southern Hemisphere. Given that much of the deep ocean floor is in contact with the more dense Antarctic Bottom Water rather than North Atlantic Deep Water, we suggest that our model is a actually a better analog of how geothermal heating affects the circulation in the South Pacific, where Antarctic Bottom Water is formed.

[11]The realized form of Rayleigh-Bénard convection in our configuration is not entirely clear; Krishnamurti (1980) found that in certain laboratory configurations with very high Rayleigh number, domain-filling circulations were possible due to up-gradient momentum transport by convection.

Our results also suggest that increased heating along mid-ocean ridges may not be as important as the broadly dispersed conductive heating, but again this requires confirmation in a model with realistic topography. In an idealized model, Thompson and Johnson (1996) show that geothermal heating and/or deep diffusion along the upward (western) slope of a mid-ocean ridge are capable of producing significant geostrophic flow. Our lack of wind forcing and single-basin ocean configuration (i.e., without a circular channel) may also affect the fundamental character of the geothermal response. To this end, the reader is referred to Adcroft et al. (2000), in which the effect of geothermal heating is examined in a more realistic global ocean model.

Chapter 5

Scaling Behavior of the MOC

5.1 Introduction

Although previous studies (e.g., Bryan 1987;Colin de Verdière 1988, Zhang et al.1999; Park and Bryan 2000) have examined the effect of varying κ in ocean general circulation models, the primary goal of these studies was to establish a scaling relationship. Marotzke (1997; hereafter M97) was more ambitious, presenting a closed theory for the MOC, yet he too provided only a cursory look at changes in the circulation and density structure given variations in κ. In the early years of ocean circulation modeling, it was also important to examine the effect of κ variations for model "tuning" purposes; to this day, diffusivity is poorly constrained by observations, and an understanding of how changes in κ affect the large-scale circulation remains a important objective. In contrast to the attention bestowed upon changes in mixing rate, the response to variations in the imposed surface ΔT has received considerably less attention [to our knowledge, this has been examined systematically in only two studies, Zhang (1998) and Huang (1999); other studies have indirectly examined this question using mixed boundary conditions, varying the rate of freshwater forcing]. In this chapter, we will revisit these scaling relationships, but will also more carefully examine changes in the underlying dynamics. Throughout, we will consider the applicability of the self-similarity assumption employed by the scaling argument discussed in chapter 1. By probing the system's behavior across parameter space, we seek a more fundamental understanding of the intrinsic roles played by mixing and surface buoyancy forcing.

A second motivation for this undertaking is that both κ and ΔT are likely to have been different in past climates. Energy for mixing is a function of wind, tidal and perhaps geothermal forcing (Munk and Wunsch 1998; Huang 1999). In an alternative climate state, it is quite possible that wind stresses at the ocean surface were markedly different; moreover, changes

in topography over geologic time scales likely affected the conversion efficiency of wind and tidal forcing into mixing energy. A plethora of paleoclimatic evidence suggests that the equator-to-pole temperature gradient has experienced considerable fluctuation in the earth's past (Crowley 1991), which would change the temperature forcing at the ocean surface. (We do not consider the effect of changes in freshwater forcing, which could also change the meridional gradient of surface buoyancy, as a consideration of mixed boundary conditions is beyond the scope of this thesis.)

By fluxing heat from the mixed layer into the ocean interior, diapycnal mixing raises the center of mass and hence increases potential energy. Unfortunately, beyond this the energetics of the ocean are not well understood. Relatively few studies examine the link between potential energy, available potential energy, and kinetic energy (see Huang 1998), hence a quantitative link between mechanical mixing energy and the ocean energy budget remains a goal for future research (see also Oort et al. 1994; Huang 1999). Our focus here is the large-scale dynamical response to parameterized changes in the diapycnal diffusivity, without regard to energy considerations.

In contrast with diapycnal mixing, buoyancy forcing is not an energy source that drives the MOC, but is clearly an essential component in the generation of a large-scale circulation. For climate modeling purposes, the coupling of the atmosphere to the ocean (i.e., how buoyancy forcing is applied to the ocean model through a surface boundary condition), is critical for development of realistic models. Unfortunately, many oceanographers have a narrow conception of the atmosphere, and the de facto coupling method for temperature is to use a simple restoring surface boundary condition on a timescale of one to three months. This choice poorly simulates the slower rate at which the ocean adjusts to temperature anomalies through radiative processes (Marotzke and Pierce 1997). Although the effect of the restoring timescale has been considered in reference to the stability of the global thermohaline circulation (e.g. Power and Kleeman 1994), its importance in the fundamental dynamics of the MOC has not been established. Accordingly, we seek to answer the following question: Does the manner in which the atmosphere forces the ocean play a fundamental role in ocean dynamics?

In addition to addressing how the large-scale circulation changes across parameter space, we examine how temperature structure is affected. With wind forcing, Samelson and Vallis (1997) suggest that a thermocline depth may be defined from the position of a diffusive "internal" boundary layer at the base of the ventilated thermocline; of course, this presumes that

diffusive mixing is sufficiently weak that the adiabatic ventilated thermocline [as described in Luyten et al. (1983)] is realized. More typically, the thermocline refers to the upper portion of the ocean characterized by rapid changes in stratification (Pickard and Emery 1990). Without wind forcing, however, defining a specific thermocline depth is somewhat problematic. Our experiments in chapter 3 naively assumed that it was possible to define a thermocline depth in terms of a distinction between deep abyssal waters, with water mass properties resulting from deep convection, and that of deep downwelling water. In other words, we are able to define a thermocline given that our simple configuration leads to production of a weakly stratified abyssal water mass. (In fact, one could take our results a step further and define the thermocline as the depth of water over which diapycnal mixing matters for the overturning maximum, although this is of limited practical use in that it requires significant computational trial-and-error). Unless one makes an attempt to distinguish between different water masses and/or changes in stratification with depth, the specification of a thermocline depth is arbitrary. In both the scaling argument and the M97 theory, for example, the assumption is that temperature decreases exponentially with depth, which suggests no particular justification for any specific thermocline depth. If the distinction between water masses is important, neither analytical treatment is able to capture the dynamical significance.

In section 5.2, we begin with a systematic series of experiments that explore the effect of changing the model's diapycnal diffusivity while holding all other parameters constant. All experiments in this chapter were run using our standard single hemisphere configuration. Scaling relationships for overturning streamfunction and meridional heat flux are computed, followed by a scaling of several proxies for thermocline depth. We extend parameter space over nearly five decades, considerably further than that of previous studies. In section 5.3, we repeat these scaling analyses across a decade of imposed surface ΔT. In the simulations presented in these two sections, the surface layer is restored using a 3-day timescale[12], which essentially prescribes SST. The effect of the surface restoring timescale is addressed separately in section 5.4. To the best of our knowledge, this is the first study that attempts a scaling analysis using (nearly) imposed SSTs, which restricts the dynamics of the MOC to its most rudimentary incarnation. The chapter ends with a summary of our major conclusions and a discussion of these results.

---

[12]In runs with $\kappa \geq 400 \times 10^{-4}$ $m^2 s^{-1}$, we reduced the restoring time-scale to 1 day. This adjustment was necessary in order to maintain SSTs close to the prescribed profile, due to the marked increase in circulation intensity.

5.2 Scaling Behavior with κ

5.2.1 Overturning Streamfunction and Meridional Heat Transport

A plot of the meridional overturning streamfunction maximum at high latitudes, the overturning maximum adjacent the equator, and the maximum meridional heat flux as a function of κ is shown in Fig. 5.1. Also displayed (to the right of the plot) are the least-squares, power law curve fits as computed over the range of $\kappa = 5 - 80 \times 10^{-4}$ m^{2}s^{-1} (our reasons for restricting the curve fit to this sub-range will soon become apparent). Remarkably, the three series show a nearly perfect linear fit over the first three decades. For $\kappa > 1000 \times 10^{-4}$ m^{2}s^{-1}, the overall maximum in overturning migrates toward the equator; in this range, values of both the heat flux and (overall) overturning maximum fall slightly below their respective curve fits. It is noteworthy, however, that the scaling of the overturning maximum roughly agrees with the predicted $\kappa^{2/3}$ power law relation (see chapter 1) across the full range of parameter space. The extreme mixing scenario at the rightmost edge of this plot reflects the limit where diapycnal mixing operates with the same order of efficiency as convective mix-

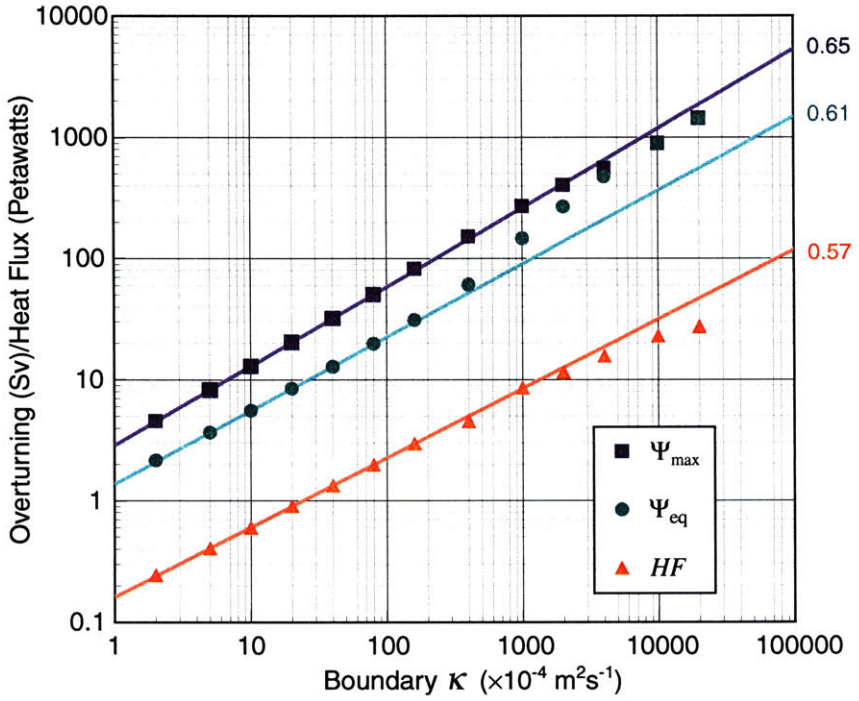

FIGURE 5.1: Plot of (overall) maximum meridional overturning streamfunction, maximum streamfunction at the equator, and the maximum meridional heat flux as a function of diapycnal diffusivity κ. Least-squares power law curve fits over the range $\kappa = 5 - 80 \times 10$ m^{2}s^{-1} are shown to the right of the plot.

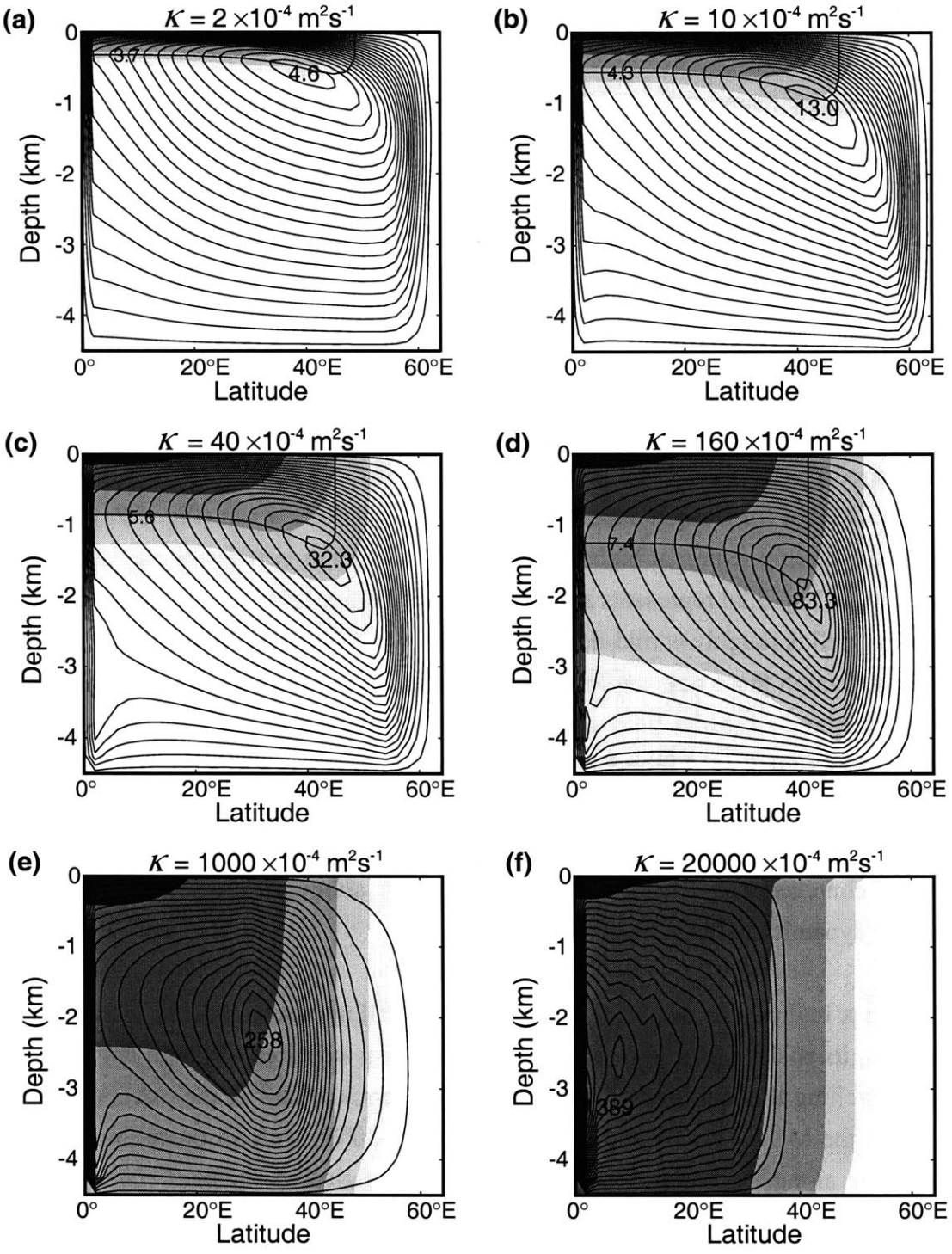

FIGURE 5.2: Meridional overturning streamfunction (contours) and zonally averaged temperature (shading), given (a) $\kappa = 2\times10$ m^{2}s^{-1}; (b) $\kappa = 2\times10$ m^{2}s^{-1}; (c) $\kappa = 2\times10$ m^{2}s^{-1}; (d) $\kappa = 2\times10$ m^{2}s^{-1}; (e) $\kappa = 2\times10$ m^{2}s^{-1}; (f) $\kappa = 2\times10$ m^{2}s^{-1}. The contour interval is 5% of the maximum overturning (indicated at cell center, in Sv), with the center contour at 97.5%. Isotherms (shaded) are at 0.05, 0.1, 0.2, 0.4, and 0.8 of ΔT=27°C. The isotherm of T_* (see definition in text) along the eastern boundary is plotted in (a)-(d).

ing[13]. This limit of similar convective and diapycnal mixing efficiency was examined, albeit with a much weaker mixing efficiency, in Marotzke and Scott (1999).

The overturning streamfunction and zonally averaged temperature for selected runs is shown in Fig. 5.2. To lowest order, the overturning circulation appears self-similar except for the extremely high mixing run (Fig. 5.2f), assuming one is willing to overlook the increasing depth of the cell center. The self-similarity is consistent with the corresponding power law fits for the equatorial and maximum overturning strength in the lower decades of κ.

We suggest that the overturning behavior can be divided into two regimes. In the low κ regime (Figs. 5.2a-5.2c), which includes the range of κ thought to reflect the real ocean's mixing efficiency, the depth of the overturning cell maximum increases in tandem with the zonally averaged thermocline. The latitude of the overturning cell center is little changed between runs except for a slight southward shift in the weakest κ run (Fig. 5.2a). Hence, the width of the sinking region at higher latitudes is also similar between these runs. The overturning plot in Fig. 5.2d represents a transition to the high κ behavior. Here, the center of the overturning cell is roughly at mid-depth, and a distinct thermocline becomes more difficult to resolve. Although these runs are less likely to have direct relevance for the real ocean, they are of interest to the broader field of geophysical fluid mechanics. We consider these runs to be approaching what is referred in the literature as the low Rayleigh number limit (the Rayleigh number is defined as $\alpha g \Delta T H^3 / \nu \kappa$, where H is the ocean depth and ν is kinematic viscosity). This limit has been investigated both numerically and in laboratory experiments in varying contexts (e.g., Rossby 1965; Rossby 1998), although here we add the complexity of rotating dynamics to the system.

In the high κ regime, the center of the overturning cell moves southward with increased κ, maintaining its position at mid-depth. Although sinking still occurs at high latitudes, there is less downwelling that contributes to the meridional circulation. In the extreme mixing run (Fig. 5.2f), the MOC only extends to approximately 30°N, with all upwelling located in a narrow zone along the equator. Convection at high latitudes becomes more widespread; north of the MOC, the ocean consists of quasi-isothermal columns that undergo constant convective adjustment. Although there is no net meridional overturning circulation at these latitudes, a large zonal overturning circulation is present, with upwelling and downwelling at

[13]Klinger et al. (1996) inferred from their non-hydrostatic, three-dimensional numerical experiments that convection is adequately parameterized by $\kappa = 10\ \mathrm{m^2 s^{-1}}$, only slightly above the maximum parameterized value of κ examined in these experiments.

the western and eastern boundaries, respectively. At $\kappa = 1000 \times 10^{-4}$ $m^2 s^{-1}$, variability sets in, with an approximate 10% and 20% standard deviation in the overturning maximum and maximum meridional heat flux, respectively. As a result, Figs. 5.2e and 5.2f show only a "snapshot" of the flow and temperature structure. By examining the behavior after a small perturbation[14] in the system's state variables, we confirmed that these very high κ runs were chaotic: for several years, the results with and without the perturbation were identical, but diverged thereafter.

Our explanation for this variability is as follows. As κ is increased, the increased upwelling of cold water in the tropics and northward advection of warm surface currents temporarily results in surface temperatures far from the restoring profile; large heat fluxes into (out of) the surface are then required to warm (cool) the surface back to this profile. Consequently, the surface boundary condition changes in character from being more like a prescribed boundary condition (i.e. Dirichlet) to that of fixed surface flux (i.e., Neumann). We speculate that as our surface restoring condition approaches a near-constant surface flux, it is not able to fully damp out growing modes that are baroclinically unstable in the western boundary current (Colin de Verdière 1999), even though the model's resolution only permits length scales that are much greater than the internal radius of deformation. In similar series of experiments with increased grid spacing, we found that the transition to chaos occurred at a higher value of κ. This result is consistent with our speculation, given that the resolution of length scales closer to the deformation radius allows for greater growth rates.

Although, these low Rayleigh number runs warrant further investigation, given their limited context to our actual ocean, our focus hereafter is on understanding the behavior in the low κ regime. Moreover, given that all rising motion occurs in an equatorial boundary layer, it is uncertain whether our limited resolution here is affecting these high κ results.

In Fig. 5.1, note that the scaling relations for the three quantities are not *exactly* equal, as would be implied by the scaling laws discussed in Chapter 1. Overturning at the equator scales with a slightly lower power law than the cell maximum, which we attribute to a slight increase in high latitude recirculation with κ (i.e., with little or no cross-isopycnal component). Accompanying this increase is a shift in the orientation of the maximum streamfunction contour from nearly horizontal in Fig. 5.2a to "vertical" (in appearance only, given the plot's aspect ratio) in Fig. 5.2d. Since the overturning through low latitudes gives rise to me-

[14]This small perturbation was accomplished by integrating over a short period using a reduced time step for the thermodynamic equations.

ridional heat transport, the latter's scaling law is also less than that of Ψ_{max}. What is perhaps surprising is that the heat flux scaling is lower still, with a power law of $\kappa^{0.57}$.

In the literature there has been considerable speculation as to what the heat flux scaling "should be," with many researchers examining whether the scaling was equal to that of the overturning maximum (Bryan 1991; Winton 1996). M97 calculated a scaling law of $\kappa^{1/2}$, and suggested that meridional advection of warm surface waters to high latitudes essentially reduced the top-to-bottom temperature difference acted upon by the MOC. Park and Bryan (2000) carried this idea further, including a "correction factor" in the scaling which took account of the change in realized surface ΔT as κvaried across parameter space. Their "corrected" results suggested that the $\kappa^{2/3}$ power law implied by the scaling arguments was indeed appropriate. Here, our very rapid surface restoring essentially imposes ΔT, yet our scaling is identical to Park and Bryan's uncorrected scaling result. Moreover, the temperature of our coldest abyssal water (or equivalently, the coldest surface temperature) changes very little for $\kappa \leq 40 \times 10^{-4}$ m^{2}s^{-1}, yet the scaling behavior is not demonstrably different for larger κ,in which the bottom water temperature is a function of mixing strength. Although there are notable differences between our model configurations, in particular due to our boundary mixing implementation, our results imply that the dynamics are less straightforward than suggested by Park and Bryan.

The surface layer meridional velocity in the western boundary current as a function of latitude is shown in Fig. 5.3a. The peak value of these curves scales almost exactly to the 1/3 power, as would be suggested by the (1.4). However, in addition to being "stretched" in magnitude, the latitudinal extent of a vigorous western boundary current increases with κ. In other words, as the MOC becomes stronger, the "separation[15]" of the western boundary current occurs increasingly to the north [this was also noted in Zhang et al. (1992)]. Moreover, observe that the aforementioned transitional behavior between low and high κ regimes occurs when the western boundary current reaches the northward extent of the model, implying a link between the vertical temperature structure and the surface horizontal flow. Note that it is only the meridional velocity at the western boundary that exhibits the latitudinal stretching; the zonal mean meridional velocity, as shown in Fig. 5.3b, appears to leading order to be stretched only in magnitude for $\kappa \leq 20 \times 10^{-4}$ m^{2}s^{-1}. For larger κ, the zonal mean velocity

[15] The western boundary current "separation" is a subject that has been examined extensively in the literature, and is commonly believed to be a function of topography and perhaps wind-forcing. We do not wish to imply any link between the "separation" observed here and that of more realistic modeling studies.

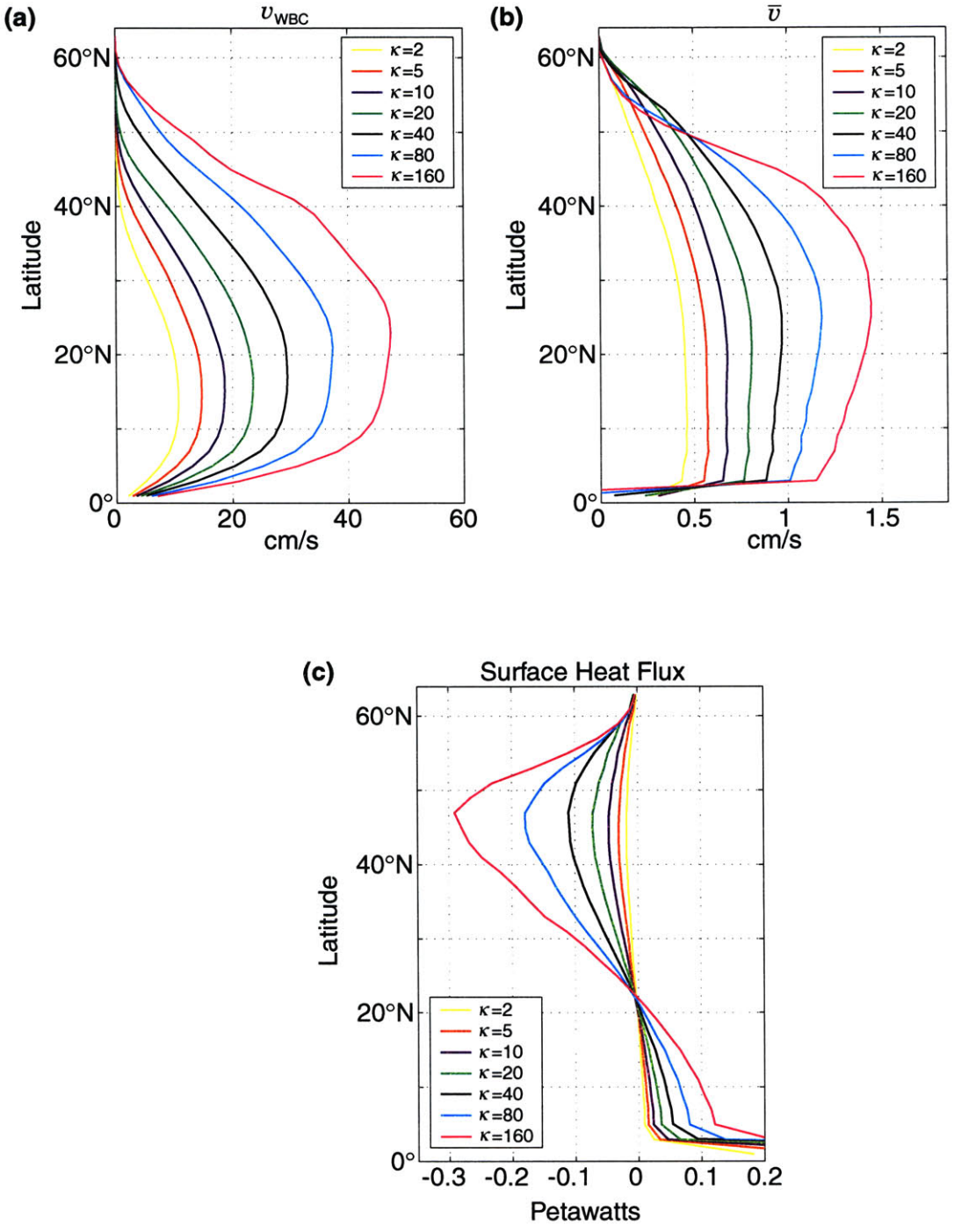

FIGURE. 5.3: (a) Plot of the surface layer meridional velocity at the gridpoint adjacent to the model's western boundary, as a function of latitude, over the range of κ shown; (b) plot of zonally averaged meridional velocity in the surface layer; (c) profile of zonally integrated surface heat flux exchanged to the "atmosphere" via the restoring boundary condition.

actually *decreases* at northern latitudes, with a more noticeable peak occurring at mid-latitudes.

Unlike the western boundary current, the zonally integrated surface boundary heat flux is remarkably self-similar over $\kappa = 2 - 160 \times 10^{-4}$ m^{2}s^{-1}, as shown in Fig. 5.3c. If scaled with κ to the 0.57 power, these curves are nearly co-incident. The crossover between surface heat input into the ocean and heat release occurs slightly northward of 20°N, near the peak in curves shown in Fig. 5.3a. The ramifications of this self-similar behavior will be discussed more fully in chapter 6.

5.2.2 Thermocline Depth

Both the scaling laws and the Marotzke theory suggest that the thermocline scale height should increase as $\kappa^{1/3}$, half that of the overturning scaling. For physical insight into the large-scale response as diapycnal mixing is increased, and why the thermocline depth exhibits a weaker response, consider the following feedback loop:

increased $\kappa \rightarrow$ greater penetration of warm water $\rightarrow$ strong zonal flows over an increased depth
$\rightarrow$ increased flow into the eastern boundary $\rightarrow$ increased downwelling at the eastern boundary
$\rightarrow$ increased depth of large E-W temperature differences $\rightarrow$ increased MOC $\rightarrow$ increased upwelling in tropics

The last step in this loop partially offsets the ability of increased diffusive fluxes to effect an increase in the thermocline depth, so that we expect a relatively weak scaling relationship.

As mentioned in the introduction, how one defines a thermocline depth is ambiguous yet seemingly important in the context of the dynamics. The most common way of defining a thermocline depth for scaling purposes is to compute a "potential energy efficiency," i.e., a quantity proportional to potential energy divided by depth-integrated temperature:

$$\frac{\int_{\text{bottom}}^{\text{top}} (T - T_{\text{bottom}})\, z\, dz}{\int_{\text{bottom}}^{\text{top}} (T - T_{\text{bottom}})\, dz} \tag{5.1}$$

(5.1) is typically computed over a low or mid-latitude column of water (e.g., Park and Bryan 2000). If the temperature structure exhibits simple exponentially decay with depth, (5.1) evaluates to:

$$\frac{D\left(n+1-e^{n}\right)}{1-e^{n}} \tag{5.2}$$

where D is the advective-diffusive scale height and n is the number of scale heights over the full depth of the ocean. Across the portion of parameter space where the ratio of the thermocline to ocean depth is small (i.e., large n), (5.2) is a reasonable approximation of D. The physical significance is less clear as this ratio becomes small. This quantity has been shown in some studies to scale roughly as $\kappa^{1/3}$, i.e., that predicted by the scaling relation, although there is no reason *a priori* that it should scale to the same power law as the level of no motion.

Here, we will investigate the scaling of the following measures of thermocline depth:

- D_* - zero-crossing depth in the tropics, with the temperature here denoted T_*
- D_Ψ - depth of the overturning maximum at the cell center (as measured by the depth of the contour given by $0.975\times\Psi_{max}$ in the thermocline, which allows for a more precise measurement)
- D_T - depth of zero vertical velocity on the eastern boundary at the latitude where T_* outcrops
- D - advective-diffusive scale height, as measured by the slope of $\mathrm{Log}(T-T_{bottom})$ from the surface to depth D_T, at the equator
- D_{PE} - calculation of (5.1), using zonally averaged temperature along the equator

Interpreting the dynamical significance of D_* and D_Ψ is straightforward: these are the depths over which east-west temperature differences result in the build-up of meridional shear via the thermal wind relation in the tropics and high latitudes, respectively. In Fig. 5.2, the depth of D_* is indicated by a contour of T_* on the eastern boundary. Note that the contour of T_* dips along with the level of vanishing meridional velocity at mid-latitudes and appears to bisect the "center" contour of the overturning cell. Although there appears to be a weak dependence of T_* on κ, with T_* outcropping further north with weaker mixing, we find it striking that

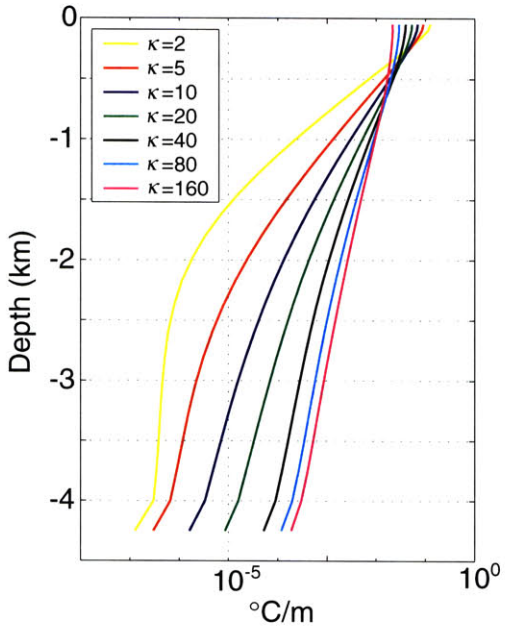

FIGURE 5.4: Plot of vertical potential temperature structure $\partial T/\partial z$ (in °C m^{-1}) versus depth, as measured at mid-basin along the equator.

to leading order the meridional position of the cell maximum occurs where T_* outcrops. In chapter 6 we will explore whether this result is fundamental to a thermodynamic conceptualization of the MOC.

The third measure of thermocline depth D_T is the most subjective, but this definition is the only one which attempts to recognize a distinction between abyssal and thermocline water masses. Our choice of T_* in this definition is somewhat arbitrary, although the aforementioned correlation between the outcrop of T_* and the center of the overturning cell has physical appeal. In the weakest mixing runs, it is possible to distinguish a transition in the plot of $\partial T/\partial z$ (Fig. 5.4) at mid-depth. However, given our limited resolution and the difficulty in using this observation to define a precise depth, we chose instead to focus our efforts on relating the thermocline depth to the downwelling branch of the MOC. At high latitudes, an area of sharp stratification is easily discerned on the eastern boundary due to the convergence of downwelling water over upwelling waters, as shown in Fig 3.1b. Upwelling water has abyssal water mass properties, which are determined as some mixture of water mass properties from deep convection and deep downwelling (Marotzke and Scott 1999). Except for the northernmost grid points (which downwell into the abyss), the downwelling water on the eastern boundary exhibits water mass properties of thermocline water. These descending columns of water at high latitude (or more specifically, north of the overturning maximum)

are unstratified until they approach the point of vanishing vertical velocity, accounting for the peak in stratification (in runs without high latitude mixing, as those examined in chapter 3, the stratification occurred in a thin internal boundary layer; similarly, a more sharply delineated zone of stratification was also apparent in our uniform mixing run). The measured value of D_T in our control mixing run ($\kappa = 10 \times 10^{-4}$ m^{2}s^{-1}) was 1300 meters, which is close to our effective depth choice in chapter 3 for our weak and strong deep mixing experiments. Recall that below this depth we had concluded that changes in diapycnal diffusivity had little effect on the circulation through the thermocline.

By defining the advective-diffusive scale height D over depth D_T, we are in effect examining the temperature structure across the thermocline water mass. Strictly speaking, denoting this quantity as a "scale height" presumes that the vertical velocity w is constant through this depth. We know from Fig 3.10b that this is a poor assumption, as there is horizontal convergence below and divergence above the depth D_*. It is difficult to estimate precisely how this variation in w affects our measurement of D; our aim is to minimize the "error" by applying a least-squares fit across the full thermocline depth. Close agreement between our observed scale height and a similarly computed slope of Log($\partial T/\partial z$) is observed, giving some measure of confidence as to the significance of D (i.e., these would be identical given pure exponential decay). In short, we suggest that the tropical temperature structure in the thermocline can be well approximated by exponential decay with depth.

The scaling behavior of D_*, D_Ψ, D_T, D, D_{PE}, and T_* is shown in Fig. 5.5. All show a reasonable linear fit over this range of κ (except perhaps the data points at the extremes), in view of the fact that precise measurement of several of these quantities is somewhat difficult. Note that the scaling of D_* and D differs, in contrast with the implicit assumption employed in the scaling law argument (see chapter 1). However, the computed power laws for D_* and D_Ψ are quite close to the predicted value of 1/3 suggested by scaling law. Both D_T and T_* show a weaker power law dependence. While it is not completely surprising that the power law for these two are similar (i.e., given that D_T is computed at a location determined by T_*), the near-equality suggests a dynamical link. As κ increases, the depth of the abyssal water mass decreases, allowing for less build-up of shear at depth; accordingly, T_* must also increase, as more shear is now required through the bottom portion of the thermocline. As suggested by (5.2), D_{PE} scales roughly with D for low κ but increases more slowly for higher κ, i.e., as thermocline depth starts to become a more significant percentage of the ocean depth.

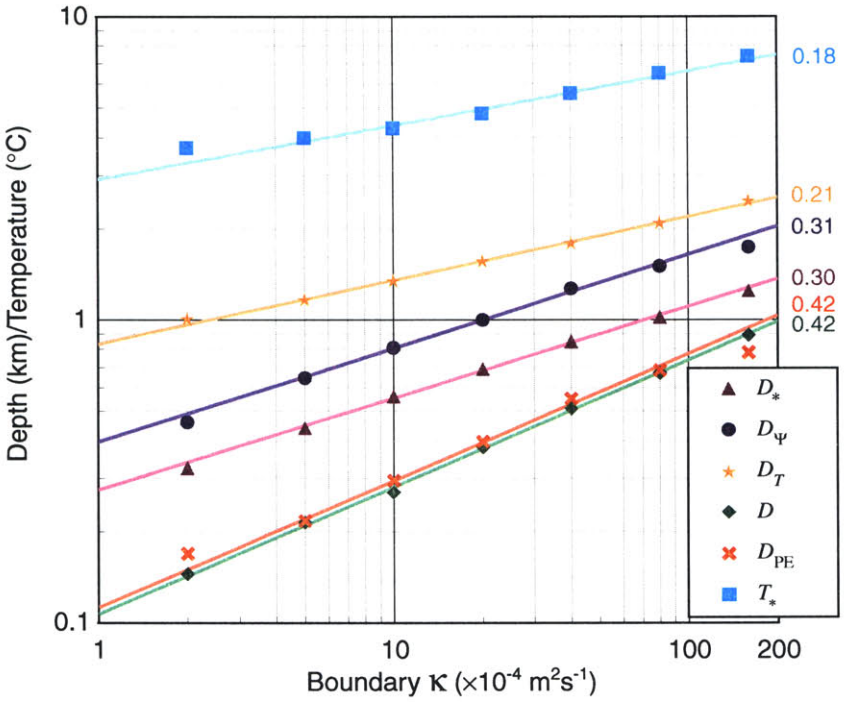

FIGURE 5.5: Plot of several measures of thermocline depth and T_* (see text for definitions) as a function of diapycnal diffusivity κ. Least-squares power law curve fits over the range $\kappa = 5 - 80 \times 10$ m^{2}s^{-1} are shown to the right of the plot.

Fig 5.6a shows the profile of $T_{\text{East}} - T_{\text{West}}$ through the center of the overturning cell, with the position of the $0.975 \times \Psi_{\max}$ contour on these curves marked by a '×' (so that the upper marking indicates the depth D_Ψ and the depth between these markings indicates a region of weak meridional velocity). Notice that to leading order, the peak in $T_{\text{East}} - T_{\text{West}}$ is independent of κ. For the lower values of κ, there is a slight decrease in the maximum $T_{\text{East}} - T_{\text{West}}$ as the peak occurs at lower depth, although the trend is broken for the two highest values of κ shown. In these runs, which are near the transition to the high κ regime, $T_{\text{East}} - T_{\text{West}}$ remains measurable in the abyss, while negative values of $T_{\text{East}} - T_{\text{West}}$ occur near the surface. The general similarity of the curves and the respective position of D_Ψ (i.e., slightly below the peak in the $T_{\text{East}} - T_{\text{West}}$ curve) suggests how the $\kappa^{2/3}$ scaling law comes about, as the maximum in Ψ is built up by integrating twice over the thermal wind relationship (M97):

$$\Psi_{\max} = \int_{D_\Psi}^{0} \bar{v}\, dz = -\frac{g\alpha}{\rho_o L_x} \int_{D_\Psi}^{0} \int_{D_\Psi}^{0} \left(T_{\text{East}} - T_{\text{West}}\right) dz dz \tag{5.3}$$

where $\bar{v}$ is the zonally averaged meridional velocity. Given that $T_{\text{East}} - T_{\text{West}}$ appears to leading order to be stretched in the vertical, the scaling is $\Psi_{\max} \sim D_\Psi{}^2 \sim \kappa^{2/3}$. In contrast, the

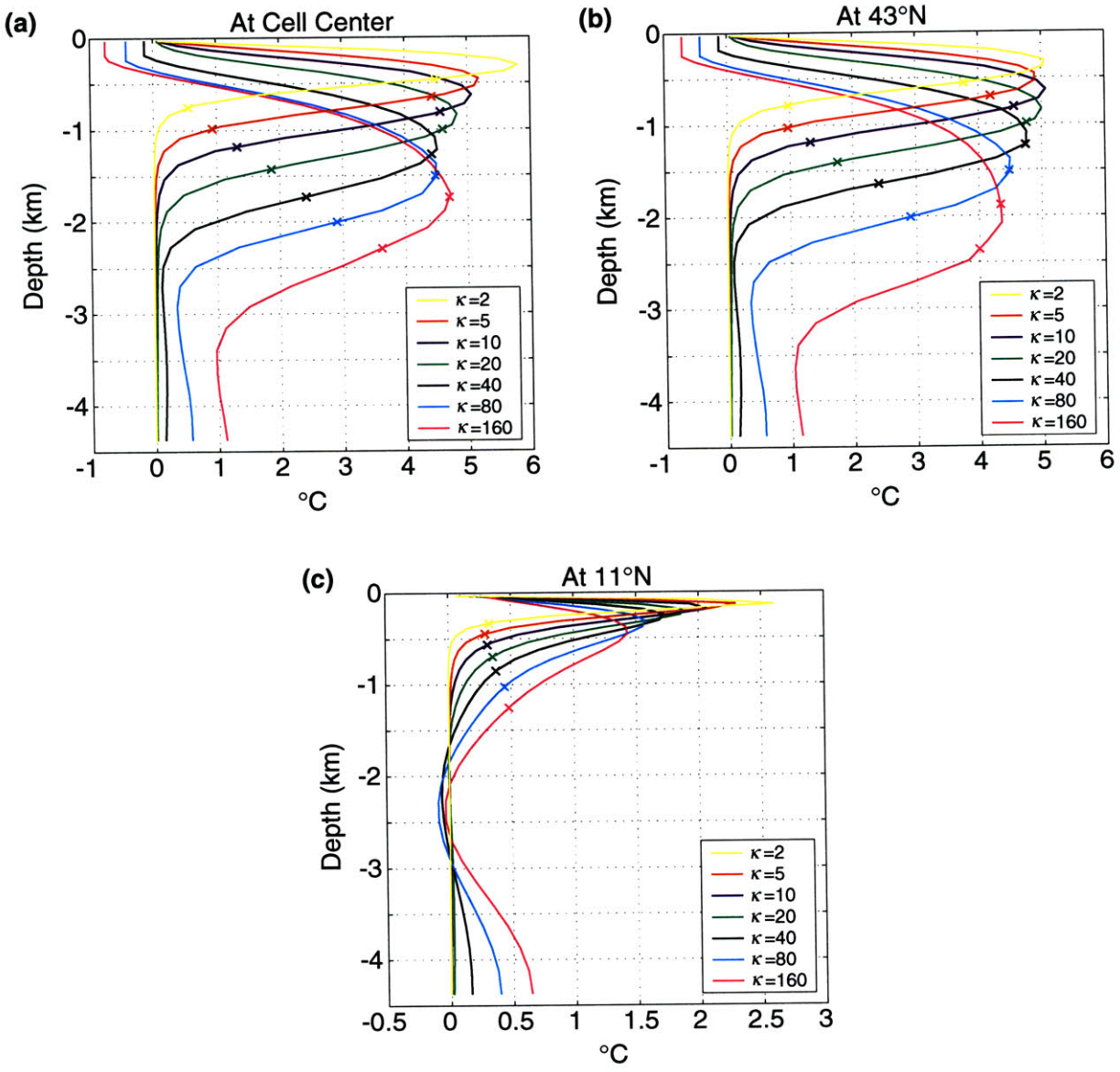

FIGURE 5.6: (a) Vertical profile of $T_{\text{East}} - T_{\text{West}}$ at the latitude given by the center of the overturning cell. The locations of the two '×' markings denote the position of the $97.5\% \times \Psi_{\max}$ contour, delineating the region of vanishing (zonally averaged) vertical velocity (so that the upper '×' marks the depth of D_{Ψ}. (b) Same as (a), except as observed at 43°N. (c) Same as (a), except as observed at 11°N. In (c), the '×' shows the depth of the tropical level of no motion D_*.

lower marked depth changes its relative position on the curve with increased κ. With weak mixing and hence a deeper abyss and weak overturning, the southward meridional velocity at depth is quite feeble and subsequently only a modest non-zero $T_{\text{East}} - T_{\text{West}}$ results in shear necessary to reverse the direction of $\overline{v}$. Conversely, with a shallow abyss and hence strong deep southward flow, the lower marking is located much higher on the curve.

The profile of $T_{East} - T_{West}$ is also shown at two specified latitudes: at 43°N (Fig. 5.6b), near the center of the cell, and at 11°N (Fig. 5.6c). In the tropics, it is less clear why the scaling of Ψ is so clean; $T_{East} - T_{West}$ is not simply stretched with increased κ, but exhibits a significant decrease in its peak value. At 43°N, the plots appears quite self-similar, even more so than observed in Fig. 5.6a (again, the large κ behavior deviates from pattern). This result seems to suggest that the system's behavior on the eastern and western boundaries is governed by similar dynamics as a function of latitude (and therefore surface temperature). The meridional positioning of Ψ_{max} is then dictated by these profiles and the requirement that southward flow at depth balance northward flow through the thermocline.

5.3 Scaling Behavior with ΔT

5.3.1 Overturning Streamfunction and Meridional Heat Transport

Fig. 5.7 shows the scaling behavior as the imposed equator-to-pole ΔT is varied over a decade (in the model we ignore phase changes of seawater, including the effects of sea ice). The quantities plotted appear to scale linearly over this range of ΔT. Immediately, we see that there is a contradiction between our results and that predicted by both the Marotzke theory

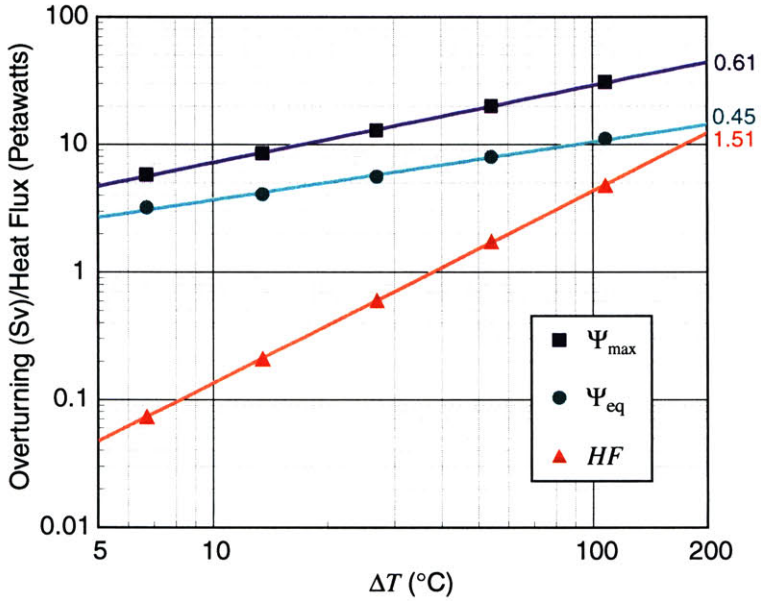

FIGURE 5.7: Plot of (overall) maximum meridional overturning streamfunction, maximum streamfunction at the equator, and the maximum meridional heat flux as a function of the restoring equator-to-pole temperature difference ΔT. Least-squares power law curve fits are shown to the right of the plot.

and the scaling argument, which suggest a $\Delta T^{1/3}$ relation for Ψ_{max}. Although our computed power law at the equator is closer to the predicted value, it would still seem overly optimistic to say that either analytical treatment captures the observed scaling behavior. The scaling of the maximum meridional heat flux is consistent with the mass transport scaling results, given that the heat flux should scale roughly as $\sim \Psi \Delta T$. The actual heat flux scaling falls between that implied by the two overturning power law exponents, which suggests that some of the high-latitude overturning operates across a considerably weaker thermal gradient.

The behavior of the zonally averaged overturning across this range of ΔT is captured in Fig. 5.8. Several trends are apparent. Most noticeably, the thermocline thins as overturning

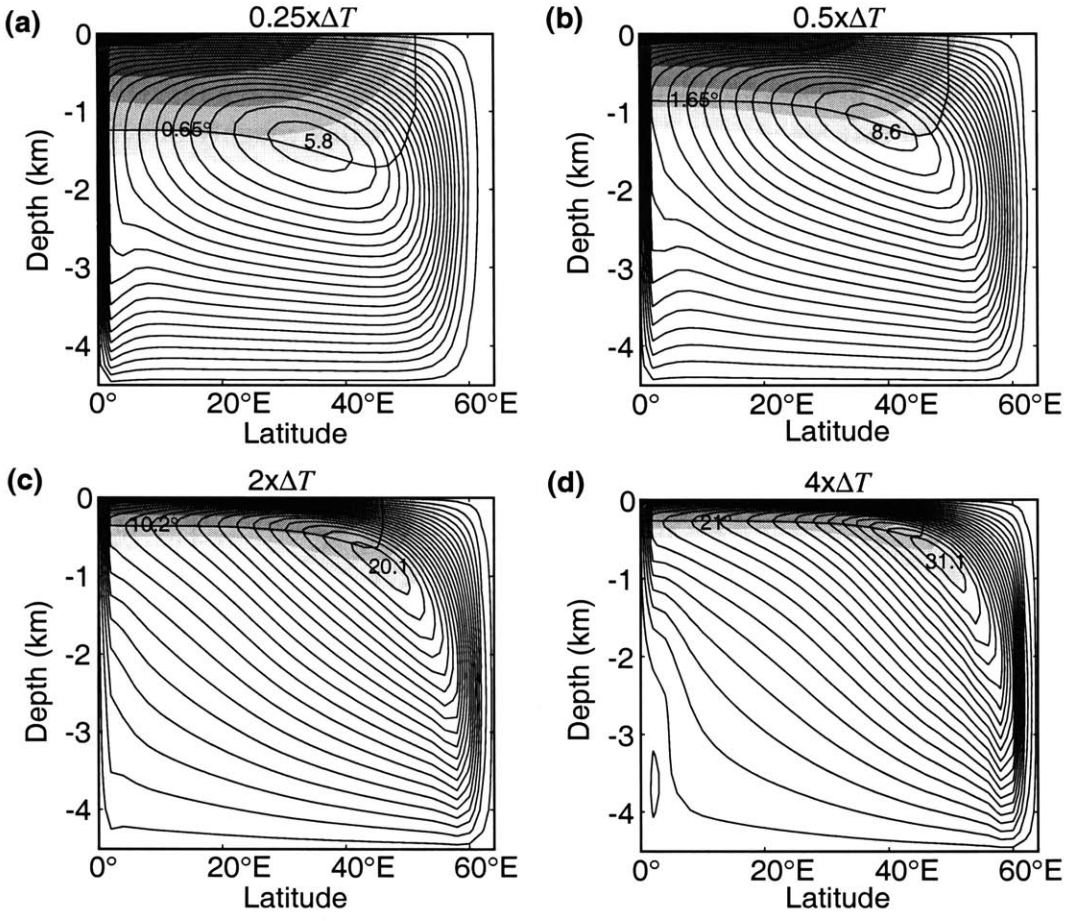

FIGURE 5.8: Meridional overturning streamfunction (contours) and zonally averaged temperature (shading), given (a) $\Delta T = 0.25 \times 27°C$; (b) $\Delta T = 0.5 \times 27°C$; (c) $\Delta T = 2 \times 27°C$; (d) $\Delta T = 4 \times 27°C$. Boundary κ was set to a constant value of 10×10 $m^2 s^{-1}$ in these runs. The contour interval is 5% of the maximum overturning (indicated at cell center, in Sv), with the center contour at 97.5%. Isotherms (shaded) are at 0.05, 0.1, 0.2, 0.4, and 0.8 of ΔT. The isotherm of T_* (see definition in text) along the eastern boundary is also shown, as labeled.

is strengthened (i.e., with increasing ΔT), in contrast with the behavior given increasing κ. As before, the increase in overturning occurs in conjunction with a shift in the primary orientation of the cell center from horizontal to vertical. A more pronounced northward shift in the position of the cell center is also apparent as ΔT is increased.

Apparently, this disparity between the predicted and observed scaling behavior has not been acknowledged in the literature, as we are aware of only two studies that even address this question through numerical experimentation. In a single hemisphere model with uniform diapycnal diffusivity, Zhang (1998) examined the scaling of maximum overturning at each latitude. Over a decade of ΔT, his power law fit roughly agrees with our result at the equator, but he found an even weaker relation in the sub-tropics, and therefore concluded that his results were consistent with the scaling argument. We suggest that Zhang's scaling at fixed latitudes obscures our more fundamental result, in light of the cell center's northward tendency with ΔT. Huang (1999) also looked at the scaling behavior across a range of ΔT in a similarly configured general circulation model (here, we refer to his prescribed κ experiments), suggesting that his observed $\Delta T^{1.43}$ scaling of heat flux roughly obeyed the scaling argument, but also noted that his $\Delta T^{0.552}$ scaling of overturning maximum hinted instead at a $1/2$ power law. (This result was tangential to the main focus of Huang's paper, and as such was not pursued any further).

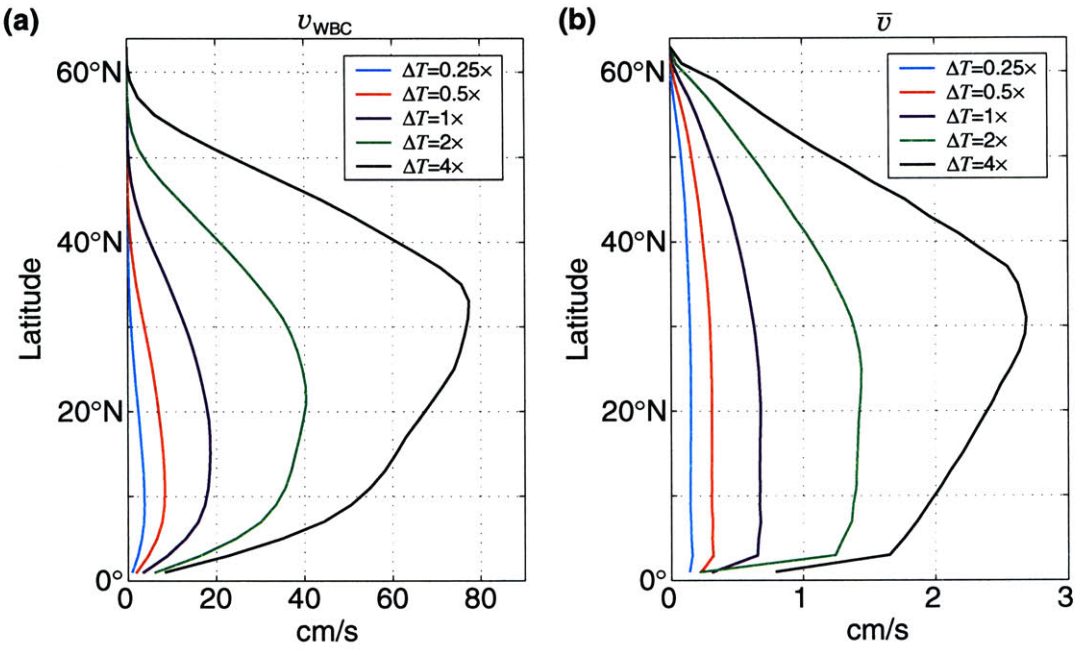

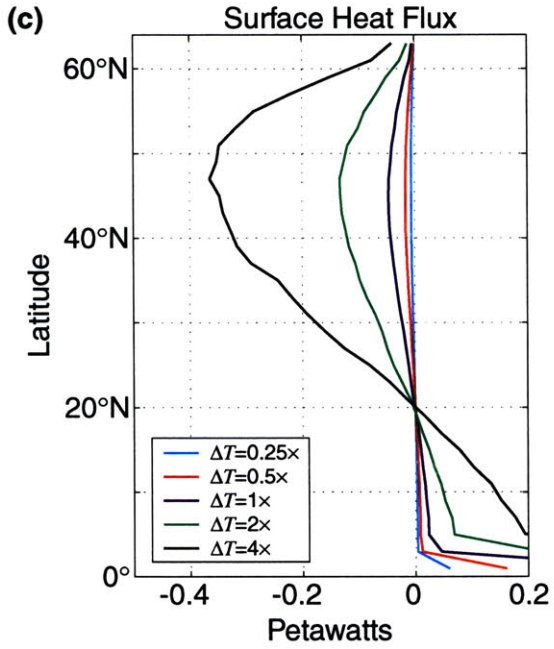

FIGURE.5.9: (a) Plot of the surface layer meridional velocity at the gridpoint adjacent to the model's western boundary, as a function of latitude, over the range of ΔT shown; (b) plot of zonally averaged meridional velocity in the surface layer; (c) profile of zonally averaged surface heat flux exchanged to the "atmosphere" via the restoring boundary condition.

Figs. 5.9a and 5.9b show the scaling behavior of the western boundary current, the zonally averaged meridional velocity, and zonally integrated surface heat flux, comparable to Figs. 5abc, respectively. Similar with the κ scaling behavior, stronger overturning produces an increasingly northward "separation" of the western boundary current. Here, the shape of the curves in Fig. 5.3a and 5.3b are less ostensibly similar, with a more pronounced peak in these profiles with greater imposed ΔT. The peak northward velocity in the western boundary current scales as $\Delta T^{1.1}$, quite different from the predicted $2/3$ power lawsuggested by (1.4). Despite these noted differences in the latitudinal profile, the profiles of surface heat flux in Fig. 5.9c are again remarkably self-similar, with a co-incident crossover between heat uptake and heat loss at about 20°N.

5.3.2 Thermocline Depth

With changes in the pole-to-equator temperature gradient, the scaling laws predict that the thermocline scale height should decrease as $\kappa^{-1/3}$. The behavior as ΔT is increased can be summarized as follows:

increased ΔT → stronger horizontal temperature gradients in the thermocline → stronger zonal flows → increased flow into the eastern boundary → increased downwelling at the eastern boundary → larger E-W temperature differences → increased MOC → increased upwelling in tropics

Unlike the feedback loop for increases in κ, the behavior for increased ΔT does not begin with a change in the depth of the thermocline. Hence, the stronger overturning circulation and accompanying increase in tropical upwelling serves to decrease the effective thermocline depth. Given this decrease in thermocline depth, downwelling at the eastern boundary is less able to penetrate to depth; thus, it is not clear *a priori* whether an increase in the magnitude of the east-west temperature difference or a broader depth of large temperature contrast has greater effect in increasing circulation with increasing ΔT.

The scaling of our defined thermocline measures with ΔT (and "normalized" T_*, i.e., scaled to account for the differences in ΔT) is shown in Fig. 5.10. In general, the linear fit achieved here is not quite as good as in the respective plot for varied κ (Fig. 5.5). The exception is D_{PE}, which exhibits a better linear fit, which we attribute to the relatively thin thermocline (as compared to the ocean depth) in these runs. Nevertheless, there remains a difference between the scaling of the advective-diffusive scale height D and D_{PE}, and both of these exhibit power laws well below the predicted value of -1/3. The difference between the maximum

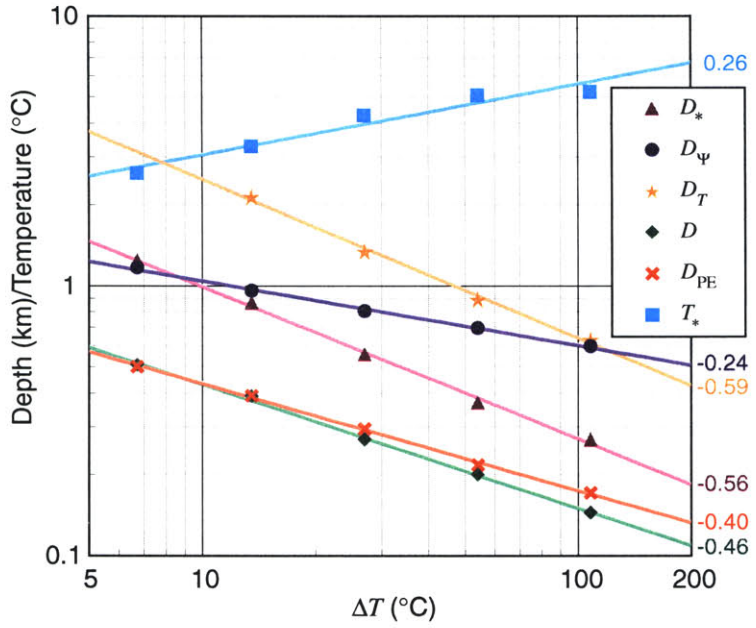

FIGURE 5.10: Plot of several measures of thermocline depth and T_* as a function of ΔT. Least-squares power law curve fits are shown to the right of the plot.

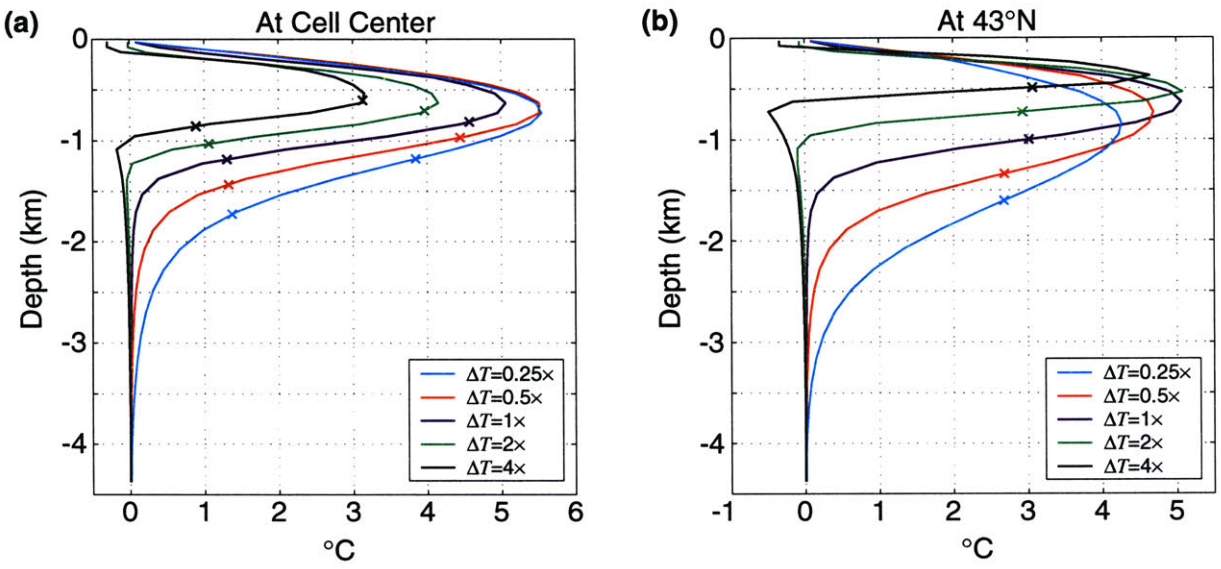

FIGURE 5.11: (a) Vertical profile of normalized $T_{\text{East}} - T_{\text{West}}$ at the latitude given by the center of the overturning cell. The locations of the two '×' markings denote the position of the $97.5\% \times \Psi_{\text{max}}$ contour, delineating the region of vanishing (zonally averaged) vertical velocity. (b) Same as (a), except as observed at 43°N; here, the single '×' shows the approximate depth of vanishing vertical velocity, as the $97.5\% \times \Psi_{\text{max}}$ contour does not extend to this latitude in the two extreme runs.

overturning at the equator and Ψ_{max} is reflected in the power law fits of D_* and D_Ψ respectively: D_* decreases more rapidly with increased ΔT, implying a decreased depth over which meridional shear is attained in the tropics, resulting in the weaker scaling of the equatorial streamfunction maximum in Fig. 6. D_T also decreases slightly faster than $\Delta T^{-1/2}$, which suggests a corresponding rapid increase in the depth of the abyssal water mass. Unlike the thermocline depth measures, T_* increases with ΔT, similar to that when increased diapycnal diffusivity led to a more vigorous overturning. It is unclear whether this change in T_* is well captured by a power law, given the rather poor fit.

Fig. 5.11a shows the profile of normalized $T_{\text{East}} - T_{\text{West}}$ (i.e., divided by the multiplicative increase or decrease in ΔT) for these runs at the cell center. A systematic decrease in the peak value is observed, except for the transition to lowest ΔT. This decrease is perhaps surprising, given that the computed power law in Fig. 5.7 is higher than that predicted by the scaling laws. In other words, one might expect to see non-similar behavior that would account for the more vigorous MOC as ΔT is increased. We attribute this observed change to the northward trend in the cell center with increasing ΔT; in comparison, recall that the meridional position of cell center varied little with κ. Conversely, at 43°N there is much weaker disparity in the peak magnitudes of these curves.

The other noticeable difference between Fig. 5.11a and the similar figure given variations in κ (Fig. 5.6a) is that while the profiles are of similar form, the curves do not intersect in the upper few hundred meters. Moreover, the depth of the peak value changes little between runs. In Fig. 5.11b, which shows $T_{\text{East}} - T_{\text{West}}$ at 43°N, the depth of the maximum changes more noticeably between runs. As in Fig. 5.11a, however, the curves are more nearly coincident near the surface. Accordingly, the vertical extent of the large $T_{\text{East}} - T_{\text{West}}$ region in both plots is much narrower with large ΔT. Since the maximum in Ψ is built up as a double integral of $T_{\text{East}} - T_{\text{West}}$, the shape of this profile is relevant; a narrow profile is most like a delta function profile, with vertical shear concentrated in an internal boundary layer, resulting in the maximum build-up of Ψ.

5.3.3 Varying both ΔT and κ

We equilibrated four additional runs, completing a 3x3 matrix with κ=5, 10, and 20×10^{-4} m^{2}s^{-1} using surface forcing of 0.5×, 1× and 2×ΔT, in order to examine the ΔT scaling relationships at an alternate value of diapycnal diffusivity. Over this more limited range of parameter space, the fitted power laws were broadly consistent with those in Figs. 5.7 and 5.10, suggesting that these relationships are not a function of parameterized mixing strength. Similarly, the power law fits for κ increases at 0.5× and 2×ΔT were broadly consistent with those in Figs. 5.1 and 5.5.

More interesting is an exploration of the synergy in responses brought about by changes to both parameters. Because both κ and ΔT obey a nearly identical overturning power law, doubling one parameter while halving the other serves to maintain the circulation intensity (Ψ_{max}= 13.0, 13.0, and 13.9 Sv along the cross-diagonal of the matrix) despite a sharp change in the thermocline depth. Conversely, by doubling both parameters the advective-diffusive scale height is maintained—notice that the power laws for D are of similar magnitude but opposite sign in Figs. 5.5 and 5.10—while the overturning increases by a factor of approximately $4^{2/3}$.

5.4 Effect of Surface Restoring Timescale

5.4.1 Varying τ

By increasing the coupling timescale of the surface restoring (τ), the ocean is allowed to self-advect temperature in the surface layer, allowing for a temperature feedback which has been shown to be important in stabilizing the thermohaline circulation (Zhang et al. 1993; Rahmstorf and Willebrand 1995; Marotzke and Stone 1995). Here, we will focus instead on the more fundamental dynamical changes that result as surface restoring is weakened.

Northward advection of warm waters in the western boundary current is the most noticeable change with weaker restoring, resulting in higher temperatures at high latitudes. In addition, in tropical regions of strong mixing the surface temperature is effectively colder, as the atmosphere can not keep pace with the diffusion of heat into the thermocline. The overall result is a weaker realized ΔT, resulting in a diminished meridional heat flux as τ is increased (Fig. 5.12). In the limit of small τ, the curve appears to converge; the difference in peak meridional heat flux between fully prescribed SSTs and surface restoring with τ set to 3 days is only 0.002 PW. In the extreme where τ is set to 450 days, the range in surface temperature is reduced by about 7°C, resulting in a considerably weaker meridional heat flux.

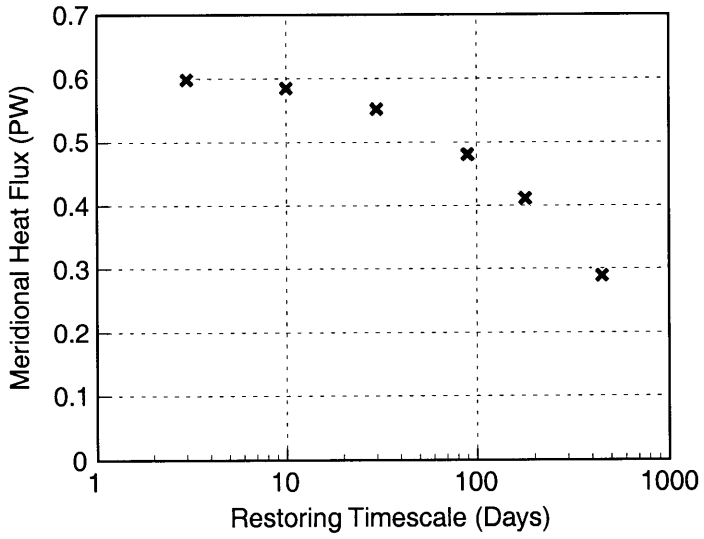

FIGURE 5.12: Plot of maximum meridional heat flux, as a function of the surface temperature restoring timescale.

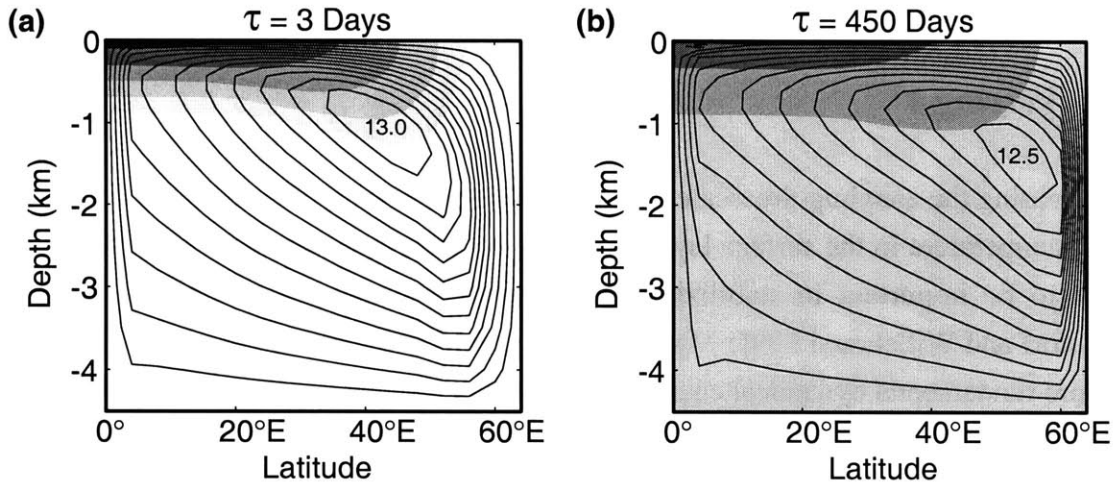

FIGURE 5.13: Meridional overturning streamfunction (contours) and zonally averaged temperature (shading), given (a) restoring timescale of 3 days; (b) restoring timescale of 450 days. The contour interval is 1 Sv. Isotherms are at 0.05, 0.1, 0.2, 0.4, and 0.8 of (restoring profile) ΔT=27°C.

A comparison of the zonally averaged MOC for the two extremes is shown in Figs. 5.13a and 5.13b. Despite a significant difference in the temperature structure, Ψ_{max} is little changed between runs (nor is it appreciably different anywhere along this spectrum of choices for τ). Since the circulation adjacent to the equator is comparable between runs, i.e., the near-equality is not accomplished through an increase in high latitude recirculation, it would appear that with weaker restoring the system is able to more efficiently convert potential energy generated by (weaker) diapycnal heat fluxes into a large-scale meridional motion. In comparison, when we effectively decreased the system's heat uptake in chapter 3 by localizing all diapycnal mixing (likewise producing cold SST anomalies where mixing occurs), the overturning circulation was sharply reduced.

The most striking difference in these plots of overturning is the northward position of the MOC. With strong restoring, we have previously shown that downwelling in the zonal average occurs across the northernmost 10-20° of the model (Figs. 5.2 and 5.8), except as noted in the very high κ regime. With weak restoring, however, all sinking into the abyss occurs in the northernmost grid points; here, deep sinking relocates from the eastern boundary to the middle of the model's back "wall" as τ becomes large, as shown in Figs. 5.14 and 5.15. Also note the difference in convective activity in Figs. 5.14a and 5.15a; with weak restoring, the depth of mixed layers is much reduced (in both runs, deep convective mixing occurs sporadically on the western side of the model's northern boundary, but is not captured during this "snapshot"). We speculate that the aforementioned improvement in efficiency occurs be-

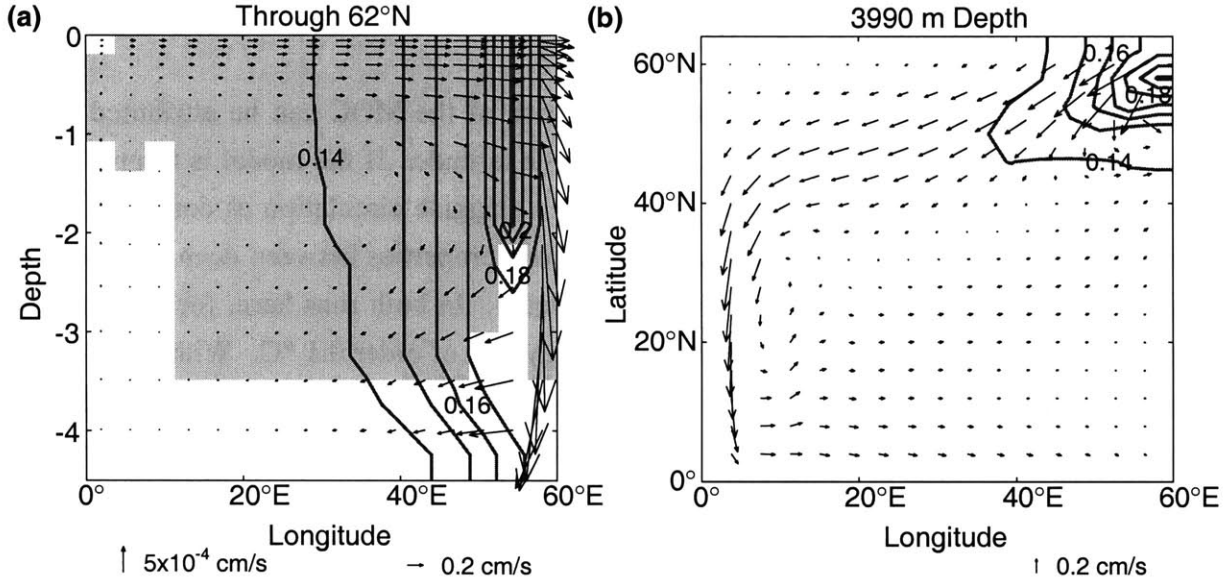

FIGURE 5.14: Temperature (contours) and circulation given a surface temperature restoring timescale of 3 days. (a) Zonal slice along the model's back wall; (b) Plan view of bottom layer. The contour interval in both plots is 0.01°C. Convective activity is indicated by shading.

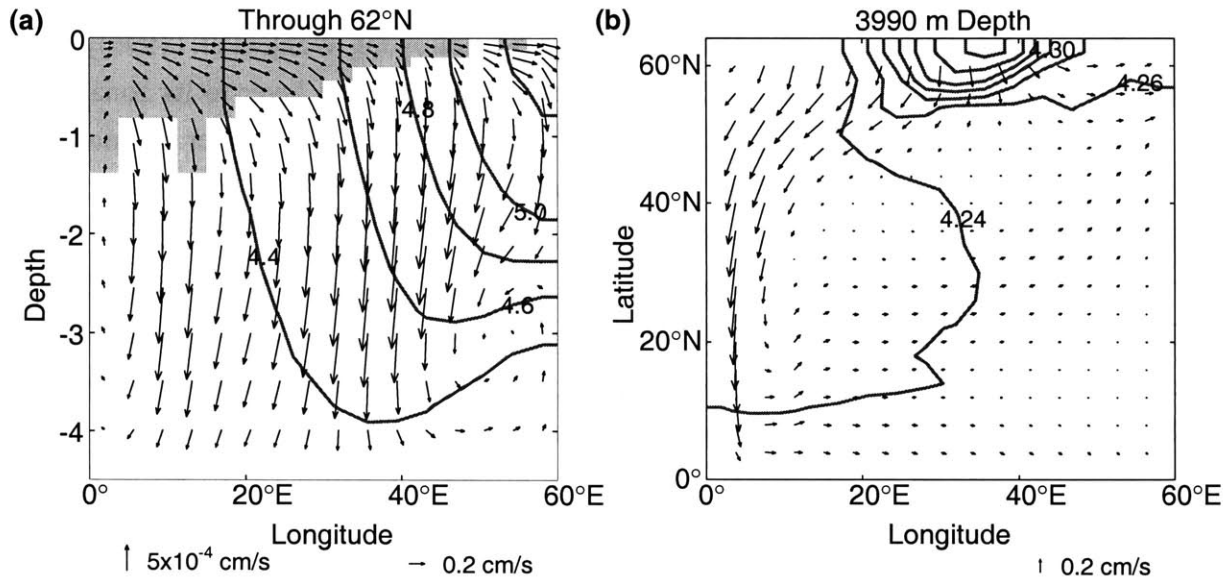

FIGURE 5.15: Same as Fig. 5.14, except using a restoring timescale of 450 days. The contour interval is 0.2°C in (a) and 0.02°C in (b).

cause convective activity weakens, inasmuch as convection removes potential energy from the system.

The shift in the location of the downwelling branch of the MOC can be attributed to the change in the pattern of surface temperature at high latitude. If the model is to produce an abyss with weak horizontal gradients (and hence a sluggish circulation as compared to the flow in the thermocline), the difference in water mass properties between deep downwelling and deep convective mixing cannot be too significant. In both runs here, for example, the horizontal variation in temperature in the bottom layer is of order 0.1 °C. With weak restoring, advection of warm water into the northeast corner results in a more substantial zonal temperature gradient in the upper waters at high latitudes. If this warm eastern water were subsequently injected into the abyss, relatively large horizontal gradients would occur, resulting in a significant enhancement of the deep circulation. Instead, deep downwelling occurs nearer to the site of deep convective mixing, so that the aforementioned small horizontal temperature variation is realized. Because the presence of a boundary is essential to the downwelling process (Colin de Verdière 1988; Marotzke and Scott 1999; Spall and Pickard 2000), all sinking must then be located adjacent to the model's northern boundary.

We ran an additional run with a more realistic atmosphere-ocean coupling, restoring to a "effective" atmospheric temperature profile with larger ΔT [following Wang et al. (1999)], using a 450 day restoring timescale. In addition, we restored the surface layer to its zonal mean using a 60 day timescale, following Kamenkovich et al. (2000). The former simulates the slow radiative adjustment of the ocean (with the atmosphere's meridional heat transport reflected in the choice of restoring profile), whereas the latter process simulates the ability of the atmosphere to disperse local SST anomalies, a much faster process (Marotzke and Pierce 1997). At steady state, the realized ΔT and meridional heat flux were comparable to our strong restoring run, with a 1 Sv increase in Ψ_{max}. Similar to our other 450-day restoring run, sinking was localized at mid-basin along the northernmost boundary (not shown).

5.4.1 Varying κ using a 30-day Restoring Timescale

We repeated the series of runs across parameter space in κ using a 30-day restoring timescale. The scaling results are shown in Fig. 5.16. Overturning streamfunction increases somewhat more slowly than with 3-day restoring in the lower κ regime (over which the curve fit is applied), but remains close to the predicted $^2/_3$ power law across parameter space. The scaling of meridional heat flux is markedly weaker, closer to the $^1/_2$ law favored in M97 (this

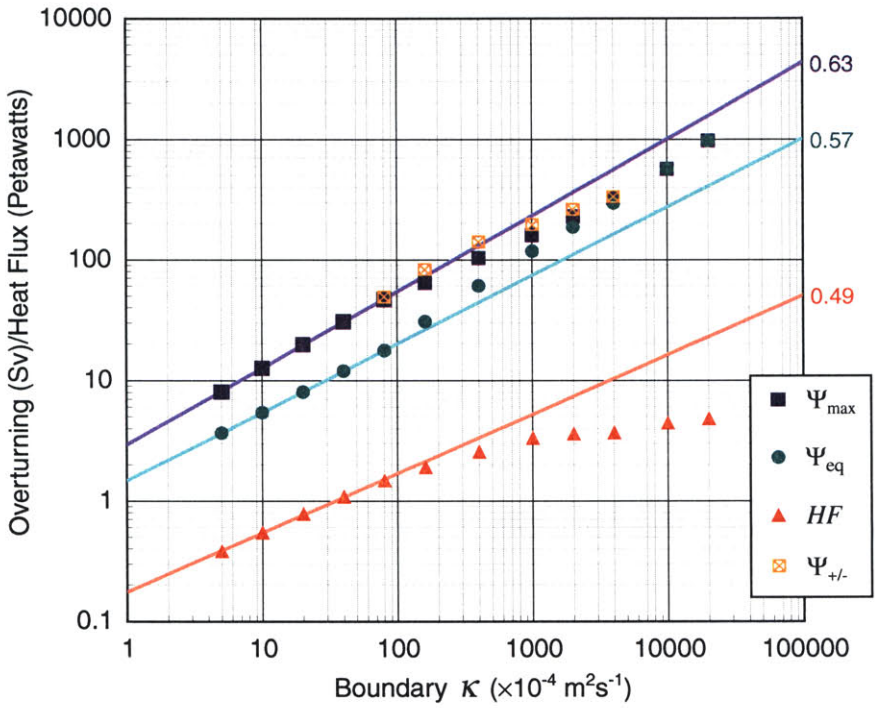

FIGURE 5.16: Same as Fig. 5.1, except here all runs employed a 30-day restoring timescale. The additional series $\Psi_{+/-}$ indicates the total downwelling at high latitudes, as computed by adding the direct MOC overturning to the indirect high latitude overturning (where present).

is not coincidental, given that Marotzke used a similarly configured model with a 30-day restoring timescale).

As the diapycnal diffusivity is increased into the higher κ regime, the increased penetration of the western boundary current results in progressively warmer conditions in the northwest corner, shutting off deep convection. Meanwhile, deep downwelling spreads southward along the eastern boundary in conjunction with stronger zonal flows, with deep convection occurring in the northeast corner. As a result, at high latitudes it becomes warmer along the west than in the east, supporting a reverse circulation. Adding the zonally averaged reverse circulation to the direct MOC gives an indication of the total downwelling (as plotted by the orange symbols in Fig. 5.16). It appears that the expansion of the reverse circulation comes at some expense to the direct circulation, although the total downwelling is increased (as suggested by their location about the curve fit). At very high κ, the reverse circulation diminishes in intensity, in tandem with the spread of deep convective activity throughout high latitudes.

Associated with this high latitude behavior is a regular 15-year oscillation, as diagnosed in M97 [a similar oscillation was noted by Fanning and Weaver (1997)]. At $\kappa = 80 \times 10^{-4}$ m^{2}s^{-1}, this oscillation is damped out as steady state is reached. At $\kappa = 160 \times 10^{-4}$ m^{2}s^{-1}, a very regular 15-year oscillation is self-sustained, associated with a regular waxing and waning of the reverse circulation between 12 and 26 Sv. As κ is increased further, the circulation becomes increasingly chaotic. At $\kappa = 1000 \times 10^{-4}$ m^{2}s^{-1} the reverse circulation completely vanishes for intermittent periods, and disappears entirely given even larger κ.

5.5 Summary and Discussion

A detailed scaling analysis of the MOC's response to variations in diapycnal mixing and equator-pole temperature gradient has been presented. These results are followed by some additional experiments with weaker surface buoyancy restoring, which allow for non-linear interaction with the ocean circulation.

For values of $\kappa < 160 \times 10^{-4}$ m^{2}s^{-1}, we find that the overturning exhibits "similar" behavior, as suggested by our examination of $T_{\text{East}} - T_{\text{West}}$ at the cell center, the horizontal position of the cell center (i.e., the width of the sinking region), and the zonal mean profile of surface heat exchange. Although the depth of the thermocline increases in conjunction with κ, the limitation of fixed ocean depth is not critical until a higher range of κ values. We also find that the northward penetration of the western boundary current increases with κ. In contrast, given changes in the imposed ΔT, the system does not exhibit similar behavior except in the profile of surface heat exchange. In these runs, the sinking region of the circulation becomes increasingly narrow as ΔT is increased, and the changes in $T_{\text{East}} - T_{\text{West}}$ at high latitudes are less easily understood.

We find that the scaling of maximum overturning increases obeys an approximate 2/3 power law with both κ and ΔT. This scaling with κ has been reported before in the literature (e.g. Park and Bryan 2000). In contrast, our result with ΔT is not only novel, but also does not agree with the power law predicted by the scaling argument. At face value, our similarity "assessment" would seem to explain this scaling discrepancy, as the scaling argument would apply only if the behavior were similar across parameter space. However, we find additional behavior not explained by the scaling argument, even in the low κ regime where the scaling argument seemingly applies. In particular, the advective-diffusive scale height increases

more rapidly than the predicted 1/3 relation; instead, we find that the depth of the level of no motion more nearly obeys this power law, which directly accounts for Ψ_{max}'s 2/3 law through a double integration of the thermal wind relation. Moreover, we find the 2/3 law is obeyed well into the high κ regime, where the response to changes in κ is fundamentally different. Hence, we conclude the "success" of the scaling argument is largely fortuitous.

Given the disparity in scaling between the advective-diffusive scale height and the level of no motion, the Marotzke (1997) theory is better suited than the scaling argument to capture the dynamical behavior of the MOC. However, the ad-hoc choice for the depth of the level of no motion (i.e., the $2|z_\rho|$ vertical scale used in the double integration of the thermal wind relation) is ultimately a function of the tropical stratification, which in turn is governed by advective-diffusive balance, so it is not altogether surprising that the theory gives rise to similar scaling predictions as the scaling argument. Hence, the Marotzke theory also fails to capture the scaling behavior given variations in ΔT.

The response of the ocean to changes in the equator-to-pole temperature gradient is an important question in the study of climate. Our results suggest that an increased gradient would lead to a significant increase in ocean circulation and meridional heat flux. This increase in heat flux would then serve to reduce the gradient, acting as a strong negative feedback. We caution, however, that our results presume sufficient energy is available so as to maintain our prescribed diapycnal diffusivity. Using a similarly configured model, Huang (1999) examined the effect of varying ΔT while prescribing a constant vertical profile of energy flux for mixing. For some parameter choices, his results showed the opposite behavior: circulation weakened with increased ΔT [a similar result was found by Lyle (1997), albeit using a crude box model]. Our study sheds light on why this behavior occurs. With a fixed energy flux, increases in the vertical gradient of temperature decreases the effective κ, which in turn serves to further increase $\partial T/\partial z$ in the upper portion of the water column and hence weaken κ further. We have previously demonstrated in this thesis (see chapter 3) that thermocline mixing is critical in order to generate a vigorous MOC. This glaring contradiction in results certainly warrants future study; in particular, it would seem a more fundamental understanding of ocean energetics is essential in order to unlock the riddles of our climate system.

When we weaken surface restoring while holding κ constant, we find a strong decrease in the maximum meridional heat flux, as would be expected given the realized decrease in ΔT. More surprisingly, we find that overturning is maintained, despite a marked change in temperature structure and the narrowness of sinking. These changes in ocean dynamics suggest

that the atmosphere-ocean coupling is important in determining ocean dynamics, and vice-versa. Hence, "realistic" ocean models that employ a rapid (e.g. 30-60 day) restoring boundary condition are not likely to accurately portray aspects of the real ocean. For process models of the ocean circulation, such as that used in this study, the use a time-scale on the order of months is in some ways counterproductive; the more fundamental processes which drive the MOC in the limit of prescribed SSTs are obscured, yet this boundary condition is a poor approximation of the true atmosphere-ocean coupling process.

The constancy of the MOC intensity given variations in the coupling timescale is remarkable, particularly in light of the observed changes to the temperature structure. This outcome would seem to suggest that any approach that makes use of the temperature structure to estimate overturning circulation is inherently flawed! The change in the narrowness of sinking also requires an explanation; recall that Stommel's (1962) pipe-model study concluded that the narrowness of sinking was not a function of the surface temperature gradient, in contrast with the results here. We will revisit these questions in the context of the ocean thermodynamics in chapter 6.

Chapter 6

Summary and Conclusions

6.1 Summary

A series of numerical experiments examining the roles of diapycnal mixing and buoyancy forcing in generating a MOC have been presented using a highly idealized, single-hemisphere ocean model. In accord with long-held thermodynamic ideas (Sandström 1908), we find that in the absence of wind forcing a steady-state MOC can only be driven by diapycnal mixing or deep buoyancy forcing. Without an imposed pole-equator temperature difference, however, deep heating does not produce a large-scale circulation; instead, these buoyancy fluxes are communicated to the surface (where they can be "radiated" to the atmosphere through the surface boundary condition) through convective mixing. Diapycnal mixing in the tropical thermocline communicates the surface buoyancy fluxes into the interior, which in turn increases potential energy. In conjunction with convective mixing at high latitudes, the penetration of heat leads to horizontal temperature gradients beneath the surface. In geostrophic balance, these temperature gradients generate strong zonal flows into the eastern boundary that subsequently downwell, leading to an east-west temperature difference that provides the vertical shear necessary for the MOC (Zhang 1992; Colin de Verdière 1993; Marotzke 1997). Thus, both of these forcing mechanisms require that surface buoyancy fluxes impose a density gradient between the equator and the pole in order to generate a large-scale circulation.

In the model, mixing at mid- and high latitudes is not critical in order to generate a MOC, given that surface temperatures there are relatively low and hence diffusive heat fluxes are much weaker than in the tropics. As required by conservation of planetary vorticity, vortex stretching or compression in the ocean interior is accompanied by meridional flow; here, we find that vortex compression in the thermocline effectively restricts the communication of

warms waters to the eastern boundary, and therefore interior mixing is less effective at driving a vigorous MOC than boundary mixing. Mixing at depth is not required to generate deep flow, and has little effect on the strength of the circulation through the thermocline. In the abyss, downwelling water is relatively warm, but is then cooled through convection and rewarmed through diffusion. Hence, with reduced mixing in the abyss a more homogeneous abyssal water mass is formed.

When the model ocean is forced by deep buoyancy fluxes on the order of our planet's geothermal heating, the resulting anomalous circulation is largely confined to the abyssal water mass, inasmuch as these fluxes are dwarfed in magnitude by buoyancy fluxes through the surface and into the thermocline. In this regard, the role of the thermocline is analogous to that of the stratosphere, in that this sharp zone of enhanced stratification effectively limits the height of any convective penetration from below. Note, however, that at steady state we find that our prescribed geothermal heating is insufficient to maintain convective mixing from below, given an anomalous advective response which increases flow along the ocean floor (i.e., reducing the transit time of a water parcel through the abyss, which in turn lessens its temperature increase). In addition to its dependence on temperature structure, the anomalous circulation is also a function of the circulation generated by diapycnal mixing, with weaker mixing resulting in a more vigorous anomalous overturning circulation. Ultimately, the heat input through the ocean floor must be conveyed to the surface in order for steady-state balance; this occurs in our model by anomalous advection of warmer waters into (high latitude) deep mixed boundary layers, which effectively pipe the heat from depth to the surface. Given the weak stratification across the abyss, the anomalous circulation transports little heat meridionally, although it might be important to climate through its capacity to advect tracers.

In response to variations in either diapycnal diffusivity or imposed equator-pole density gradient, we find that the strength of the MOC can be predicted using an approximate $^2/_3$ power law relation. It is rather surprising that changes to either parameter leads to a nearly identical scaling behavior, especially since they lead to a similar in magnitude yet opposite effect on a measured advective-diffusive scale height in the tropics. Although the scaling behavior of the overturning maximum is quite close to that predicted by scaling arguments and the Marotzke (1997) theory for variations in κ, it does not match the $^1/_3$ power law predicted for changes in ΔT.

It is not clear whether either the Marotzke (1997) theory and/ or the scaling argument accurately captures the dynamical behavior over the lowest decades of κ parameter space, given a

fixed ΔT. In this regime, the horizontal position of the MOC center remains constant, but decreases in depth as the thermocline thickens. At this latitude, the vertical profile of the temperature difference between the eastern and western boundaries appears to leading order to be "stretched" in the vertical in response to changes in κ. It could therefore be argued that the system's behavior across this parameter space is "self-similar" in regard to this critical variable, as would be required by the scaling argument (Park and Bryan 2000). On the other hand, our scaling of the advective-diffusive scale height differs from that of the level of no motion, which are assumed equivalent in the scaling argument. The Marotzke theory has no such stipulation, and in this regard is superior to the scaling argument even though the later quantity is determined through an ad hoc assumption. The Marotzke theory also incorporates the fundamental dynamic behavior into its temperature structure on the east and west boundaries. Our results suggest that simple exponential decay is a reasonable assumption through the tropical thermocline, as implied by advective-diffusive balance, even though vertical velocity is not constant. It is less certain to what extent the mid- and high latitude temperature structure is captured by the theory.

The transition to the high κ regime is marked simultaneously by two developments: the western boundary current reaches the northward extent of the model and the MOC center reaches mid-depth. Given further increases in κ, the center of the overturning circulation advances southward, so that in the limit of extremely high κ all upwelling occurs adjacent to the equator. Despite the transition, the overturning scaling behavior does not change until this upper limit is approached. In this regime, it seems less plausible that either the scaling argument or the Marotzke theory applies, yet it is puzzling as to why the scaling behavior remains little changed.

The behavior exhibited as the surface restoring timescale is increased is equally puzzling. Here, the maximum meridional heat flux decreases sharply in tandem with the decrease in realized ΔT, but the maximum in overturning streamfunction remains nearly constant over the full extreme of parameter space investigated. Given that the ocean's temperature structure is also strongly affected by changes in the surface boundary condition, it is unclear why the overturning maximum remains constant.

Also noted was a general decrease in convective activity with increasing τ, along with a narrowing of the ocean's sinking region. We interpret this response as follows. With weakened surface restoring, the surface pattern of temperature is to large degree governed by surface currents. As a result, the northeastern corner of the model warms due to cross-basin advec-

tion of the western boundary current, with temperatures well above that of waters undergoing deep convection. Although the water mass properties of deep downwelling are warmer than that of deep convective mixing, the difference must be relatively small, or else downwelling would not be able to penetrate to depth. Hence, deep downwelling (which must along occur at a boundary) is located nearby to deep convective mixing, at mid-basin adjacent to the model's northern boundary, rather than spread along the eastern boundary at northern latitudes. The concomitant decrease in convective heat loss contradicts the explanation in Rossby (1965) as to narrowness of sinking. Rossby's argument, which apparently has become standard (Marotzke and Scott 1999), states that convection is an efficient mechanism of heat loss, whereas diapycnal mixing is inefficient and therefore requires a larger area over which to act. Although his argument is also flawed in that it does not distinguish between convection and downwelling, it begs an interesting question: Does convection play an important role in the heat loss of the ocean?

6.2 Thermodynamic Conceptualization

Building on the results in chapters 3-5, we now present an abstract thermodynamic model of the MOC, followed by some speculation related to our observed scaling behavior. Our general approach follows that of Walin (1982), although here we have additional insight gleaned from our suite of numerical experiments

An abstract depiction of the MOC is shown in Fig. 6.1. In Fig 5.3c and Fig. 5.9c we observed that the latitude separating surface heat input and output was little changed between runs, located at approximately 20°N. Here, we consider all diapycnal mixing (and hence upwelling) to occur in this tropical region, where, all heat input occurs, and for simplicity will assume a single surface temperature for this region, T_{tropics}. SSTs are prescribed in mid- and high latitudes as a function of latitude. The heat flux through the surface boundary is given by Q, so that the maximum meridional heat flux is obtained through an area integral of this quantity over the tropical region. We have also shown the position of two isotherms on the western boundary, one at temperature T_* (i.e., the temperature at the depth of no motion in the tropics) and the other at some arbitrary temperature greater than T_*.

In chapter 5, we found that the profile of the zonally integrated surface heat exchange did not change shape given variations in κ and ΔT, but varied in magnitude according to a power law relation. Except for high latitude convection, we assume the interior of the ocean away from

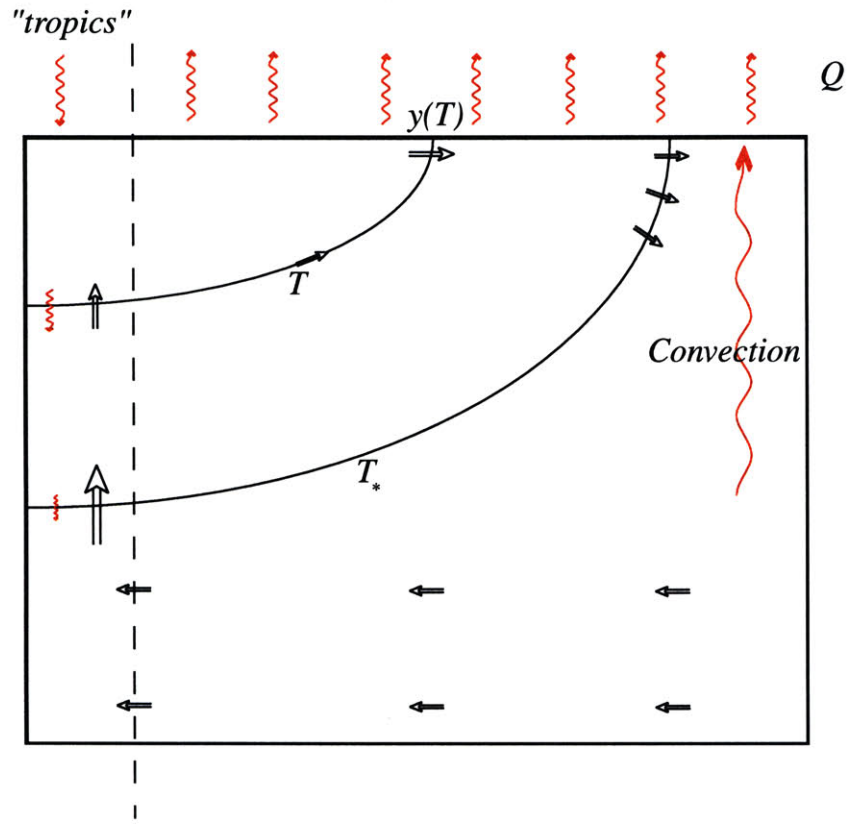

FIGURE 6.1: Conceptual model of the MOC. A heat flux is indicated by red arrows, with black arrows indicating flow. The two isotherms depict temperature on the western boundary.

the tropics to be adiabatic. Thus, as long as we remain south of deep convection and deep mixed boundary layers, heat balance furnishes the following relation:

$$\int_0^L \int_0^{y(T)} Q\,dy\,dx \quad = \quad c_p \rho A_{\text{tropics}} \kappa \left.\frac{\partial T}{\partial z}\right|_{z(t)} \tag{6.1}$$

(6.1) implies that the heat flux through an isotherm in the tropics is equivalent to the heat flux lost to the "atmosphere" across the area to the north of the isotherm's outcropping latitude. Since our choice of temperature is arbitrary, (6.1) could be re-written to say that the diffusive convergence of heat flux into a layer bounded by T_1 and T_2 is equivalent to the surface heat flux lost between the latitudes $y(T_1)$ and $y(T_2)$.

Since we have observed that the scaling behavior of the LHS of (6.1) behaves according to a power law, the RHS must also follow. We will further assume that the tropical temperature structure is governed by advective-diffusive balance (as was found in chapter 3) and is rea-

sonably well approximated in the thermocline by exponential decay so that $\partial T/\partial z \sim TD^{-1}$, where D is an advective-diffusive scale height. For changes in κ, we see that this term implies that the power law exponents for meridional heat flux and D must sum to unity; this is in fact what we observed (the exponents were 0.57 and 0.42, respectively). Similarly, for changes in ΔT these power law exponents must also sum to one (1.51 and -0.45). Thus, through simple application of thermodynamics, (6.1) provides a relationship between meridional heat flux and advective-diffusive scale height. While it is true that the standard scaling argument also predicts exponents for these quantities that sum to unity, our observations do not agree with the predicted scalings of the additional components; in contrast, our thermodynamic "scaling" for this sum of exponents is upheld by the numerical results..

In the tropics, convergence of diffusive heat fluxes serves to warm upwelling waters. It has been suggested in the literature (e.g., Rossby 1965; Rahmstorf 1995) that an upward convective flux of heat must balance the downward diffusive flux. In other words, heat that is injected at depth must be balanced by heat loss through convective mixing into the surface layer, where it is subsequently lost via the surface boundary condition. Although the simplicity of this argument is appealing, we suggest that this "budget" is incomplete. Rather, much of the heat input into the ocean is balanced by heat loss from northward advection of water in the surface layer, particularly in the western boundary current. As shown In Fig. 6.1, above the level of no motion w decreases with height, with the diverging water flowing northward and upward along isotherms until it reaches the surface. Given the requirement that diffusive heat flux convergence at an isotherm match heat loss at the corresponding outcrop latitude, there is a direct connection between surface layer advection and the temperature structure in the tropics.

At high latitudes, i.e., north of the outcrop of T_*, heat is removed from the deep ocean by convective mixing. One can think of a convecting column as an extension of the surface mixed layer (here we refer to the surface as roughly the upper 50 meters), so that flows over an increased depth effectively become diabatic. We saw in chapter 4 that the system makes use of this convective pathway to communicate geothermal heat fluxes to the surface.

In summary, the heat flow "pathway" is as follows. Above the level of no motion, some of the warmed upwelling water diverges from the tropical region and flows to the surface along isotherms, while some continues upward and is warmed further. Although we do not claim to understand how the system arrives at a balance between upward and diverging flow, the divergence out of the upwelling column is critical is setting the vertical structure of the west-

ern boundary current (i.e., or else the western boundary current would be realized only in the surface layer). Below the level of no motion, flow is converging into the tropical region, so all water warmed by the convergence of heat flux continues upward, and is subsequently warmed further. Thus, here we can directly consider a balance between the heat loss by convective "preconditioning" and the convergence of heat flux at depth.

In Fig. 6.2 we show the pattern of surface heat flux (contours) and convective heating of the surface layer (shading) for three different runs. Fig. 6.2a show results using our standard values of $\kappa = 10 \times 10^{-4}$ m^{2}s^{-1} and $\Delta T = 27°$C, whereas Fig. 6.2b was run with $\kappa = 40 \times 10^{-4}$ m^{2}s^{-1} and Fig 6.2c with $\Delta T = 4 \times 27°$C. Given our scaling results in chapter 5, the bottom two plots show a similar increase in overturning strength (approximately $\times 4^{2/3}$) as compared to the standard run. T_* is also shown for reference. In all plots, heat input occurs where tropical mixing occurs, as follows from our discussion in chapter 3. Also in common is a large area of heat loss associated with the surface advection of the western boundary current. Since the northward penetration of the western boundary current is a function of overturning strength (see chapter 5), there is additional heat in western high latitudes in Figs. 6.2b and 6.2c, to the north of T_*.

In contrast, the pattern of convective surface heating varies markedly between runs. In Fig. 6.2a, note that the contours of heat loss coincide with enhanced convective warming in the northeast. Also note that convective activity occurs primarily to the north of the latitude given by T_* (although there is also a slight deepening of the mixed layer associated with the mid-latitude western boundary current, as would be suggested by the shading pattern). As follows from our discussion in chapter 4, there is little heat loss from deep convective mixing (in the northwest corner). When κ is increased, convective activity increases throughout high latitudes. Hence, it would seem that increasing κ results in greater warming of the surface layer through convective mixing, in keeping with the increased convergence of diffusive heat flux at depth. Also note that the horizontal extent of convective activity changes little between Figs. 6.2a and 6.2b, although we would expect convection to extend southward in the high κ regime.

Given an increase in ΔT, the area of convective activity is more confined to the northern extreme of the model. This result is consistent with Fig. 5.8d, which showed a narrower sinking region in the zonal average, inasmuch as deep mixed boundary layers on the east are colocated with deep sinking. Although a tongue of enhanced surface heat loss is again present at the eastern boundary, there is less visible correlation between this pattern and that of con-

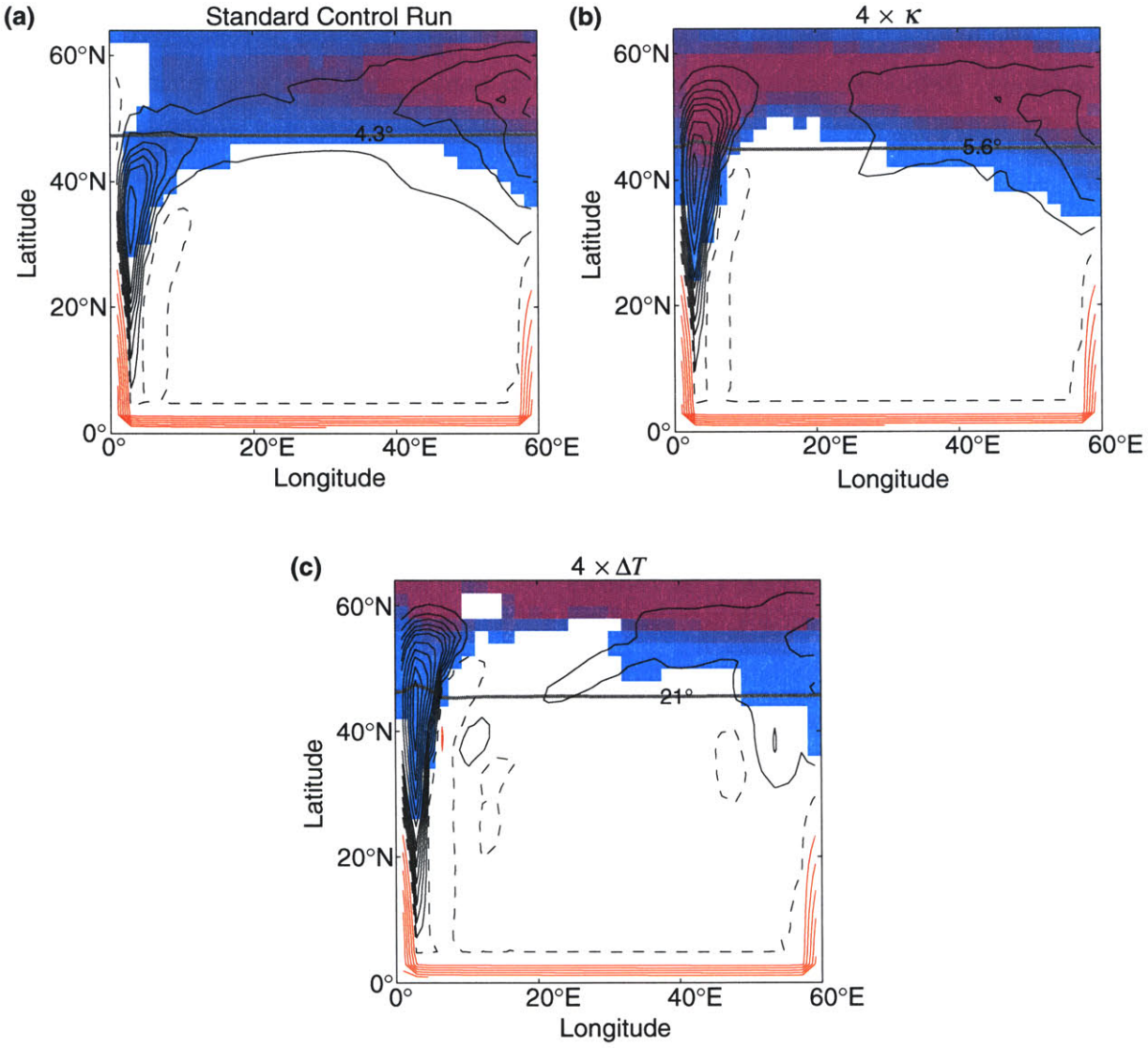

FIGURE 6.2: Plan view of surface heat exchange (contours) and convective warming of the surface layer (shading). The zero heat flux contour is shown as a dashed line; the heavy gray line shows the outcropping of the T_*; solid black contours indicate heat loss and red contours indicate heat gain. The scale of surface layer convective warming ranges from weak heating (blue) to strong heating (magenta). (a) Results from our standard control run, with $\kappa = 10 \times 10^{-4}$ m^{2}s^{-1} and ΔT =27°C; contour interval is 25 and 50 W m^{-2} for black and red contours, respectively. (b) Results with $\kappa = 40 \times 10^{-4}$ m^{2}s^{-1}; contour interval is 55 and 110 W m^{-2} for black and red contours, respectively. (c) Results with ΔT = 4×27°C; contour interval is 203 and 405 W m^{-2} for black and red contours, respectively. The contour interval in (b) and (c) has been scaled in accord with the maximum meridional heat flux, in order to facilitate a comparison with (a).

vective surface warming, suggesting that surface meridional flow accounts for a greater proportional of heat loss. In this run, the abyss is very homogeneous, implying weaker heat flux convergence there, which is consistent with less heat loss through the convective pathway.

In short, from a thermodynamic perspective, variations to κ and ΔT result in very different behavior, with increases in ΔT resulting in a decreased proportion of heat loss by convection. We speculate that since convection acts to reduce potential energy, it is not surprising that the system does not scale according to either the "self-similar" scaling argument or the Marotzke (1997) theory, neither of which consider the thermodynamics of the system. This notion is consistent with our results using weaker surface restoring, in that we again found surprisingly strong overturning, albeit with significantly decreased convective activity as compared to our fast restoring runs.

6.3 Concluding Remarks

In this thesis, we have examined the roles of diapycnal mixing, geothermal heating, and surface buoyancy forcing in the context of the oceanic meridional overturning circulation. We find that the thermodynamics of the system, often overlooked in the field of oceanography, are of fundamental significance. On the basis of our numerical experiments, we are able to fully explain both the role of mixing location and the impact of geothermal heating; both can be understood only through a synthesis of dynamics and thermodynamics.

Our experimental results suggest that downwelling and convective mixing are fundamentally different processes (see also Marotzke and Scott 1999). Moreover, deep downwelling and deep convective mixing cannot be co-located, which has important dynamical consequences. In contrast, the prevailing view in the literature is that warm (and salty) surface currents extend into high latitudes, are cooled, and then subsequently sink to depth as the "convective" downward branch of the large-scale circulation (e.g., McCartney and Talley 1994). Although or model lacks representation of many processes thought to be important for high latitude processes—in particular, convective flow and entrainment—and lacks sufficient resolution and topographic details to represent local current systems, we submit that this distinction between downwelling and convective mixing is relevant to the real ocean. More result studies that examine observational evidence (Mauritzen 1996; Spall and Pickard 2000) support this conclusion.

Although we are able to provide insight into our scaling results (many of which have not been previously reported in the literature), these results seemingly raise more questions than they provide answers to. Our diagnostics imply that the standard scaling argument is flawed; so why does the argument so nearly predict the observed scaling behavior with κ? And why

does the depth of the level of no motion vary so nearly as $\kappa^{1/3}$ in this series of runs, whereas the tropical advective-diffusive scale height varies with a different power law? Since we have not furnished an alternative analytical argument that provides the correct MOC scaling, it would be rash to completely dismiss the scaling argument and/or the Marotzke theory. However, we would suggest than any successful theory will require careful treatment of the system's thermodynamics.

These difficulties in understanding the system's scaling behavior underscore the complexity of the overturning circulation, even as studied in its simplest incarnation. Of course, the many considerations omitted from our model (in particular, wind forcing, topography, seasonal forcing, and salinity effects) are likely also to play a major role in governing the large-scale circulation, and must be included in any realistic modeling study. Other researchers have included wind forcing when examining the scaling behavior of maximum overturning (in a single hemisphere) with κ, and found that wind is important only when κ is very small (Zhang 1998; Vallis 2000; we confirmed these results in a series of runs not presented in this thesis, finding that wind forcing changes the scaling behavior only if the boundary κ is 1×10^{-4} m^2s^{-1} or less). Zhang et al. (1999) examined the scaling behavior using mixed boundary conditions, although a dynamical understanding of this more complicated system remains a challenge for future researchers, in light of the difficulties in understanding the behavior of the model presented in this thesis.

It is critical that we better understand ocean energetics and the processes which lead to diapycnal mixing, as it remains an open question whether the oceans are driven primarily by diapycnal mixing or through the direct effect of wind-forcing in the Southern Hemisphere, as suggested by Toggweiler and Samuels (1998). In addition, our results emphasize the need for realistic atmosphere-ocean coupling in climate models, given that surface forcing plays an important role in governing ocean dynamics.

References

Adcroft, A., J. R. Scott, and J. Marotzke, 2000: Impact of geothermal heating on the global ocean circulation. Submitted to *Geophysical Research Letters*.

Bryan, F., 1987: Parameter sensitivity of primitive equation ocean general circulation models. *J. Phys. Oceanogr.*, **17**, 970-985.

Bryan, F., 1991: Poleward heat transport in the ocean. A review of a hierarchy of models of increasing resolution. *Tellus*, **43**, 104-115.

Bryan, K., 1969: A numerical method for the study of the circulation of the world ocean. *J. Comput. Phys.*, **4**, 347-376.

Bryan, K., and M. Cox, 1967: A numerical investigation of the oceanic general circulation. *Tellus*, **19**, 54-80.

Colin de Verdière, A., 1988: Buoyancy driven planetary flows. *J. Mar. Res.*, **46**, 215-265.

Colin de Verdière, A., 1989: On the interaction of wind and buoyancy driven gyres. *J. Mar. Res.*, **47**, 593-633.

Colin de Verdière, A., 1993: On the oceanic thermohaline circulation. *Modelling Oceanic Climate Interactions*, J. Willebrand and D.L.T. Anderson, eds., NATO ASI Series, Springer, Berlin, 151-183.

Colin de Verdière, A., and T. Huck,1999: Baroclinic instability: an ocean wavemaker for interdecadal variability. *J. Phys. Oceanogr.*, **29**, 893-910.

Cummins, P., 1991: The deep water stratification of ocean general circulation models. *Atmos.-Ocean*, **19**, 563-575.

Cummins, P. F., G. Holloway, and A. E. Gargett, 1990: Sensitivity of the GFDL ocean general circulation model to a parameterization of vertical diffusion. *J. Phys. Oceanogr.*, **20**, 817-830.

Cushman-Roisin, B., 1994: *Introduction to Geophysical Fluid Dynamics*. Prentice Hall, 320 pp.

Crowley, T. J., 1991: *Paleoclimatology*. Oxford University Press, 352 pp.

Emanuel, K. A., 1994: *Atmospheric Convection*. Oxford University Press, 580 pp.

Faller, A. J., 1968: Sources of energy for the ocean circulation and a theory of the mixed layer. *Proc. U.S. Congress of Applied Mechanics*, 651-672.

Fanning, A. F., and A. J. Weaver, 1997: A horizontal resolution and parameter sensitivity study of heat transport in an idealized coupled climate model. *J. Climate*, **10**, 2469-2478.

Garrett, C., 1991: Marginal mixing theories. *Atmos.-Ocean*, **29**, 313-339.

Gent, P. R., and J. C. McWilliams, 1990: Isopycnal mixing in ocean circulation models. *J. Phys. Oceanogr.*, **20**, 150-155.

Gerdes, R. C., C. Köberle, and J. Willebrand, 1991: The influence of numerical advection schemes on the results of ocean general circulation models. *Clim. Dyn.*, **5**, 211-226.

Gill, A. E., 1982: *Atmosphere-Ocean Dynamics*. Academic Press, 662 pp.

Gill, A. E., and K. Bryan, 1971: Effects of geometry on the circulation of a three-dimensional southern-hemisphere ocean model. *Deep-Sea Res.*, **18**, 685-721.

Gregg, M. C., 1987: Diapycnal mixing in the thermocline: A review. *J. Geophys. Res.*, **92**, 5249-5286.

Helfrich, K. R., and K. G. Speer, 1995: Oceanic hydrothermal circulation: mesoscale and basin-scale flow. *Seafloor Hydrothermal Systems: Physical, Chemical, Biological, and Geological Interactions, Geophysical Monograph No. 91*, Americal Geophysical Union, pp. 347-356.

Huang, R. X., 1998: Mixing and available potential energy in a Boussinesq ocean. *J. Phys. Oceanogr.*, **29**, 727-746.

Huang, R. X., 1999: Mixing and energetics of the oceanic thermohaline circulation. *J. Phys. Oceanogr.*, **29**, 727-746.

Huck, T., A. J. Weaver, and A. Colin de Verdière, 1999: On the influence of the parameterization of lateral boundary layers on the thermohaline circulation in coarse-resolution ocean models. *J. Mar. Res.*, **57**, 387-426.

Jeffreys, H., 1925: On fluid motions produced by differences of temperature and humidity. *Quart. J. Roy. Meteor. Soc.*, **51**, 347-356.

Joyce, T. M., and K. G. Speer, 1987: Modeling the large-scale influence of geothermal sources on abyssal flow. *J. Geophys. Res.*, **92**, 2843-2850.

Joyce, T. M., B. A. Warren, and L. D. Talley, 1986: The geothermal heating of the abyssal subarctic Pacific Ocean. *Deep-Sea Res.*, **33**, 1003-1015.

Kadko, D., J. Baross, J. Alt, 1995: The magnitude and global implications of hydrothermal flux. *Seafloor Hydrothermal Systems: Physical, Chemical, Biological, and Geological Interactions, Geophysical Monograph No. 91*, American Geophysical Union, pp. 446-466.

Kamenkovich, I., J. Marotzke, and P.H. Stone, 2000: Factors affecting heat transport in an ocean general circulation model. *J. Phys. Oceanogr.*, **30**, 175-194.

Klinger, B. A., and J. Marotzke, 1999: Behavior of double hemisphere thermohaline flows in a single basin. *J. Phys. Oceanogr.*, **29**, 382-399.

Klinger, B. A., and J. Marotzke, 2000: Meridional heat transport by the subtropical cell. *J. Phys. Oceanogr.*, **30**, 696-705.

Klinger, B. A., J. Marshall, and U. Send, 1996: Representation of convective plumes by vertical adjustment. *J. Geophys. Res.*, **101**, 18,175-18,182.

Krishnamurti, R., 1980: Theory and experiment in cellular convection. *Mechanisms of Continental Drift and Plate Tectonics*, P. A. Davies and S. K. Runcorn, Eds., Academic Press, pp. 245-257.

Ledwell, J. R., A. J. Watson, and C. S. Law, 1993: Evidence for slow mixing across the pycnocline from an open-ocean tracer release experiment. *Nature*, **364**, 701-703.

Ledwell, J. R., E. T. Montgomery, K. L. Polzin, L. C. St. Laurent, R. W. Schmitt, and J. M. Toole, 2000: Evidence for enhanced mixing over rough topography in the abyssal ocean. *Nature*, **403**, 179-182..

Lupton, J. E., 1995: Hydrothermal plumes: near and far field. *Seafloor Hydrothermal Systems: Physical, Chemical, Biological, and Geological Interactions, Geophysical Monograph No. 91*, American Geophysical Union, pp. 317-346.

Lupton, J. E., and H. Craig, 1981: A major ^{3}He source on the East Pacific Rise. *Science*, **214**, 13-18, 1981

Luyton, J. R., J. Pedlosky, and H. Stommel, 1983: The ventilated thermocline. *J. Phys. Oceanogr.*, **13**, 292-309.

Lyle, M., 1997: Could early Cenozoic thermohaline circulation have warmed the poles? *Paleoceangr.*, **12**, 161-167.

Macdonald, A. M., and C. Wunsch, 1996: The global ocean circulation and heat flux. *Nature*, **382**, 436-439.

Marotzke, J., 1997: Boundary mixing and the dynamics of three-dimensional thermohaline circulations. *J. Phys. Oceanogr.*, **27**, 1713-1728.

Marotzke, J., and B. A. Klinger, 2000: The dynamics of equatorially asymmetric thermohaline circulations. *J. Phys. Oceanogr.*, **30**, 955-970.

Marotzke, J., and D. W. Pierce, 1997: On spatial scales and lifetimes of SST anomalies beneath a diffusive atmosphere. *J. Phys. Oceanogr.*, **27**, 133-139.

Marotzke, J., and J. R. Scott, 1999: Convective mixing and the thermohaline circulation. *J. Phys. Oceanogr.*, **29**, 2962-2970.

Marotzke, J., and P. H. Stone, 1995: Atmospheric transports, the thermohaline circulation, and flux adjustments in a simple coupled model. *J. Phys. Oceanogr.*, **25**, 1350-1364.

Mauritzen, C., 1996: Production of dense overflow waters feedning the North Atlantic across the Greenland-Scotland Ridge. Part I: Evidence for a revised circulation scheme. *Deep-Sea Res.*, **43**, 769-806.

Mauritzen, C., and S. Häkkinen, 1999: On the relationship between dense water formation and the "Meridional Overturning Cell" in the North Atlantic Ocean. *Deep-Sea Res.*, **46**, 877-894.

McCartney, M. S., and L. D. Talley, 1994: Warm-to-cold water conversion in the northern North Atlantic Ocean. *J. Phys. Oceanogr.*, **14**, 922-935.

McDermott, D. A., 1996: The regulation of northern overturning by Southern Hemisphere winds. *J. Phys. Oceanogr.*, **26**, 1234-1255.

Munk, W., 1966: Abyssal recipes. *Deep-Sea Res.*, **13**, 707-730.

Munk, W., and C. Wunsch, 1998: Abyssal recipes II: energetics of tidal and wind mixing. *Deep-Sea Res.*, **45**, 1977-2010.

Murton, B. J., L. J. Redbourn, C. R. German, and E. T. Baker, 1999: Sources and fluxes of hydrothermal heat, chemicals and biology within a segment of the Mid-Atlantic Ridge. *Earth Planet. Sci. Lett.*, **171**, 301-317.

Oort, A. H., L. A. Anderson, and J. P. Peixoto, 1994: Estimates of the energy cycle of the oceans. *J. Geophys. Res.*, **99**, 7665-7688.

Pacanowski, R. C., 1996: MOM 2.0 documentation, user's guide, and reference manual. GFDL Ocean Tech. Rep. 3.1, Geophysical Fluid Dynamics Laboratory/NOAA, Princeton, NJ. [Available from GFDL/NOAA, Princeton University, P.O. Box 308, Princeton, NJ 08542.]

Pacanowski, R. C., and G. Philander, 1981: Parameterization of vertical mixing in numerical models of the tropical ocean. *J. Phys. Oceanogr.*, **11**, 1142-1451.

Park, Y.-G., and K. Bryan, 2000: Comparison of thermally driven circulations from a depth coordinate model and an isopycnal layer mode: Part. I. A scaling law - sensitivity to vertical diffusivity. *J. Phys. Oceanogr.*, **30**, 590-605.

Pedlosky, J., 1996: *Ocean Circulation Theory*. Springer, 453 pp.

Peters, H., M. C. Gregg, and J. M. Toole, 1988: On the parameterization of equatorial turbulence. *J. Geophys. Res.*, **93**, 1199-1218.

Pickard , G. L., and W. J. Emery, 1990: *Descriptive Physical Oceanography*. Pergamon Press, 320 pp.

Polzin, K. L., J. M. Toole, J. R. Ledwell, and R. W. Schmitt, 1997: Spatial variability of turbulent mixing in the abyssal ocean. *Science*, **276**, 93-96.

Power, S. B., and R. Kleeman, 1994: Surface heat flux parameterization and the response of ocean general circulation models to high latitude freshening. *Tellus*, **46A**, 86-95.

Rahmstorf, S., 1995: Multiple convection patterns and thermohaline flow in an idealized OGCM. *J. Climate*, **8**, 3028-3039.

Rahmstorf, S. and J. Willebrand, 1995: The role of temperature feedback in stabilizing the thermohaline circulation. *J. Phys. Oceanogr.*, **25**, 787-805.

Redi, M. H., 1982: Oceanic isopycnal mixing by coordinate rotation. *J. Phys. Oceanogr.*, **12**, 1154-1158.

Robinson, A. R., and H. Stommel, 1959: The oceanic thermocline and the associated thermohaline circulation. *Tellus*, **11**, 295-308.

Robinson A. R., and P. Welander, 1963: Thermal circulation on a rotating sphere; with application to the oceanic thermocline. *J. Mar. Res.*, **21**, 25-38.

Rossby, H. T., 1965: On thermal convection driven by non-uniform heating from below: an experimental study. *Deep-Sea Res.*, **12**, 9-16.

Rossby, T., 1998: Numerical experiments with a fluid heated non-uniformly from below. *Tellus*, **50A**, 242-257.

Salmon, R., 1990: The thermocline as an "internal boundary layer." *J. Mar. Res.*, **44**, 695-711.

Samelson, R. M., and G. Vallis: 1997: Large-scale circulation with small diapycnal diffusion: the two-thermocline limit. *J. Mar. Res.*, **55**, 223-275.

Samelson, R. M., 1998: Large-scale circulation with locally enhanced vertical mixing. *J. Phys. Oceanogr.*, **28**, 712-726.

Sandström, J. W., 1908: Dynamische Versuche mit Meerwasser. *Annalen der Hydrographie und Maritimen Meteorologie,* **36**, 6-23.

Sclater, J. G., C. Jaupart, and D. Galson, 1980: The heat flow through oceanic and continental crust and the heat loss of the earth. *Rev. Geophys. and Space Phys.*, **18**, 269-311.

Scott, J. R., and J. Marotzke, 2000: Diapycnal stirring and the meridional overturning circulation: Does it matter where the mixing occurs? Submitted to *J. Phys. Oceanogr.*

Scott, J. R., J. Marotzke, and A. Adcroft, 2000: Geothermal heating and its influence on the meridional overturning circulation. Submitted to *J. Geophys. Res.*

Spall, M. A., 2000: Large-scale circulations forced by mixing near boundaries, submitted.

Spall, M. A., and R. S. Pickart, 2000: Where does dense water sink? A subpolar gyre example, submitted.

Speer, K. G., 1989: The Stommel and Arons model and geothermal heating in the South Pacific. *Earth Planet. Sci. Lett.*, *95*, 359-366, 1989.

Stein, C. A., S. Stein, and A. M. Pelayo, 1995: Heat flow and hydrothermal circulation. *Seafloor Hydrothermal Systems: Physical, Chemical, Biological, and Geological Interactions, Geophysical Monograph No. 91*, pp. 425-445.

Stommel, H., 1961: Thermohaline convection with two stable regimes of flow. *Tellus*, **13**, 224-230.

Stommel, H., 1962: On the smallness of the sinking regions of the ocean. *Proc. Natl. Acad. Sci. USA*, **48**, 766-772.

Stommel, H., 1982: Is the South Pacific helium-3 plume dynamically active? *Earth Planet Sci. Let.*, **61**, 63-67.

Stommel, H., and A. B. Arons, 1960: On the abyssal circulation of the world ocean - I. Stationary planetary flow patterns on a sphere. *Deep-Sea Res.*, **6**, 140-154.

Stommel, H. and J. Webster, 1962: Some properties of the thermocline equations in a subtropical gyre. *J. Mar. Res.*, **20**, 42-56.

Thompson, L., and G. C. Johnson, 1996: Abyssal currents generated by diffusion and geothermal heating over rises. *Deep-Sea Res.*, **43**, 193-211.

Toggweiler, J. R., and B. Samuels, 1995: Effect of Drake Passage on the global thermohaline circulation. *Deep-Sea Res.*, **42**, 477-500.

Toggweiler, J. R., and B. Samuels, 1998: On the ocean's large-scale circulation near the limit of no vertical mixing. *J. Phys. Oceanogr.*, **28**, 1832-1852.

Toole, J. M., and K. L. Polzin, 1999: A fine- and microstructure section across the continental slope and Gulf Stream. *EOS, Transactions*, American Geophysical Union, **80**, OS124.

Vallis, G. K., 2000: Large-scale circulation and production of stratification: effects of wind, geometry, and diffusion. *J. Phys. Oceanogr.*, **30**, 933-954.

Veronis, G., 1975: The role of models in tracer studies. Numerical models of the ocean circulation, Nat. Acad. of Sciences, Washington DC, 14 pp.

Walin, G., 1982: On the relation between sea-surface heat flow and thermal circulation in the ocean. *Tellus*, **34**, 187-195.

Wang, X., P. H. Stone, and J. Marotzke, 1995: Poleward heat transport in a barotropic ocean model. *J. Phys. Oceanogr.*, **25**, 256-265.

Wang, X., P. H. Stone, and J. Marotzke, 1999: Global thermohaline circulation. Part I: Sensitivity to atmospheric moisture transport. *J. Climate*, **12**, 71-82.

Welander, P., 1971: The thermocline problem. *Phil. Trans. Roy. Soc. London*, **A270**. 415-421.

Weyl, P. K., 1968: The role of the oceans in climate change: A theory of the ice ages. *Causes of Climate Change, Meteor. Monogr.*, No. 30, Amer. Meteor. Soc., 37-62.

Winton, M., 1995: Why is the deep sinking narrow? *J. Phys. Oceanogr.*, **25**, 997-1005.

Winton, M., 1996: The role of horizontal boundaries in parameter sensitivity and decadal-scale variability of coarse-resolution ocean general circulation models. *J. Phys. Oceanogr.*, **26**, 289-304.

Wunsch, C., 1996: *The Ocean Circulation Inverse Problem.* Cambridge University Press, 442 pp.

Wunsch, C., 1998: The work done by the wind on the ocean circulation. *J. Phys. Oceanogr.*, **28**, 2331-2339.

Young, W. R., and G. R. Ierley, 1986: Eastern boundary conditions and weak solutions of the ideal thermocline equations. . *J. Phys. Oceanogr.*, **14**, 1884-1900.

Zhang, J., 1998: Impacts of double-diffusive processes on the thermohaline circulation. Ph. D. thesis, Massachusetts Institute of Technology and Woods Hole Oceanographic Institution, 157 pp.

Zhang, J., R. W. Schmitt, and R. X. Huang, 1999: The relative influence of diapycnal mixing and hydrologic forcing on the stability of the thermohaline circulation. *J. Phys. Oceanogr.*, **29**, 1096-1108.

Zhang, S., R. J. Greatbatch, and C. A. Lin, 1993: A reexamination of the polar halocline catastrophe and implications for coupled ocean-atmosphere modeling. *J. Phys. Oceanogr.*, **23**, 287-299.

Zhang, S., C. A. Lin, and R. J. Greatbatch, 1992: A thermocline model for ocean-climate studies. *J. Mar. Res.*, **50**, 99-124.